THERMAL-HYDRAULIC ANALYSIS OF TIGHT LATTICE LIGHT WATER REACTORS

by

WILLIAM ARTIS BOYD

B.S., Alliance College (1973)

M.S., Drexel University (1975)

SUBMITTED IN PARTIAL FULFILLMENT
OF THE REQUIREMENTS FOR THE
DEGREE OF

MASTER OF SCIENCE IN NUCLEAR ENGINEERING

at the

MASSACHUSETTS INSTITUTE OF TECHNOLOGY

May 1977

Signature of Author..... William A. Boyd
Department of Nuclear Engineering, May 1977

Certified by..... Lothar Wolf
Thesis Supervisor

Accepted by..... C. J. Henry
Chairman, Department Committee

MASS. INST. TECH.
JUL 26 1977
LIBRARIES

THERMAL-HYDRAULIC ANALYSIS OF TIGHT LATTICE LIGHT WATER REACTORS

by

William Artis Boyd

ABSTRACT

This thesis investigates the thermal-hydraulic sensitivity of the Main Yankee core with respect to changes in rod diameter, rod spacing, linear heat generation rate and axial heat flux shape using a specially developed steady-state, single channel code (WABCORE) for this purpose.

A review of the information available in the open literature on the effects of small rod spacings is presented to bring into perspective, the type of thermal-hydraulic changes that can be expected to occur with core geometry changes. This review will also give insight into the necessary thermal-hydraulic effects that must be considered and modeled by WABCORE.

WABCORE has been designed such that the large amount of computer runs needed for a sensitivity study of this kind is performed in a fast and orderly fashion with a minimum of computer processor (CPU) time. Results of a particular set of calculations can be automatically plotted. Verification of the results obtained by WABCORE were made by comparison with those obtained by COBRA IIIC/MIT for examples representative of PWR and BWR core designs. The agreement in most of the parameters is surprisingly good.

The physical models used in the code to represent the phenomena in the fuel pin, and its associated coolant channel are discussed in detail. An analytical approach is used in WABCORE to represent the axial flux shape. This representation allows a very elegant solution of the axial DNBR shape correction factor. Finally, the limitations of the correlations used in the code are summarized to indicate where further improvement should be made.

Results of the sensitivity study indicate that the linear heat generation rate of the Main Yankee core could be increased from 5.7 KW/ft to 10.0 KW/ft using a flat heat flux profile while maintaining the initial total mass flow, core cross-sectional area, and total power. This increase is achieved by decreasing the rod length and increasing the

rod diameter over the initial values. The minimum allowable DNBR for steady-state operation is reached before centerline temperature becomes unsafely high for the suggested linear heat generation rate. Other results of the sensitivity study indicate that

- the core pressure loss is independent of the axial heat flux profile
- the axial distribution of the rod centerline temperature and DNBR closely follow the axial heat flux profile.

Finally, optimized regions for steady-state operation at linear heat generation rates greater than the initial of 5.7 KW/ft are outlined graphically.

Thesis Supervisor: Professor Lothar Wolf
Title: Associate Professor of Nuclear Engineering

ACKNOWLEDGEMENTS

This thesis is dedicated to my family, who may not understand any portion of the work contained herein, but have supported and believed in me from the very beginning.

The author wishes to thank Professors Wolf and Driscoll for the guiding, suggestions and financial assistance received over the preceeding year.

NOMENCLATURE

A_c - Core area

A_{cif} - Channel flow area

A_f - Flow area of liquid phase

A_g - Flow area of vapor phase

C_p - Specific heat

D_{ei} - Hydraulic diameter

d_R - Rod diameter

g_c - Conversion factor

G_i - Channel mass flux

h - Enthalpy

h_i - Inlet enthalpy

h_{fg} - Latent heat of vaporization

h_{ci} - Heat transfer coefficient at inside clad surface

h_{fs} - Heat transfer coefficient at fuel pellet surface

h_g - Heat transfer coefficient of fuel rod gap

K_c - Thermal conductivity of clad

K_f - Thermal conductivity of fuel

L - Core length

L_N - Length between nodes

L' - Normalized core length

N_{eff} - Effective number of rods in core

N_n - Number of nodes

P - Pressure

p - Pitch

q - Total thermal power

q' - Linear heat generation rate

q'' - Heat flux

$q''_{DNB,N}$ - CHF for nonuniform flux shape

$q''_{DNB,U}$ - CHF for uniform flux shape

q'''_{PEAK} - Peak power density

R_e - Renold's number

R_{ci} - Clad inside radius

R_{co} - Clad outside radius

R_{fs} - Fuel pellet radius

S - Slip factor

T_{ci} - Inside clad surface temperature

T_{co} - Outside clad surface temperature

T_f - Coolant temperature

T_{fs} - Fuel pellet surface temperature

T_g - Rod gap temperature

TPM - Two-phase multiplier

V_f - Liquid velocity

V_g - Vapor velocity

W_f - Liquid mass flux

W_g - Vapor mass flux

X - Quality

Z_{FDB} - Length at which fully developed boiling starts

Z_{sc} - Length at which subcooled boiling starts

Z^* - Length at which thermodynamic equilibrium is reached

α - Void fraction

ρ_f - Liquid density

ρ_g - Vapor density

ϕ_{SPE} - Shape function

μ_f - Liquid viscosity

μ_g - Vapor viscosity

ν_f - Liquid specific volume

ν_g - Vapor specific volume

LIST OF TABLES

LIST OF FIGURES

TABLE OF CONTENTS

CHAPTER I

INTRODUCTION AND BACKGROUND

MIT began work in 1976 to examine improvements in LWR breeding performance (MIT LWR Thorium Project). Two of the approaches taken to study these improvements included work on thorium utilization and on tight-pitch LWR lattices. The immediate objectives of this work was to:

- Develop a model which would predict ore requirements for a variety of systems composed of LWR reactors using various combinations of fertile and fissile species.
- Use the model to project savings which could be achieved through improvements in reactor performance characteristics, and through thorium utilization, for a range of reactor characteristics.
- Identitify the most promising mode of fuel utilizations in a symbiotic LWR economy and the magnitude of the resulting savings relative to conventional options.

Current reactor conditions were used as a starting point in these studies, and advancements were made toward the stated goals. The newly established reactor characteristics made for these advancements were within the realm of current state of the art technology. These changes were not, however, checked to determine whether they would combine to produce a physically relizable thermal-hydraulic reactor system.

A preliminary study was carried out the summer of 1976 to evaluate the thermal-hydraulic constraints applicable to tight-pitch lattices installed in as built PWR's[5]. It was considered to be sufficient for the initial phase of this work to use a hand-calculational procedure, together with some backup checks using COBRA-IIIC/MIT. With the Main Yankee reactor chosen as the base case, these preliminary studies were expected to show relative sensitivities of reactor characteristics to design changes. It was also thought that preliminary limits could be established on a portion of the reactor parameters. This would enable the fuel management and lattice studies to continue with an upper and lower limit of parametric variation. These added restraints would aid the fuel management and lattice analyst in determining whether their newly established reactor characteristics would be feasible at all.

This first approach to the thermal-hydraulic question did indeed show that:

- The core pressure drop was very sensitive to changes in the pitch-to-diameter ratio and
- The axial power profile has a major effect upon the fuel centerline temperature as well as on DNB.

Several questions did, however, remain unanswered in this preliminary study. These included:

1. What design changes lead to a reduction of the high pressure drop resulting from a tight pitch?

2. What is the sensitivity of DNB to local flux irregularities?

3. Can the mass flow rate and power rating of current PWR designs be maintained for the redesign?

4. What is the most promising spacer design, grid or wire wrap?

At this point, it was felt that a more accurate and flexible tool than the initial hand- calculational procedure was needed, and which was, at the same time much cheaper to operate than COBRA IIIC/MIT. The development of this computational tool was considered necessary in order to cope with the vast amount of parametric information to be handled. It would also provide the fuel management and lattice analyst with a quick and inexpensive tool to examine the feasibility of their reactor characteristic changes.

This thesis presents:

1. The development of a steady-state one-dimensional code (WABCORE) capable of performing a thermal-hydraulic analysis of both PWR's and BWR's.

2. Results of comparison checks made with COBRA IIIC/MIT to validate WABCORE as a useful thermal-hydraulic tool.

3. Results of a sensitivity study performed on the Main Yankee reactor to answer the above four questions and

a final thermal-hydraulic area of interest to the MIT LWR thorium project.

4. Detailed COBRA IIIC/MIT checks of the sensitivity studies final results.

1.1 Geometric Effects Upon the Thermal-Hydraulic Behavior of Rod Bundles

Certain water-cooled reactor concepts employ rod arrays with very small clearances between the rods. Because these designs have a relatively low water-to-metal ratio, it seems possible that considerable adverse local flow redistributions might occur within a typical coolant channel, particularly under boiling conditions. As a result of this, flow staivations may occur causing the power level at which CHF conditions are reached to be substantially lower than the power level corresponding to complete mixing of the fluid in the channel. Also, substantial increases in the channel pressure losses can be expected as a result of the very small clearances between the rods compared to the normal LWR rod spacing.

The following section will present the results of a literature survey covering both theoretical and experimental evidence.

1.1.1 Effect of Rod Spacing on CHF

Green et al.[11] reported CHF data for water at pressures ranging from 1200 to 2000 PSIA in a 48. inch long vertical electrically heated channel simulating the narrow gap of a triangular lattice as shown in Figure 1.1A. His results show that the measured CHF data for 15 and 30 mil gaps, assuming complete mixing, agree closely with CHF data obtained with rectangular channels having spacing of 59 to 97 mils. These results agree with those obtained by Towell in a differently shaped test section[12], shown in Figure 1.1B, in which the rod spacing was varried from .018 in. to .05 in. No effect on CHF was found at a water mass velocity of 1×10^6 lbm/hr ft^2 and at a pressure of 1000 PSIA having a constant average exit quality in the range of 15 to 45%.

These results also agree with those found by DaSilva and Andrade[5], who performed a thermal-hydraulic evaluation of a core substitution with the constraints of maintaining the initial total mass flow and core thermal power. They concluded that there would be no advantage in using a triangular array over a square array other than to obtain a very low pitch over diameter ratio.

It should be noted that the above mentioned gap effects upon CHF were obtained for a geometry where gaps were changed uniformly in a rod bundle. In case that a single gap should be reduced in a rod bundle, the CHF would be affected

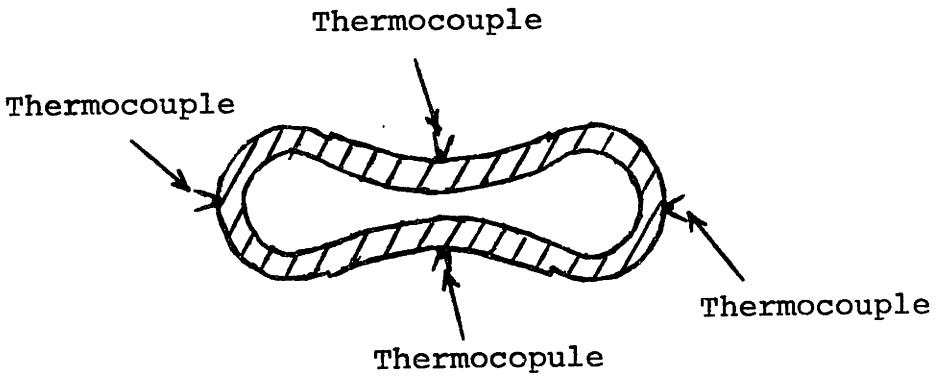

Figure 1.1A

Simulated Rod Gap in a Triangular Lattice Rod Bundle

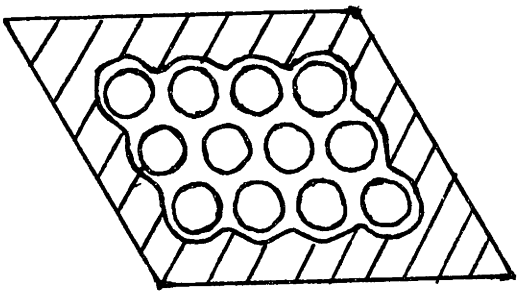

Figure 1.1B

Towell's "Star" Rod Bundle

by the local reduction of gap flow in comparison with the average bundle flow.

1.1.2 Effect of Rod Length on CHF

In the 19-rod bundles tested by Matzna et al.[13] and Moeck et al.[14], results indicate a radial shift of CHF locations from the outer channels to the inner channels as the bundle length increases from 18 inches to 108 inches. This shift was explained by Tong with the help of Figure 1.2[3]. In the group of outer channels, the mass velocities in the long rod bundles are lower, thus, CHF occurs in the relatively low mass velocity channel. However, the flow at CHF in the outer channel rod groups should be higher than that of the inner channel group due to the higher power and the cold walls surrounding the outer channels. DaSilva and Andrade[5] analyzed the possibility of increasing q' in a PWR while maintaining the initial total mass flow and core thermal power. They found that changing length would cause less drastic changes in DNBR, centerline temperature and core pressure loss than changing core area.

1.1.3 Flow Regime and Cold Wall Effects on CHF

Gellerstedt et al.[15] have reported the CHF data obtained from a 9-rod, 6 foot long bundle with a uniform axial heat flux. The rod outside diameter is .42 inches with a gap of .138 inches between rods, and a gap of .069 inches between the rod and wall. The CHF data were obtained for

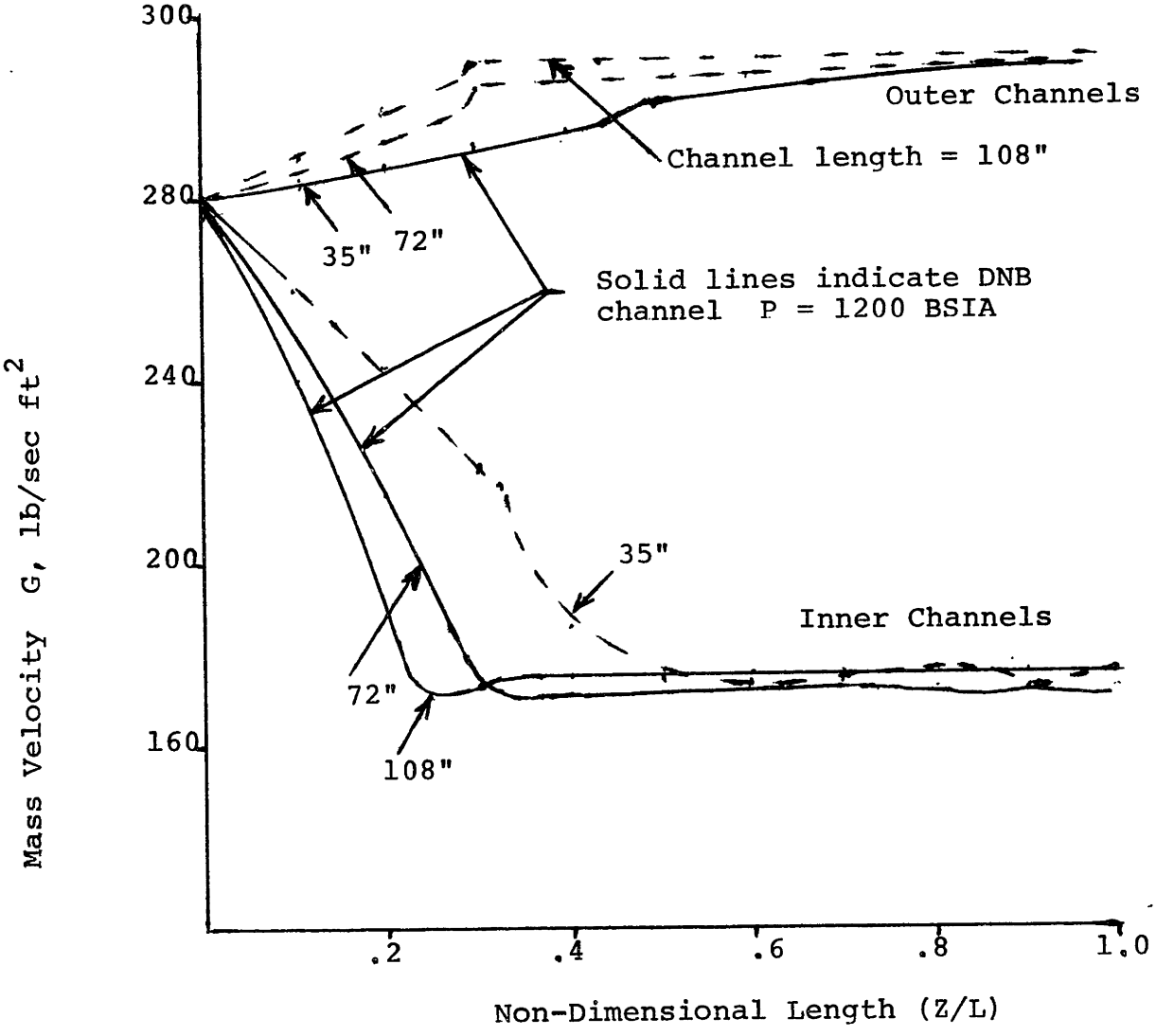

Figure 1.2

Axial Subchannel Flow Distribution
in a 19-Rod Bundle

mass fluxes ranging from .2 to 3.5 x 10^6 lbm/hr ft^2 and in a pressure range from 1000 to 2400 PSIA. The resulting average exit quality varied from - 5% to + 75%. They found that the cold wall effect on CHF differs in three distinct flow regimes as shown in Table 1.1. These results indicate that the cold wall effect is more important at higher void fractions.

Bergles[16] also found that for all flow regimes, a strong tendency exists for the liquid to channel into the more restricted corner subchannel of a 4-rod, 24 inch long bundle. Under adiabatic conditions, large variations in the thickness of the wall liquid films in annualr flow were noted. The wall film thickness were consistantly thinner on the portion of the rod which faced the interior subchannel. The test results also indicated that flow regime boundaries are shifted to lower qualities with heat addition.

1.1.4 Effect of Grids on CHF

Janssen et al.[17] have reported on CHF data obtained from 72 inches long, 16-rod bundles with uniform axial heat flux for steam-water flow at pressures ranging from 600 to 1250 PSIA. The effect of grid-type spacers on CHF is dependent on their axial positions. With the last spacer located 4 inches upstream from the end of the heated length, CHF is improved. On the other hand, with the last spacer located 18.5 inches upstream from the end of the heated length, CHF at high flows is reduced.

Table 1.1

Subchannel Critical
Heat Flux Location

Flow Regime	Critical Heat Flux Location (% of total data points in the given flow regime)
High Quality	Corner Cell: 75% Wall Cell: 25% Unit Cell: 0%
Annular Flow	Corner Cell: 22% Wall Cell: 77.5% Unit Cell: 0.5%
Nucleate Boiling	Corner Cell: 30% Wall Cell: 0% Unit Cell: 70%

1.1.5 Effects of Improvements in CHF

A steady-state reactor analysis was performed by William's[18] to aid in reactor design improvements. For the purpose of this analysis, a hypothetical hot-channel-fuel plate was selected. Channel conditions were defined as:

- Mass flux = 3×10^6 lb/hr ft^2
- Average thermal flux level = 3×10^5 BTU/hr ft^2
- Film heat transfer coefficient = 1×10^4 BTU/hr ft^2 °F
- Hydraulic diameter = .01333 ft
- Channel length = 3.5 ft .

It was reported that improvements in CHF may be achieved by channel inserts and fluid mixing. If the improvement in CHF is measured from the DNBR = 1.0 point, the gain in operational power is shown in Figure 1.3. For example, if DNB could be increased by 100% (by any method), the iti-tial system could operate at 140% of its current limiting heat flux with a maximum fuel plate temperature of 880°F. Again, this analysis considered only the steady state per-formance of a pressurized water core.

1.1.6 Effects on Pressure Loss

Towell[12] also used his test section (Figure 1.1B) to correlate pressure loss data versus exit quality for rod spacings of .018 and .05 inches. Figure 1.4 shows the results of his measurements and indicates that there is approximately a two-to-one relationship between the pressure

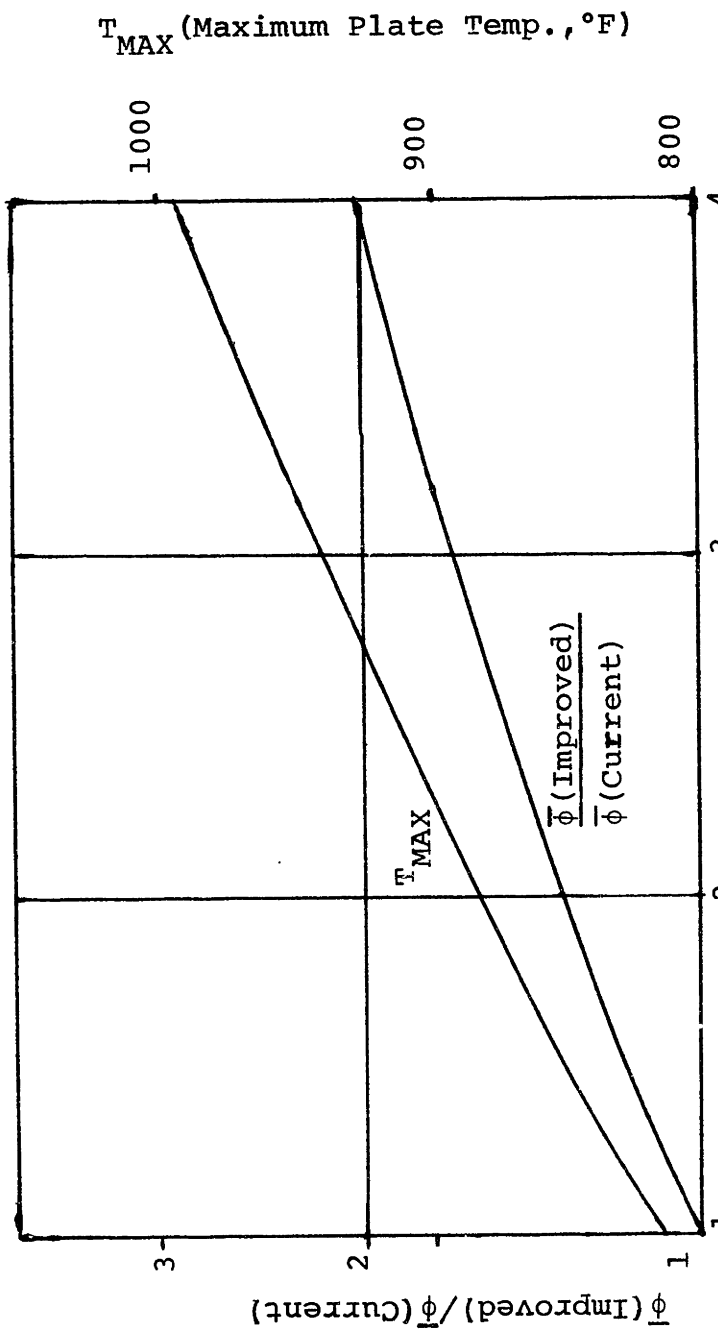

Figure 1.3: Variation of Allowable Operational Power Level and T_{MAX} for Improved DNB Flux Level (Uniform Axial Flux)

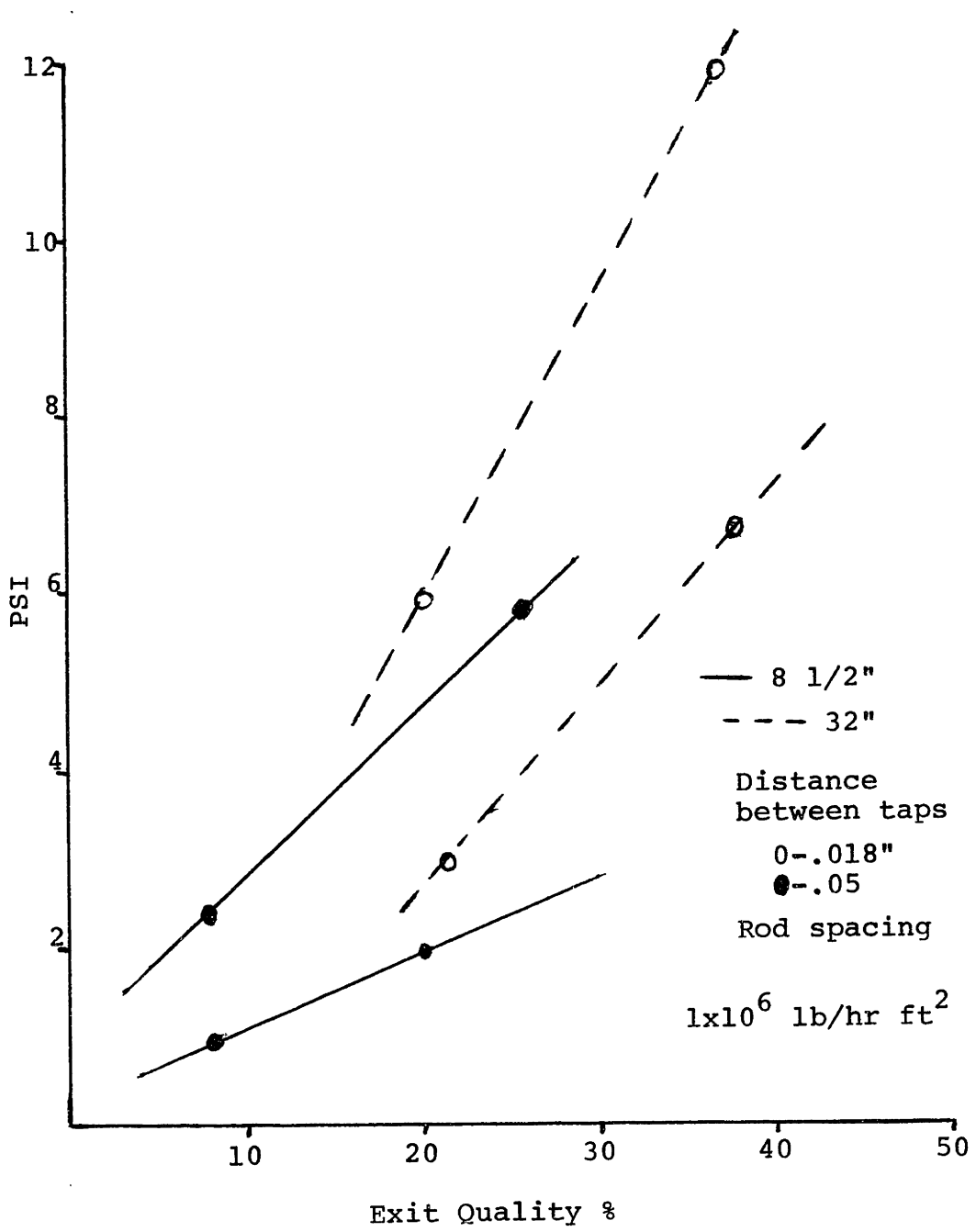

Figure 1.4

Exit Quality Versus Pressure Loss
For Various Rod Spacings

loss of the .018 inch and .05 inch rod bundle spacings.

Castellana et al.[19] report that calculations show that for high heat flux densities the magnitude of the subcooled boiling friction factor in the wall voidage region can be as much as several times the isothermal value. Thus, it must be concluded that to neglect the wall voidage region, and to only apply a bulk boiling two-phase multiplier (TPM) in the detached voidage region can result in substantial underpredictions of the friction pressure drop for conditions of low exit quality where these regions are of substantial length. At present, however, there is no generally accepted method for the accurate prediction of (α) and (TPM) over a wide range of pressures, qualities, and flow rates. Therefore several methods must be used to accurately predict (α) and (TPM) over a wide range of flow conditions.

Isothermal pressure drop tests were performed on a square rod bundle with several spacer types by LeTourneau et al.[20] to determine an effective friction factor, assuming that the spacer pressure loss was distributed along the length of the rod bundle. The Selmi-type spring clip spacers resulted in friction factors which could be represented by $f = .155\ Re^{-.11}$ while all other spring collar spacers had friction factors that could be represented by $f = .244\ Re^{-.168}$. These friction factor results

were based on

- Rod length = 90.79 inches
- Flow area = $3.89 \times 10^{-2} ft^2$
- Heated area = $20.9 ft^2$
- Wetted perimeter = 43.9 inches
- Hydraulic diameter = .516 inches .

DeStordeui[21], on the other hand, developed drag coefficients for fuel-element spacers and concluded that the coefficients were independent of the height of the spacers.

1.2 Survey Conclusions

As a result of the preceeding literature survey, the following dev opments are included in WABCORE:

- Fluid properties are determined at each axial location for more precise CHF and voidage calculations.
- Provisions for including the effects of grid spacers through both the drag coefficient method recommended by DeStrodeui[21] or the channel averaging method by LeTourneau[20].
- Two slip factors are applied to the homogeneous two-phase flow model to enable more accurate voidage calculations in the low voidage flow region.

Also, because of the results obtained from the literature survey, the sensitivity study will:

- only investigate hexagonal arrays if an increase cannot be obtained in the linear heat generation rate while

maintaining established constraints (discussed in Chapter 4).

- not vary the core corss-sectional area, but will vary core length

- assume DNB will always occur in the interior channles for the Main Yankee core .

CHAPTER II

DESCRIPTION AND LOGIC OF WABCORE

2.1 Problem Formulation

The task of all thermal-hydraulic codes is to generate results that agree with the actual behavior of the reactor core being modeled. Of course, the cost to build and to run a thermal-hydraulic code that models an entire reactor core exactly is much too expensive, and consequently, no such codes have been built. What is commonly done is to formulate a code capable of modeling a reactor assembly exactly and surround this assembly with other assemblies represented as modes. These results are then used to represent a reactor core (i.e., MEKIN, THINC IV). The cost of this process is not altogether inexpensive and in the case of using such a code for the many runs needed in a sensitivity study, the final cost would be quite high.

To reduce this cost further, an additional simplification is made on the reactor assembly resulting in the isolated single channel approximation as shown in Figure 2.1. These single channel results will forseeably be conservative because of its isolation for neighboring subchannels. This isolation does not allow for the exchange of mass, momentum or energy in the x-direction into the neighboring subchannels, thus resulting in this conservatism. The cross

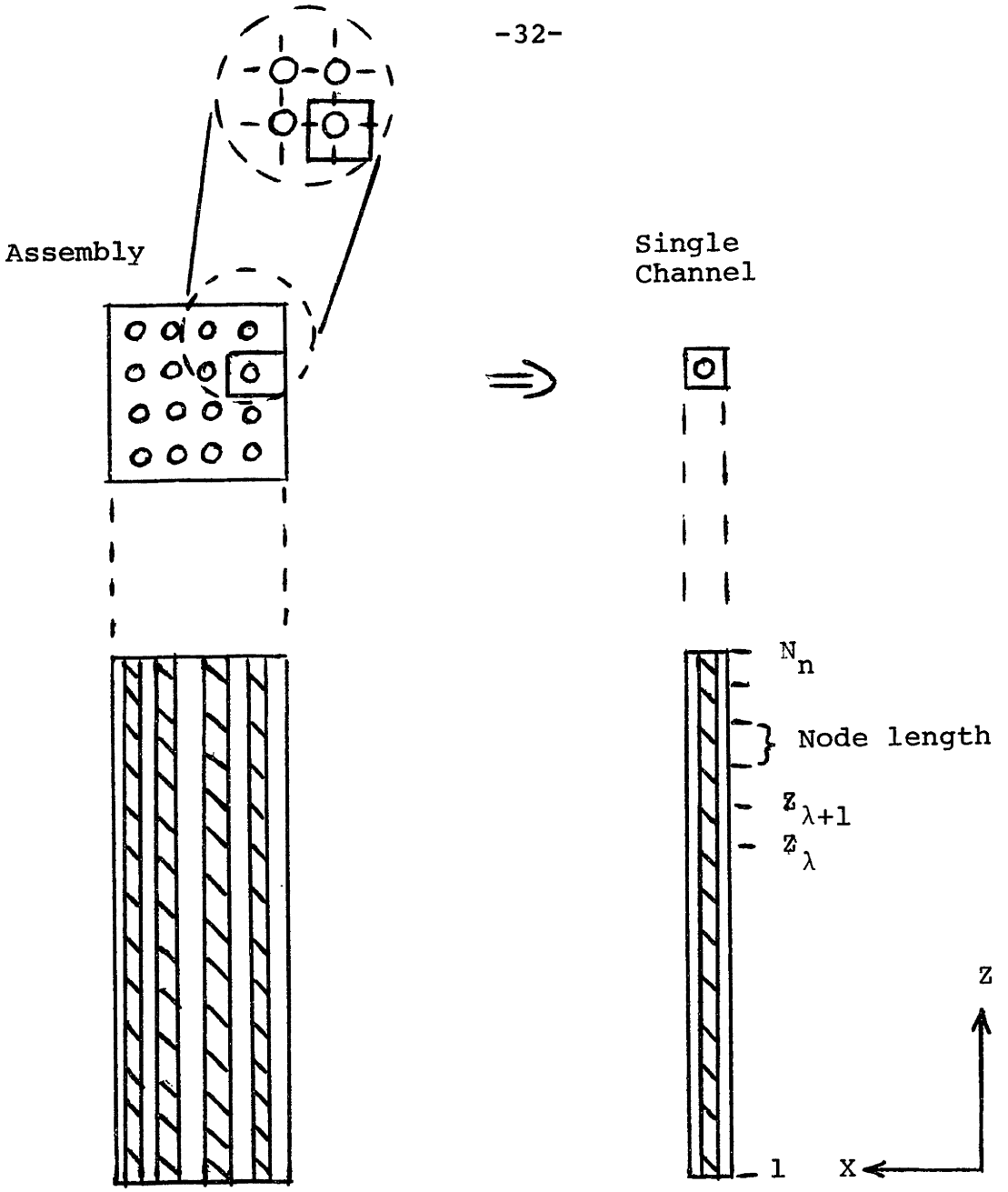

EQUIVALENT ASSEMBLY AND SINGLE CHANNEL

FIGURE 2.1

flow caused by this transversal exchange is not a serious problem unless there are several radial and axial flux peakings or any phenomenon which will cause transeverse pressure gradients in the rod bundle being modeled. In this case the single channel approach will not produce results representative of the bundle or any single channel of the bundle. As a result of the single channel approach, only one spatical variable exists in the z-direction and all transvere momentum calculations are eliminated.

This single channel technique is developed into a steady-state one-dimensional code (WABCORE) to model the thermal-hydraulics of a reactor channel. The results will then be applied to the entire reactor core. An attempt has been made to develop a tool capable of performing the computational work of a sensitivity study in a fast and orderly fashion. To do this, the following general considerations went into the development of the code.

1) An imput format which can quickly and easily be understood.

2) A minimum of computer processor usage (CPU) time.

3) Printed output of all results in tabular form with computer plottings made of all important reactor design variables.

4) Possible deviations of less than 10% towards conservatism when compared with established multisubchannel

thermal-hydraulic codes.

These considerations led to the preliminary logic illustrated in Figure 2.2 and resulted in the following:

1) The correlations used in WABCORE produce very accurate results while requiring a minimum amount of calculation time. Naturally trade-offs had to be made between accuracy and calculation time.

2) Decreasing the solution time by having one calculational pass made through the core by the code (Figure 2.2).

The loss of accuracy caused by this will be discussed at a latter point.

3) Solution of algebraic equations to integrate up the channel length, thus decreasing the computational time necessary while increasing accuracy over the numerical integration schemes normally used.

4) An unlimited number of cases can be calculated in a single run while up to five of these cases may be plotted on a single plot.

5) Water property correlations which are the same as those used in HAMBO and COBRA III C.

2.2 Conservation Equations

A simplified one-dimensional analysis of two-phase flow can be made by considering the system in Figure 2.3.

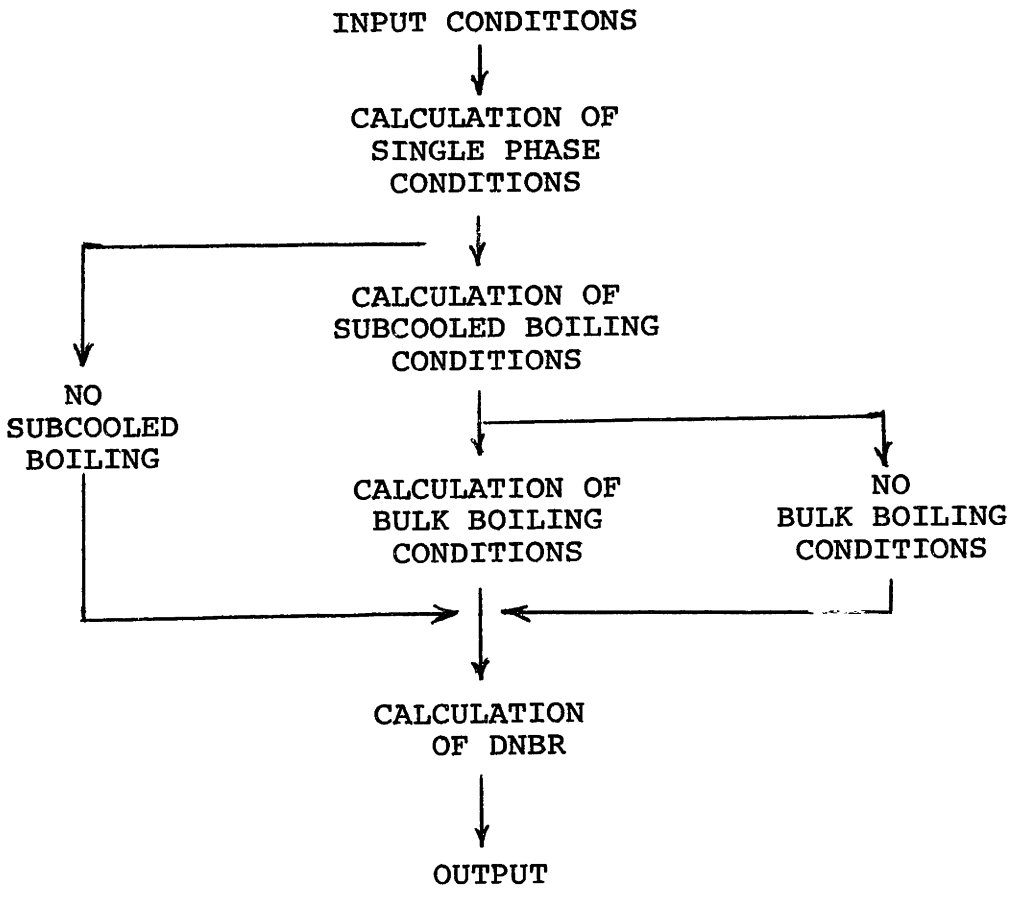

Figure 2.2

Elementary Single-Pass Flow Logic

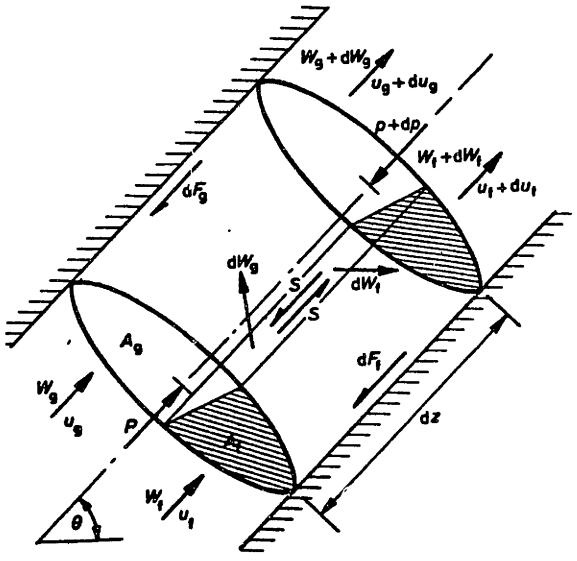

Figure 2.3

Simplified Model for Two-Phase Flow
Over Element of Channel

This shows a flow in an inclined pipe under conditions where there is a mass transfer between the phases (i.e., evaporation or condensation). The flow is assumed to be steady and mean values of the velocity and density of each phase are assumed to exist across a plane normal to the flow. It is further assumed that the pressure across any plane normal to the channel axis is uniform and the sum of areas occupied by the vapor and liquid in this plane equals the channel cross-sectional area.

2.2.1 Conservation of Mass

The equations expressing conservation of mass in the channel in the absence of any addition or removal of mass through the channel walls are

$$\begin{aligned} w &= w_g + w_f \\ dw_g &= - dw_f \\ w_g &= A_g \rho_g v_g = wx \\ w_f &= A_f \rho_f v_f = w(1 - x) \end{aligned} \tag{2.1}$$

2.2.2 Conservation of Momentum

The forces acting on each phase can be equated to the rate of change of momentum of that phase. Therefore, for the vapor phase,

$$PA_g - (P + dP)A_g - dF_g - s - A_g dz\ \rho_g g \sin\theta = (w_g + dw_g)(V_g + dV_g) - w_g V_g - dw_g V_f \qquad (2.2)$$

where

dF_g = vapor function forces on solid surface

s = vapor function forces at gas-liquid interface .

A similar relationship is derived for the liquid phase.

$$- A_f dP - dF_f + s - A_f dz\ \rho_f g \sin\theta = w_f dV_f \quad . \qquad (2.3)$$

The basic differential momentum equation for this one-dimensional approach is obtained by adding equations 2.2 and 2.3.

$$- AdP - dF_g - dF_f - g \sin\theta\ dz(A_f\ \rho_f + A_g\ \rho_g) = d(w_f V_f + w_g V_g) \qquad (2.4)$$

The net functional force may be expressed in terms of the area:

$$(dF_g + dF_f) = - A \left(\frac{dP}{dz}\right)_F dz \quad . \qquad (2.5)$$

Substitution of equation 2.5 into 2.4 yields after rearrangement

$$\left(\frac{dP}{dz}\right) = \left(\frac{dP}{dz}\ F\right) + \left(\frac{dP}{dz}\ a\right) + \left(\frac{dP}{dz}\ z\right) \tag{2.6}$$

where acceleration losses are

$$-\left(\frac{dP}{dz}\ a\right) = \frac{1}{A}\frac{d}{dz}\left(w_g V_g + w_f V_f\right) = G_i^2 \frac{d}{dz}\left[\frac{x^2 \nu_g}{\alpha} + \frac{(1 - x^2)\nu_f}{(1 - \alpha)}\right] \tag{2.7}$$

and the elevation losses are

$$-\left(\frac{dP}{dz}\ z\right) = g \sin\theta\left[\frac{A_g}{A}\ g + \frac{A_f}{A}\ f\right] = g \sin\theta\left[\alpha\rho_g + (1 - \alpha)\rho_f\right] . \tag{2.8}$$

The above derivation illustrates the use of momentum equations to relate the total static pressure gradient in terms of the separate components of friction, acceleration and static head. It should be pointed out that the frictional term has been defined in terms of the force $(dF_g + dF_f)$ and will be expanded upon in Section 2.3.

2.2.3. Conservation of Energy

The equation describing the conservation of total energy for both phases is,

$$(\delta q - \delta w) = wdh + d\left[\frac{w_g V_g^2}{2} + \frac{w_f V_f^2}{2}\right] + wg \sin\theta \, dz \quad . \quad (2.9)$$

For the purpose of this work:

- the work performed by the fluid on the surroundings is assumed to be zero

- the kinetic energy and potential energy phases does not contribute to the internal energy.

Therefore:

$$\delta q = wdh \quad . \quad (2.10)$$

2.2.4 Equation of State

For a given mass of fluid at equilibrium in either the major or liquid phase, a relationship exists among the pressure, temperature and the density. The relation is written symbolically as

$$f(P,T,\rho) = 0 \quad .$$

That is, for any given equilibrium state of the mass of fluid specification of any two of these parameters determines the value of the third one.

The water property correlations used in WABCORE are polynomial fits to steam table data. The exact equation of state for water as given by the Keenan and Keyes Steam Tables[10] is

$$P = \rho RT \left[1 + \rho Q + \rho^2 \left(\frac{\partial Q}{\partial \rho}\right)\right]$$

and

$$h = RT \left[\rho t \left(\frac{\partial Q}{\partial t}\right) + 1 + \rho Q + \rho^2 \left(\frac{\partial Q}{\partial \rho}\right)\right] + \frac{d(\psi_o t)}{dt}$$

where

$$\psi_o = \sum_{i=1}^{6} C_i / t^{i-1} + C_7 \ell n\, T + C_8 \ell n\, T/t$$

$$Q = (t - T_c) \sum_{j=1}^{7} (t - t_{aj})^{j-2} \sum_{i=1}^{8} A_{ij} (\rho - \rho_{aj})^{i-1} + C^{-E} \sum_{i=9}^{10} A_{ij} \rho^{i-9} \quad .$$

The coefficients are

$C_1 = 1857.06$ $\quad C_4 = 36.66$ $\quad C_7 = 46.0$

$C_2 = 3229.12$ $\quad C_5 = -20.55$ $\quad C_8 = -1011.25$

$C_3 = -419.46$ $\quad C_6 = 4.85$

and

$R = 4.6151$ bar $cm^3/g°K$ $\quad T$ = temperature in °K

ρ = density in g/cm^3 $\quad T_c = 1.54$

$t = 1000$ K $\quad E = 4.8$

2.3 Friction Loss

The friction loss term of the momentum conservation equation is expressed by the Darcy formula

$$-\frac{dP}{dz}F = f\frac{L}{D_{ei}}\frac{\rho V^2}{2g_c}(TPM) \qquad (2.11)$$

where the Darcy-Weisbach friction factor is

$$f = \frac{.221}{(D_{ei}V\rho/\mu)^{.2}} = \frac{.221}{Re^{.2}}$$

and (TPM) is the two-phase multiplier applied in the boiling region. This multiplier will be discussed at a later point in Section 2.9.

2.4 Grid Loss

From the continuity and energy equations, the mass flow rates for liquid and vapor are

$$w_f = A_f'(2g_c\rho_f(dP)_f)^{.5} \qquad (2.12)$$

$$w_g = A_g'(2g_c\rho_g(dP)_g)^{.5} \qquad (2.13)$$

where through an orifice

$$A_f' = C_d \frac{A_f}{\left(1 - \left(\frac{A}{A_c}\right)^2\right)^{.5}}$$

$$A_g' = C_d \frac{A_g}{\left(1 - \left(\frac{A}{A_c}\right)^2\right)^{.5}}$$

A = orifice area

A_c = channel area

C_d = a coefficient of discharge, obtained from experiments or published data.

The two-phase loss is therefore, from Equations 2.12 and 2.13.

$$(dP)_{TP} = (dP)_f + (dP)_g$$

$$= C_s\left(\frac{w_f}{A_f'}\right)^2 \frac{1}{2g_c\rho_f} + C_s\left(\frac{w_g}{A_g'}\right)^2 \frac{1}{2g_c\rho_g} \qquad (2.14)$$

$$= \frac{C_s}{2g_c}\left[\frac{G_{if}^2}{\rho_f} + \frac{G_{ig}^2}{\rho_g}\right]$$

$$(dP)_{TP} = \frac{C_s}{2g_c}\frac{G_i^2}{\bar{\rho}}$$

where

$$C_s = \frac{1}{C_d}$$

$$\bar{\rho} = \alpha\rho_g + (1 - \alpha)\rho_f \quad .$$

Equation 2.14 is applied in all flow conditions and its accuracy depends on the loss coefficient C_s . If there is no void (i.e., single phase), then the liquid density is the only density term in Equation 2.14.

It has been shown that the pressure drop from grids is not a function of grid length[1]. This indicates that the pressure loss is primarily a form loss rather than a friction loss.

2.5 Other Losses

For added versatility, the effects of spacer length and thickness can be included. These will effect the channel geometry (i.e., D_{ei} , G_i , A_{cif}), thereby causing an increase in the frictional loss term. Losses induced by wire wraps are included this way and there are no loss coefficients for them.

WABCORE does not consider any other type of pressure losses in either the single-phase or two-phase region. The flow is assumed to propagate up a single channel without expansions or contractions. Orifices are only considered through the effects of grid losses.

2.6 Heat Flux Shape Function

2.6.1 Shape Correlation

The basis of the analytical approach used in the code is the analytical shape correlation. This correlation is versatile enough to represent the most common reactor heat flux shapes while still remaining a simple analytical function. This simplicity becomes extremely beneficial when the correlation is integrated into the code through the heat flux and temperature equations.

The basic mathematical correlation consists of the superposition of two exponentials as shown in Figure 2.4 and are added together to yield:

$$\phi_{SPE}(z) = K_n\left[NA(B - Z)C^{(Z-B)A} + KCZC^{-ZC}\right] \quad . \qquad (2.15)$$

The different shapes are generated by varying the constants (K_n, N, A, K, C) of the equation. Some possible shapes from this correlation are illustrated in Figure 2.4 with $(B = 1)$.

2.6.2 Normalization

To represent the heat flux profile of a reactor core, the z axis of Figure 2.5 must correspond to the height of the core. Secondly, the dimensionless abscissor must coincide with the 1.0 at the peak value of the shape function.

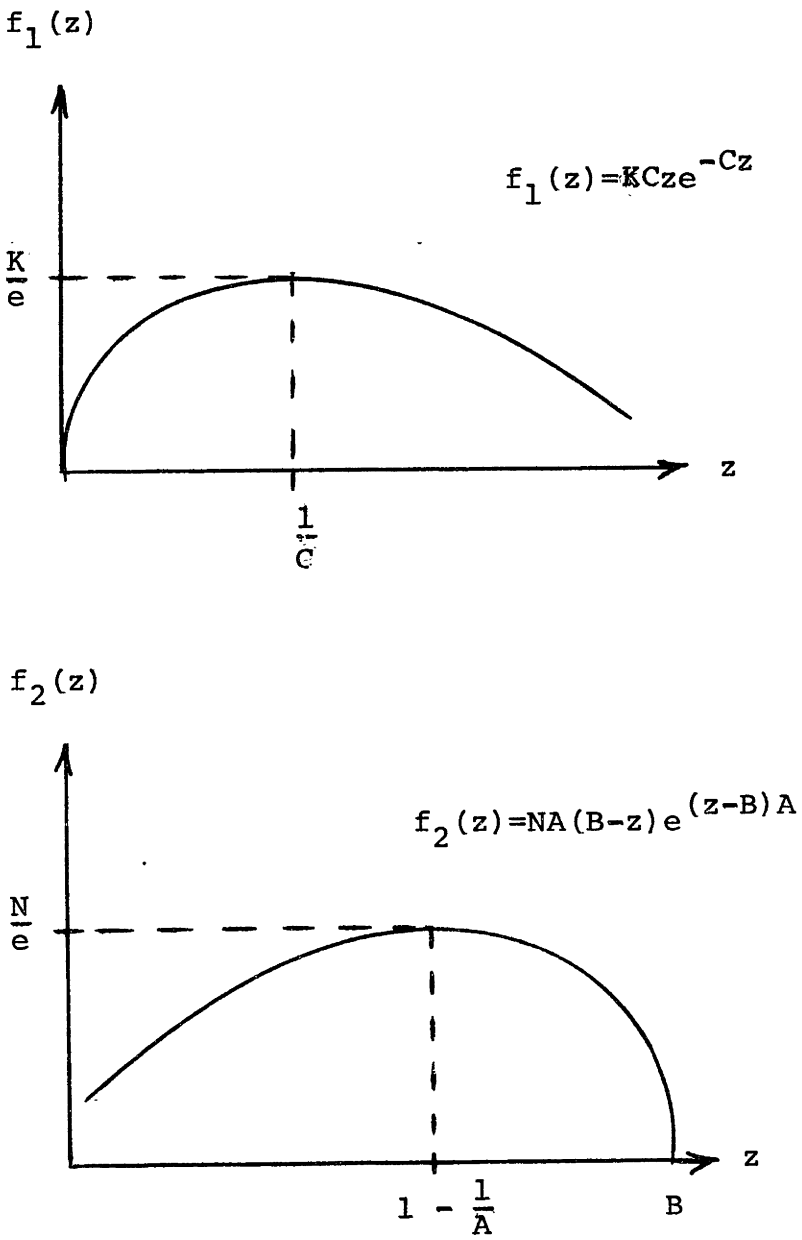

Figure 2.4

Shape Correlation Exponentials

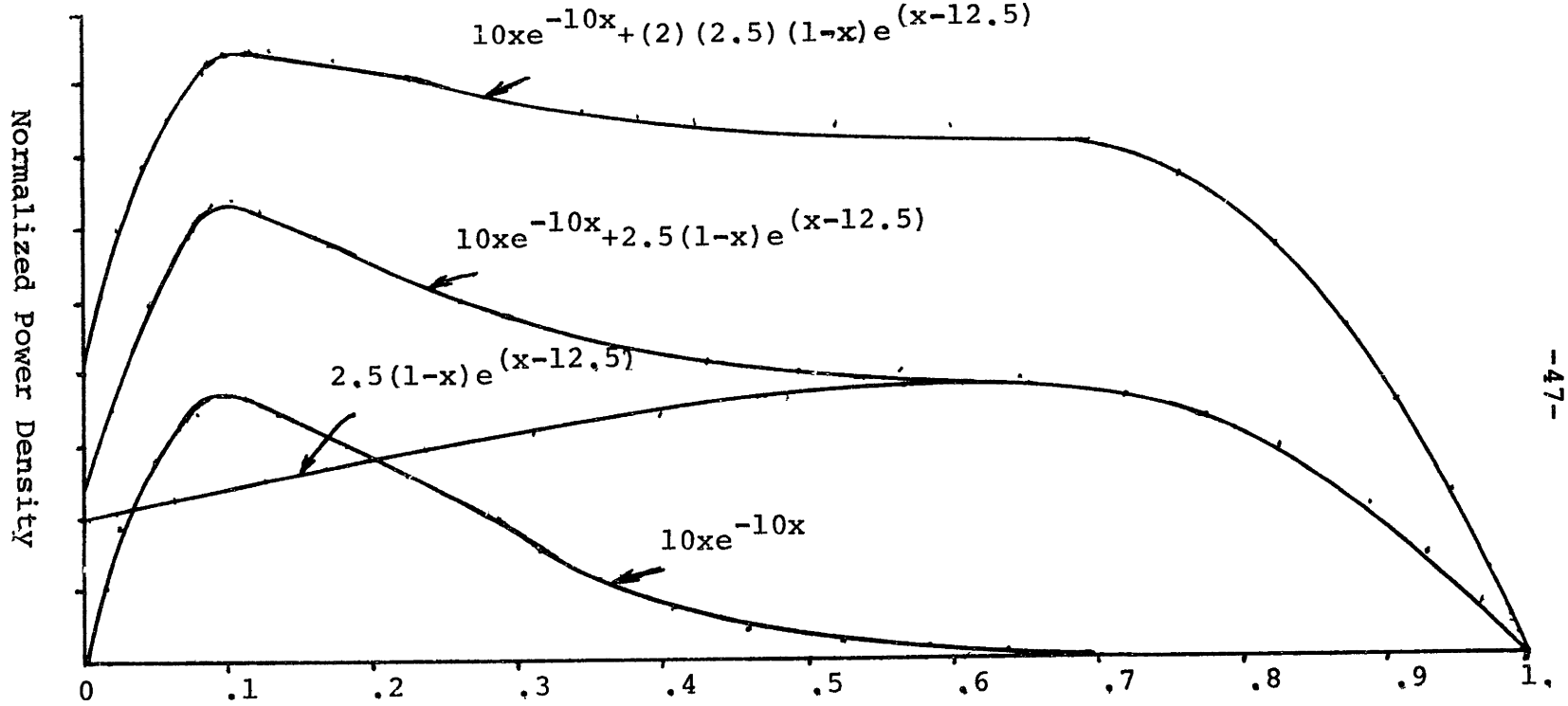

Figure 2.5

Sample Power Profiles Which Can Be Represented by Parametric Equation

This second condition is easily alleviated by using the constant, K_n to equalize the reactor and correlation abscissa values. The first condition requires a more involved, but straight forward approach.

Since $\phi_{SPE}^{(z)}$ is only a function of z, it need only be multiplied by some constant to convert it to the true reactor length. Mathematically, the multiplier is L'/B, where the normalized length (L') is

$$L' = \frac{L}{B - 0} B = L \quad .$$

If the entire length of the z axis is not used to represent the core length, but only a portion between z_1 and z_2 (Figure 2.6), then

$$L' = \frac{L}{(B' + s) - s} B = \frac{L}{B'} B \quad ,$$

where

$$s = z_1$$

$$B' + s = z_2 \quad .$$

This normalization multiplier is also valid when the correlation is integrated over limits anywhere between $-\infty$ and $+\infty$. For use in WABCORE, B has been set to <u>one</u>.

2.6.3 <u>Heat Flux</u>

The heat flux used for further computation at each axial

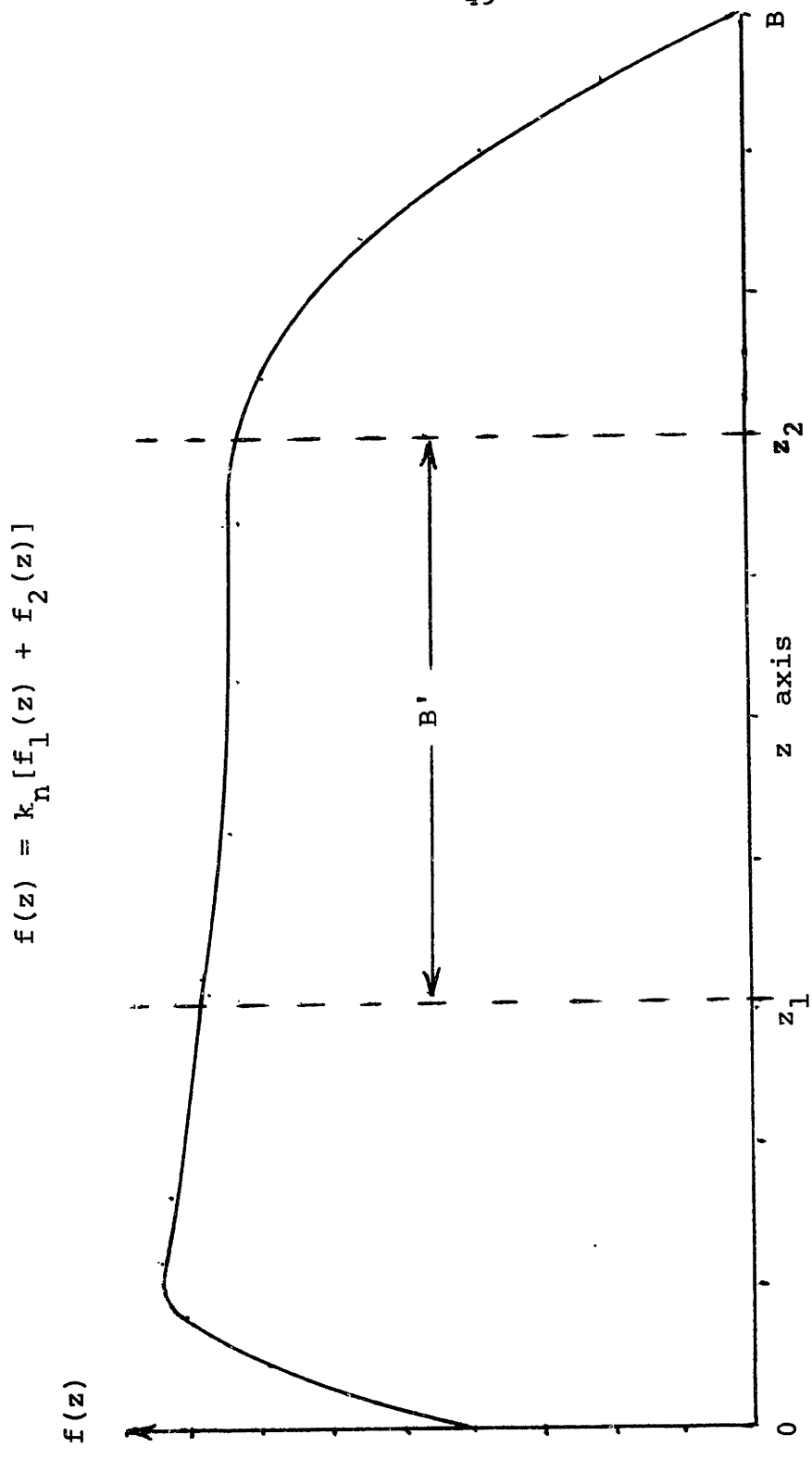

FIGURE 2.6

PARTIAL SHAPE REPRESENTATION

step is an averaged value over the length of the incremental step. This average incremental flux is calculated from

$$q'' = q'''_{PEAK} \frac{R_{fs}^2 L'}{d_r L_N B} \int_{z_i}^{z_{i+1}} \phi_{SPE}(z)dz \qquad (2.16)$$

where

$$q'''_{PEAK} = \bar{q}'' d_r L / R_{fs}^2 \frac{L'}{B} \int_{s}^{B'+s} \phi_{SPE}(z)dz \qquad (2.17)$$

$$L_N = \frac{L}{N_n - 1} \quad .$$

z_i and z_{i+1} are the inlet and outlet positions of an incremental length (node length). See Figure 2.1.

The more irregular the heat flux shape, the smaller the axial increments (i.e., more nodes) that should be used. This will decrease the irregularities of the calculated data between nodes. It will not, in any case, make a large difference in outlet conditions.

2.7 Coolant and Fuel Pin Models

2.7.1 Coolant Temperature

The temperature of the coolant is calculated at each axial node by applying the energy balance equation (Equation 2.10) over the preceeding axial node length

$$\delta q = w c_p (\delta T) = w \delta h \quad . \qquad (2.18)$$

From Equation (2.17)

$$\delta q = q'''_{PEAK} \frac{R_{fs}^2 L'}{B} \int_{z_i}^{z_{i+1}} \phi_{SPE}(z)dz \quad .$$

Therefore

$$\delta T_f = \frac{q'''_{PEAK} R_{fs}^2 N_{eff} L'}{c_p w B} \int_{z_i}^{z_{i+1}} \phi_{SPE}(z)dz \quad . \quad (2.19)$$

2.7.2 Clad Temperature

The energy balance is again applied at the coolant-clad interface. The temperature difference between clad and coolant is directly proportional to the heat flux and the heat transfer coefficient. From this, it can be written

$$T_w - T_f = \frac{q'''_{PEAK} R_{fs}^2 L'}{h d_R B} \phi_{SPE}(z) \quad (2.20)$$

where, in the single phase and subcooled boiling region,

$$h = B_c \frac{K_f}{D_{ei}} Re^{.8} (Rr)^{.33} \quad . \quad (2.21)$$

B_c is the Weisman[2] coefficient for

square lattice - $B_c = .042\left(\frac{P}{d_r}\right) - .024$ for

$$\left(1.1 \leq \frac{P}{d_r} \leq 1.35\right)$$

and

triangular lattice - $B_c = 0.26\left(\frac{P}{d_r}\right) - .006$ for

$$\left(1.1 \leq \frac{P}{d_r} \leq 3.5\right) \quad .$$

The Weisman coefficient is chosen to readjust the single channel heat transfer coefficient to that representative of a square or triangular lattice. The Chen correlation is used to determine h in the bulk boiling region. This will be discussed in Section 2.10.

2.7.3 Fuel Surface Temperature

To determine the temperature difference between the clad outside surface and fuel pellet surface, two, one-dimensional radial heat transfer equations were solved. For the clad region

$$q' = - k2\pi R \frac{dT}{dR} \quad . \tag{2.22}$$

Solving this equation yields:

$$T_{ci} = T_{co} + \frac{q'}{2\ k_c} \ln \frac{R_{co}}{R_{ci}} \quad . \tag{2.23}$$

The solution in the gap region is approached by first solving a one-dimensional energy balance in the region illustrated in Figure 2.7. The equations describing the energy flow across this region are:

$$- q = 2\pi R_{ci} h_{ci} L (T_{ci} - T_g)$$

$$q = 2\pi R_{fs} h_{fs} L (T_{fs} - T_g) \quad .$$

Solving for T_{fs} yields

$$T_{fs} = \frac{q'}{2\pi R_{fs} h_{fs}} + \frac{q'}{2\pi R_{ci} h_{ci}} + T_{ci} \quad . \tag{2.24}$$

Combining Equations 2.23 and 2.24 results in

$$T_{fs} = T_{co} + \left[\frac{1}{2k_c} \ln \frac{R_{co}}{R_{ci}} + \frac{1}{2h_g R_{fs}} + \frac{1}{2h_g R_{ci}} \right] \cdot \frac{L'}{B} R_{fs}^2 \, q'_{PEAK} \, \phi_{SPE}(z) \tag{2.25}$$

where

$$h_g = h_{ci} = h_{fs}$$

$$q' = \pi R_{fs}^2 \, q'''_{PEAK} \, \frac{L'}{B} \, \phi_{SPE}(z)$$

Because the gap heat transfer coefficient is applied to both the fuel pellet and the inside clad wall, the results from Equation 2.25 will be conservative. This conservatism will be amplified and appear in the center-line temperature

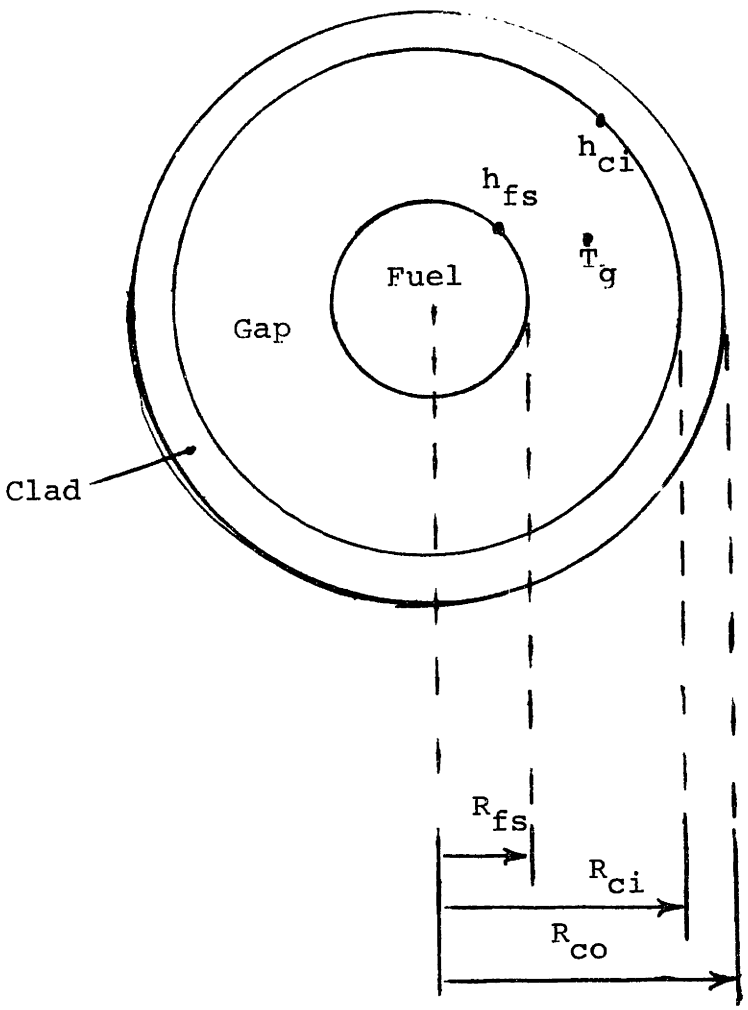

Figure 2.7

Fuel Pin Model

results. The centerline temperatures calculated from WAB-CORE can always be interpreted as an upper limit because of this.

2.7.4 Center-Line Temperature

The center-line temperature is determined by solving the one-dimensional Poisson equation. This results in

$$T_{cL} = T_{fs} + \frac{R_{fs}^2 L'}{4k_f B} \; q'''_{PEAK} \; \phi_{SPE}(z) \qquad (2.26)$$

for

$$R = 0 \quad .$$

2.8 DNB

2.8.1 Critical Heat Flux Correlation

The W-3 correlation is used to calculate the CHF in the subcooled and boiling regions.

$$\begin{aligned} q''_{DNB,u} = {} & [(2.02 - .43P/10^3) + (.172 - .1P/10^3) \\ & \exp(18.2\,x - 4.13\,x\,P/10^3)] \cdot [1.16 - .87x] \\ & \cdot [(.148 - 1.6\,x + .173\,x|x|)G_i/10^6 + 1.04] \\ & \cdot [.166 + .836 \exp(-3.15 D_{ei})] \\ & \cdot [.826 + .0008(H_{SAT} - H_i)] \end{aligned} \qquad (2.27)$$

This correlation has not been tested in quality ranges greater than 15%. This will naturally limit the code to flow situations where quality is less than 15%. Several other limitations are listed in Section

2.8.2 Shape Correction Factor

The form factor developed by Tong[3] in conjunction with the W-3 correlation is used in the code. The CHF correlation and form factor are applied at each interval along the axis. The results of this application account better for the fact that all quantities used in this calculation are local and no averaging is performed over the core length[3]. The form factor is defined as:

$$F = q''_{DNB,u}/q''_{DNB,N}$$

$$F = \frac{C_1 \int_{z_1}^{z_z} q''(z)\exp[-C(z_2 - z)]dz}{q''_{loc}[1 - \exp(-C(z_2 - z_1))]} \qquad (2.28a)$$

where

$$C_1 = .44(1 - x_2)^{7.9}/(G_i/10^6)^{1.72} \text{ in}^{-1}$$

$$x_2 = \text{quality at } z_2 \quad .$$

This integral can be exactly evaluated because $q''(z)$ is an analytical function of z given by Equations 2.16 and 2.15.

Substituting and solving results in

$$F = \left[\frac{C_1 q'' R_{fs}^2 k_n L'}{q_i''(1 - C^{-C_1 \ell_i L'/B} d_R B}\right] \left[\frac{NAB}{F}\left(C^{-D} C^{z_i F}\right)\right.$$

$$- \frac{NA}{F^2} C^{-D}\left((Fz_i - 1)C^{z_i F} - (FS - 1)C^{z_{i-1} F}\right) \qquad (2.28b)$$

$$\left. + \frac{kC}{G^2}\left((Gz_i - 1)C^{z_i G} - (Gz_{i-1} - 1)C^{z_{i-1} G}\right)\right]$$

where

$$D = AB + C_1 \ell_i B/L' \qquad E = C_1 \ell_i B/L'$$

$$F = A + C_1 B/L' \qquad G = C_1 B/L' - C$$

q_i'' = heat flux at mode i

ℓ_i = distance between nodes i and $i - 1$.

It should be noted that this form factor correlation should not be used with other CHF correlations because it has been developed in concurrence with one CHF correlation and can only produce consistent results with that correlation. Tong's form factor and the W-3 correlation form a consistent set in the sense. The B + W correlation for CHF and shape correction are another consistent set.

2.9 Subcooled Boiling Region

2.9.1 Boiling Lengths

WABCORE uses several correlations to determine the lengths at which fully developed boiling starts, where subcooled boiling ends, and where thermal equilibrium is reached (Figure 2.8). These correlations are applied at each axial step and checks are made as to whether the calculated length is less than the node length (length of axial interval).

Boiling is not considered until bubbles depart from the wall (FDB). The accuracy lost as a result of not considering the region between (ONB) and (FDB) is not considered to perpetuate any sizable errors. This conclusion has been upheld through the verification checks (Chapter 3) made on WABCORE. Ease of computation has been obtained as a result of the slight loss in accuracy.

The combined length of regions A and B of Figure 2.8 is the total subcooled length (Z_{sc}), given by

$$Z_{sc} = \frac{G_i C_p D_{ei}}{4q''} (T_{SAT} - T_{fi}) \quad . \qquad (2.29)$$

Bowring's[9] model for bubble detachment (FDB), which is recommended as the best available at present, is also used in WABCORE. His empirical development leads to

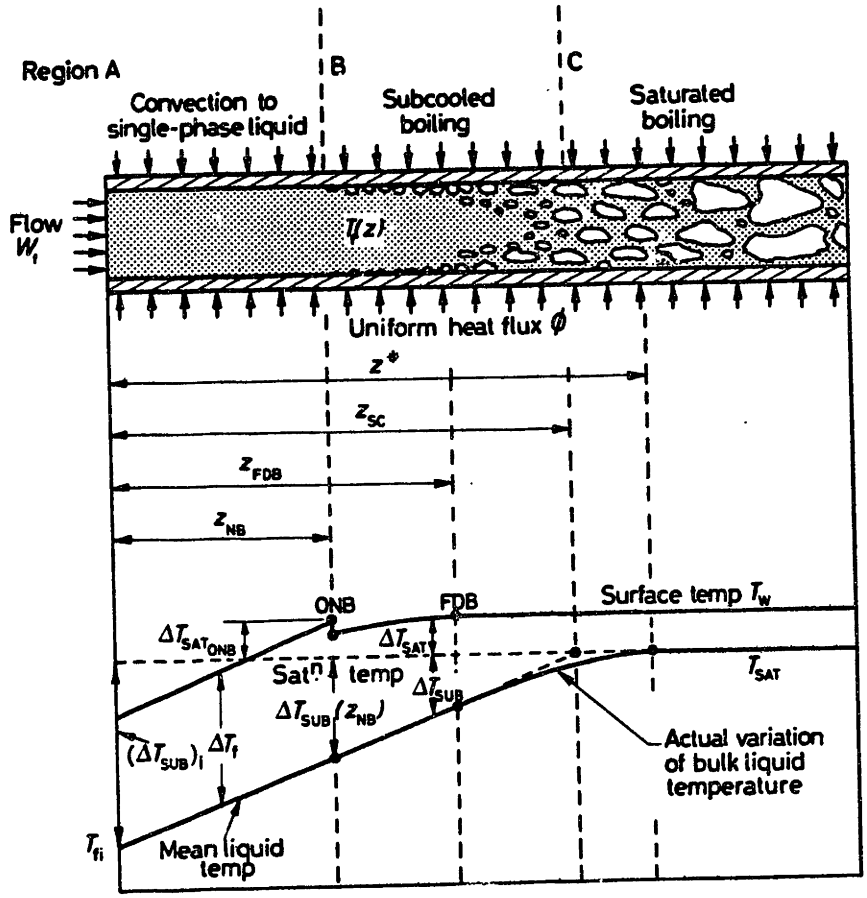

Figure 2.8

Surface and Liquid Temperature Distributions in Subcooled Boiling

$$Z_{FBD} = \frac{G_i C_p D_{ei}}{4}\left[\frac{T_{co} - T_{fi}}{q''} - \frac{\eta}{G_i \nu_f}\right] \qquad (2.30)$$

where

$$\eta = .067[14. + .0068P]$$

in British Engineering units. The length for reaching thermal equilibrium (Figure 2.8) is determined from

$$Z^* = \frac{G_i C_p D_{ei}}{4}\left[\frac{(T_{co} - T_{fi})}{q''} + \frac{\eta}{G_i \varepsilon \nu_f}\right] \qquad (2.31)$$

where

$$(1 + \varepsilon) = 2.6$$

from Bowring's empirical relationship. It is used in this case to generate consistency among the boiling length correlations.

2.9.2 TwoPhase Friction Multiplier and Void Fraction

Two correlations can be selected from the homogeneous model for calculation of the friction multiplier. Results of the homogeneous model have been determined to be very good in most of the flow regimes pertinent to reactor design.

$$TPM = \left[1 + x\,\frac{\nu_g - \nu_\ell}{\nu_\ell}\right] \cdot \left[1 + x\left(\frac{\mu_\ell}{\mu_g} - 1\right)\right]^{-.25} \qquad (2.32a)$$

and

and

$$TPM = \left[1 + x\,\frac{\nu_g - \nu_\ell}{\nu_\ell}\right] \cdot \left[1 + x\left(\frac{\mu_g}{\mu_\ell} - 1\right)\right]^{.25} \qquad (2.32b)$$

with

$$\alpha = x\nu_g/(x\nu_g + (1 - x)\nu_f s) \quad . \qquad (2.32c)$$

The void fraction is calculated using the homogeneous slip model. Two slip multipliers are used. The first is used up to the subcooled boiling length (Z_{sc}) and the second thereafter. However, caution must be exercised when these slip factors are applied. A discontinuity will be introduced in the void fraction profile when different slip factors are used. This is due to the sudden change in vapor implied by the model at the point of slip factor change.

The third two-phase multiplier and void correlation which can be selected for use in WABCORE is the Armad-Treschev model

$$TPM = (1 - x)^{1.75}/(1 - \alpha)^{1.2}$$

$$\alpha = \left(.833 + .05\ \ell n\ \frac{\beta}{14.22}\right)\beta \qquad (2.33)$$

$$\beta = \frac{\rho_f x}{\rho_g(1 - x) + \rho_f x} \quad .$$

This correlation is considered the most reliable in the bulk boiling region and is highly recommended[4].

2.9.3 Quality

WABCORE does not calculate any negative qualities. Bowring's relationship

$$x(z^*) = \frac{C_p \eta q''}{G_i h_{fg} \varepsilon \nu_f} \tag{2.34}$$

is used to calculate quality at the thermal equilibrium point. A straight line is then calculated through the coordinates $[x(x^*), Z^*]$ and $[0, Z_{FDB}]$. This line is then used to represent quality as a function of distance between these points as shown in Figure 2.9. This is again a calculational simplification which presumably results in a loss of accuracy. For the purpose of this code however, the loss is considered justified by the gain of computational time.

2.10 Bulk Boiling Region

In the bulk boiling region, the same two-phase multiplier and void fraction correlations are applied as in the subcooled boiling region (Section 2.9.2). A second slip factor is used in this region.

The quality calculated from the straight line approximation continues into the bulk boiling region to the thermal

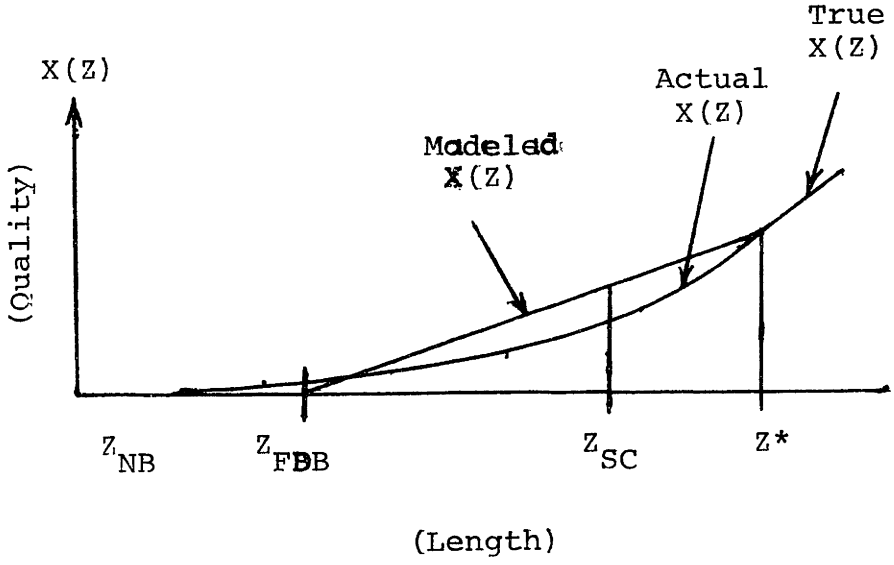

Figure 2.9

Illustration of Quality Model
Compared to Physical Reality

equilibrium point. Once this point is reached quality is calculated by

$$x(z) = \frac{4q''}{D_{ei} G_i h_{fg}} (z_2 - z_1) \qquad (2.35)$$

for each node length to the end of the channel. This computation will continue in all cases no matter what value the heat flux assumes and no vapor condensation calculations are made if the heat flux should suddenly drop to zero or any other very small value.

The Chen correlation for calculation of the clad wall heat transfer coefficient is applied in this region. It can readily be used in the subcooled boiling region but it is a time consumming computation. The increased accuracy nevertheless is considered to justify the increased computational time in the bulk boiling region.

Because Chen is not applied in the subcooled boiling region, the resulting peak wall temperature will be over predicted in this region.

2.11 Solution Logic

2.11.1 Initial Conditions

The preceeding correlations and models are solved in WABCORE using the following initial conditions:

- Inlet temperature

- Inlet mass flow, which is assumed constant
- Total power output
- Coolant inlet pressure .

There are no outlet conditions specified except that implied with the use of inlet mass flow and total power. Mainly,

$$h_o = h_i + q/w \quad .$$

Each outlet condition is tied directly or indirectly to the inlet conditions, but only one or two of the inlet conditions will cause a charge of a specific outlet condition. As a result of this, the outlet conditions can be changed predictably using inlet conditions after running the first case. This will be seen more clearly in Chapter 4.

The temperature, pressure and enthalpy equations are solved at each axial node in the following order in WABCORE

START, i = 0

1) $H_{(i+1)}$ $i \neq 1$

2) $T_{F(i+1)}$ $i \neq 1$

3) $h_{(i+1)}$

4) $T_{c(i+1)}$

5) $T_{fs(i+1)}$

6) $T_{cL(i+1)}$

7) $\delta P_{f(i+1)}$ $i \neq 1$

8) $\delta P_{SPACER(i+1)}$ $i \neq 1$

9) $\delta P_{ACC(i+1)}$ $i \neq 1$.

The clad, fuel surface and centerline temperatures are solved for at the first axial node of the channel. This is thought to lead to better results than from starting with the second axial node such as COBRA IIIc/MIT does.

2.11.2 Input Logic

WABCORE is capable of accepting two forms of geometrical input conditions. The first of these are spacific input conditions for the single subchannel (i.e., flow area, rod diameter, etc.) which are used directly by the code and are not discussed further at this point.

The second option provides input information on an entire reactor core. This is added to aid the user with design problems of a nature concerning general core changes. WABCORE will accept this information and reduce it to single channel data for its analysis. This option is normally not available on subchannel codes and will be further explained in the remaining paragraphs of this section.

A rod diameter relationship using available input data

can be derived from

$$q = \bar{q}''\pi d_R L\, N_{eff} \quad . \tag{2.36}$$

The single channel cells are assumed to be equally distributed throughout the core area. Therefore,

$$N_{eff} = \frac{A_c}{p^2} \quad . \tag{2.37}$$

Combining Equations (2.36) and (2.37) and multiplying by d_R^2 ;

$$qd_R^2 = \bar{q}''\pi d_R L\, A_c \Big/ \left(\frac{p}{d_R}\right)^2 \quad .$$

Therefore,

$$d_R = \frac{\bar{q}''\pi L\, A_c}{q\left(\frac{p}{d_R}\right)^2} \quad . \tag{2.38}$$

The code then calculates subchannel geometry parameters (i.e., D_{ei}, G_i, A_{cif}) using the effective number of fuel rods to reduce the data to single channel data.

Wire wraps can be chosen with hexagonal or square pitch geometries. The wire diameter is used in the geometry calculations to determine the flow area and hydraulic diameter of the channel. The pressure loss caused by the wire wrap is then included in the friction and acceration losses

calculated using the adjusted geometry. The wire diameter is determined by

$$d_s = P - d_R \quad .$$

In reality, this is not strictly true, because of small gaps existing between the rod and spacer wire. The error caused by this approximation is considered small enough to justify the calculational simplification.

2.11.3 Flow Chart

The logic used in WABCORE is illustrated in the flow chart shown in Figure 2.10. The brackets on the figure enclose:

A) Two forms of input conditions that are possible with the code. (1) Conditions for the full reactor core, which are reduced by the code to represent a single channel and rod. (2) Conditions for the single channel and rod.

B) Calculations of thermal-hydraulic results at each axial step up to the end of the channel or until thermal equilibrium is reached ($L_{EQ.}$) .

C) Calculation of quality and two-phase pressure drop multiplier at each axial location from the point of fully developed boilign (L_{FDB}), to the point of subcooled boiling (L_{sc}).

Figure 2.10

WABCORE Flowchart

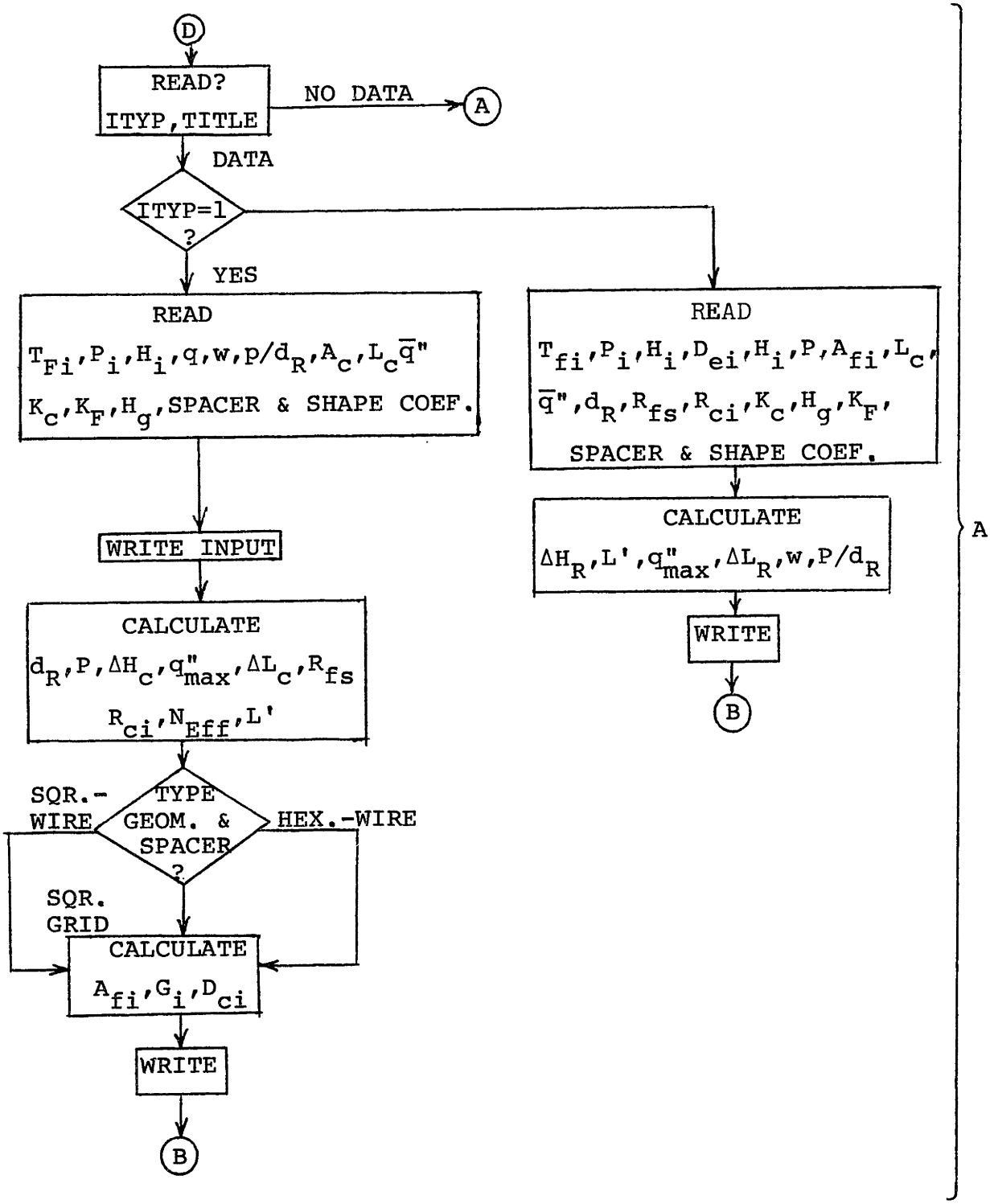

Figure 2.10 (Cont.)

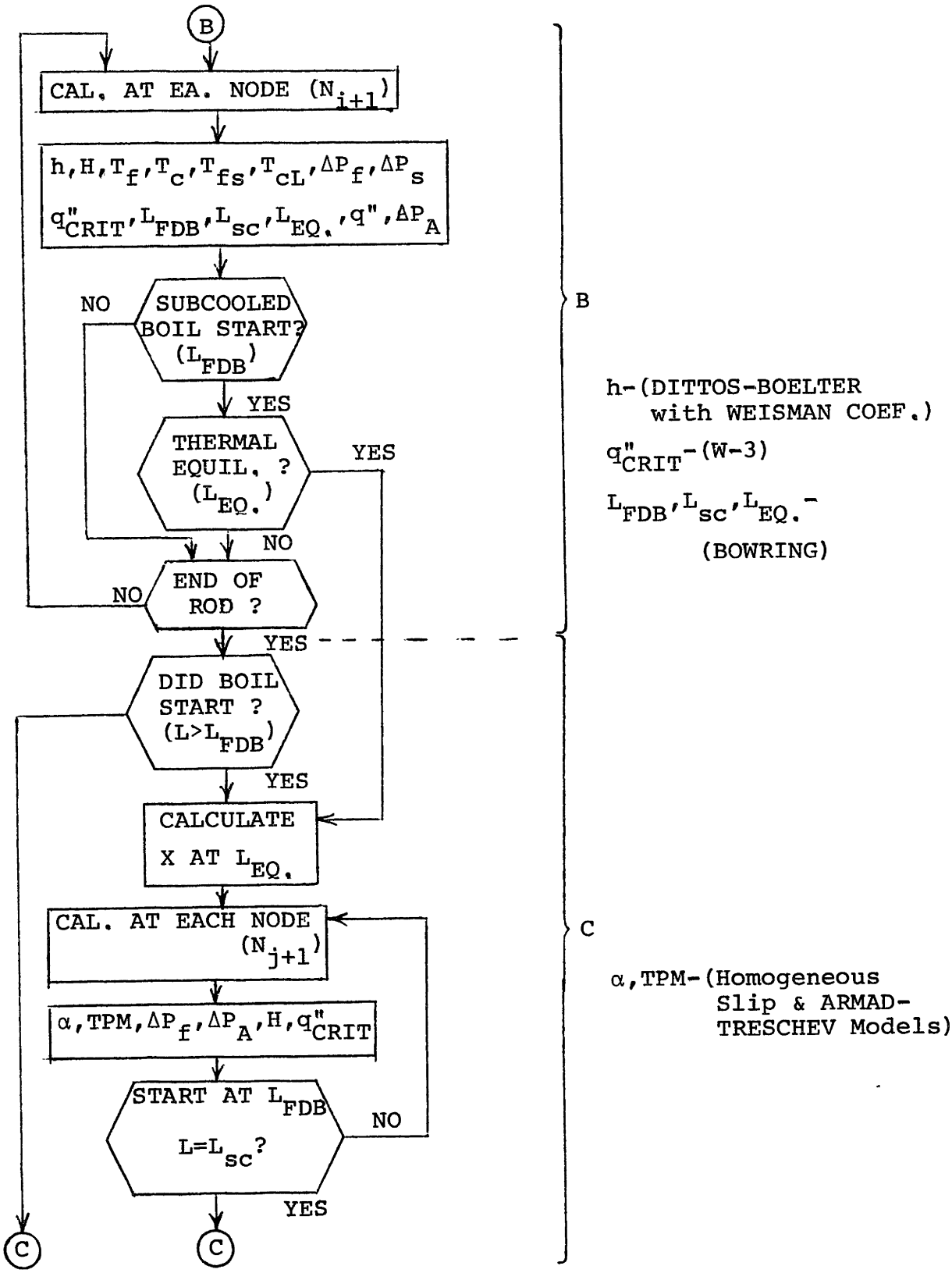

Figure 2.10 (Cont.)

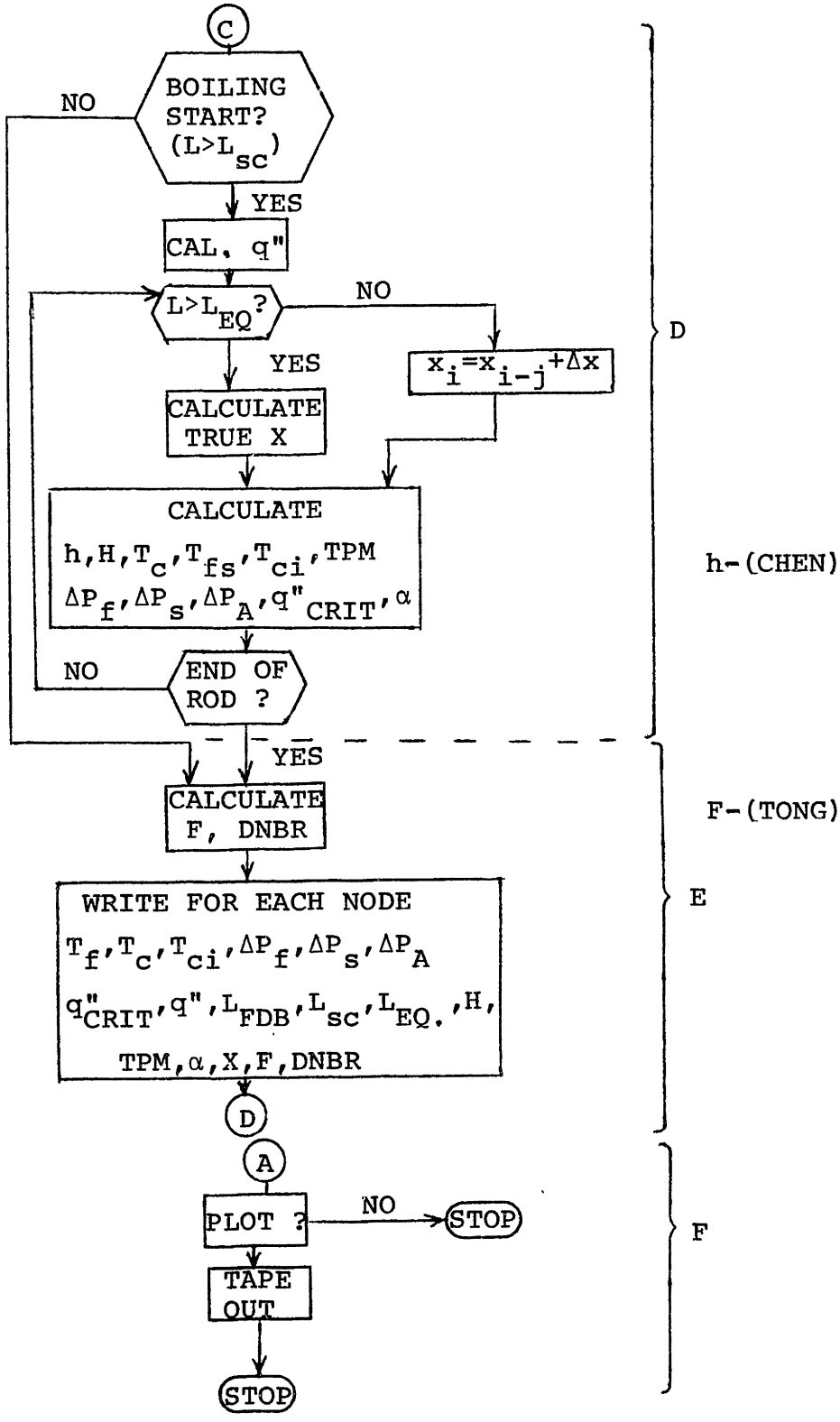

D) Calculation of all thermal-hydraulic results for each axial location from the point of subcooled boiling (L_{sc}), to the end of the channel. Calculation of the subcooled boiling quality is explained in Chapter 3.

E) Calculation of heat flux shape correction factor (F), DNBR, and printing of all results at each axial location.

F) Plotter output: At the Laboratory of Nuclear Science facility (LNS), figure plottings are recorded on magnetic tape which are in turn, displayed by the user on a Calcomp unit (Appendix A).

2.12 Correlation Limitation Summary

The correlations used in WABCORE and their ranges of applicability as reported in the literature are listed in Table 2.1. These limits are also the limits of WABCORE. The first seven entries in Table 2.1 are water property correlations used in WABCORE, whereas the remaining entries are associated with the various correlations used in the code.

Table 2.1

Correlation Limitation Summary

Correlation	Limitation
1-Saturation Temperature	P > 450, PSI
2-Liquid Density	P > 450, PSI, 450° $\leq$ T $\leq$ 650°F
3-Liquid Enthalpy	P > 265, PSI
4-Vapor Density	P > 450, PSI
5-Vapor Enthalpy	P > 450, PSI
6-Steam Viscosity	405 $\leq$ P $\leq$ 2250, PSI
7-Saturation Pressure	Triple point $\leq$ T $\leq$ Critical point
8-B_c (Equation 3.10A)	$1.1 \leq \frac{P}{d_b} \leq 1.35$ Square lattice
	$1.1 \leq \frac{P}{d_i} \leq 3.5$ Triangular lattice
9-$q''_{DNB,U}$ (Equation 3.15)	1000 $\leq$ P $\leq$ 23-0, PSI
	- .15 $\leq$ X $\leq$ 15
	D_e = .2 - .7 in
	$\frac{6}{10^6}$ = 1 - 5 lb/he ft^2
10-F (Equation 3.16)	SAME
11-Homogeneous TPM (Equation 3.20)	Only high flow regimes
12-Timed-Trechev TPM (Equation 3.21)	150 $\leq$ r $\leq$ 2700, PSI
	$\beta \leq .9$ (Equation 2.33)

CHAPTER III

COMPARISON OF WABCORE WITH THE MULTISUBCHANNEL CODE COBRA-IIIC/MIT

The validity of the results as obtained by WABCORE as a reliable thermal-hydraulic tool will be established by testing these results against those results computed by COBRA IIIC/MIT. The range of these test cases will include two axial heat flux distributions (i.e., flat, cosine), as well as PWR and BWR operational conditions. Naturally, all results are steady-state results.

The two reactors chosen for this test were the Main Yankee PWR and the Shoreham BWR. Due to the availability of the Preliminary Safety Analysis Reports (PSAR) on both reactors, results will also be presented from these reports where applicable.

The major design parameters for the Main Yankee reactor are shown in Table 3.1. These parameters were used as input to both codes and held constant for the different axial heat flux shapes. Results of these calculations are shown in Tables 3.2 and 3.3.

Note that there is very good agreement between all parameters of both Main Yankee cases except for the centerline temperature and the MDNBR. As pointed out in Chapter 2, because the rod gap region is treated separately in WABCORE,

Table 3.1

Main Yankee Core Nominal Design Parameters

Fuel Rod Array, square	14 x 14
Fuel Rod Pitch, inches	.58
Spacer Grids	
Number of Spacer Types	2
Number Per Assembly	8
Pellet Diameter, inches	.3795
Pellet Density, lb/ft^3	650
Number of Fuel Types	1
Fuel Thermal Conductivity, BTU/hr ft°F	1.4
Fuel Specific Heat, BTU/lb°F	.08
Clad Thickness, inches	.024 nominal
Clad Density, lb/ft^3	410
Clad Thermal Conductivity, BUT/hr ft°F	8.8
Clad Specific Heat, BTU/lb°F	.0780
Fuel to Clad H.T. Coefficient, BTU/hr ft^2°F	600
Core Cross-Sectional Area, ft^2	94.37
Core Power, BTU/hr	8.995×10^9
Active Core Length,ft	11.392
Avg. Heat Flux, BTU/hr ft^2	1.695×10^5
Hydraulic Diameter, ft	.0444
Wetted Perimeter, ft	.1151
Inlet Conditions	
Core Mass Flow, lbm/hr	1.316×10^8
Mass Flux, lbm/hr ft^2	2.545×10^6
Temperature, °F	541
Pressure, PSI	2100
Enthalpy, BTU/lbm	537.6

Figure 3.2

Main Yankee Core Results
With Cosine-Heat Flux Distribution

(British Engineering Units)

	WABCORE	COBRA IIIC/MIT	PSAR
Outlet Liquid Temp.	592.7	592.5	
Outlet Clad Temp.	602.1	609.5	
Inlet Clad Temp.	550.7	559.0[2]	
Outlet Centerline Temp.	1421.5	1400.1	
Peak Centerline Temp.	2820.9	2449.1	
Inlet Centerline Temp.	1370.1	1349.3	
Pressure Drop	13.1	12.35	
Outlet Enthalpy	605.9	606.4	
MDNBR	6.06	7.30[1]	2.4 (Hot CHN.)) ~ 7.2 (Nominal)

1 - W-3 CHF Correlation
2 - Taken from second node from channel inlet.

Figure 3.3

Main Yankee Core Results
With Flat Heat Flux Distribution

(British Engineering Units)

	WABCORE	COBRA IIIC/MIT	PSAR
Outlet Fluid Temp.	592.7	592.5	
Outlet Clad Temp.	613.1	624.1	
Inlet Clad Temp.	562.3	575.0[2]	
Outlet Centerline Temp.	2396.5	2099.0	
Inlet Centerline Temp.	2364.9	2066.7	
Pressure Drop	13.1	12.4	
Outlet Enthalpy	605.9	606.4	
MDNBR	7.35	7.85[1]	2.4 (Hot CHN.) 7.2 (Nominal)

1 - W-3 CHF Correlation

2 - Taken from second node from channel inlet.

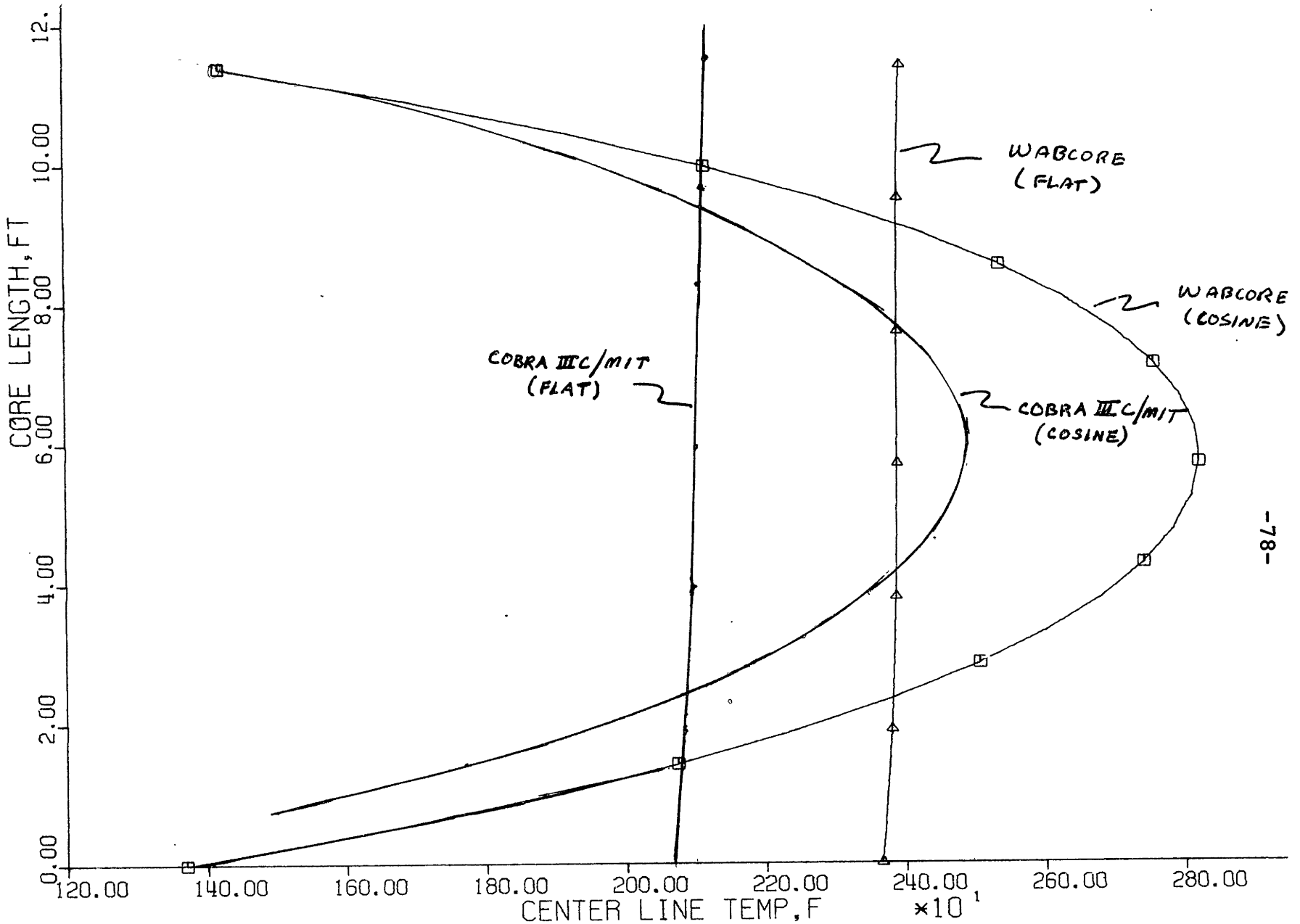

FIGURE 3.1, MAIN YANKEE CENTER LINE TEMP. DISTRIBUTION

a conservative centerline temperature is obtained. On the other hand, COBRA IIIC/MIT lumps the clad and gap region into one resistance and solves for the fule surface temperature.

$$\frac{1}{h_g'} = \frac{1}{h_g} + \frac{T_{co}}{k_f} \quad .$$

It is not known how accurate this relationship is or whether it even produces a conservative result as compared to experiments.

The descrepancy in MDNBR value is due to the COBRA IIIC/MIT code not applying the shape correction factor (F) in the single phase region. This correction factor however, results in conservative values for DNBR obtained from WABCORE.

The Shoreham BWR design parameters are shown in Table 3.4. These parameters were again used as input for both the flat and cosine heat flux shapes and the calculated results are illustrated in Tables 3.5 and 3.6.

Good agreement is again achieved between the two codes except for the centerline temperature and MDNBR values. The centerline temperature deviation is again due to the model solution technique, and the consistant conservatism of WABCORE is seen in the plots of Figure 3.2.

Table 3.4

Shoreham Core Nominal Design Parameters

Fuel Rod Array, square	7 x 7
Fuel Rod Pitch, inches	.738
Spacer Grids	
Number of spacer types	2
Number per assembly	8
Pellet Diameter, inches	.487
Pellet Density, lb/ft^3	650
Number of Fuel Types	1
Fuel Thermal Conductivity, BTU/hr ft°F	1.4
Fuel Specific Heat, BTU/lb °F	.08
Clad Thickness, inches	.032
Clad Density, lb/ft^3	410
Clad Thermal Conductivity, BTU/hr ft°F	8.8
Clad Specific Heat, BTU/lb °F	.078
Fuel to Clad HT Coefficient, BTU/hr ft^2°F	600
Core Cross-Sectional Area, ft^2	108.2
Core Power, BTU/hr	8.331×10^9
Active Core Length, ft	12.0
Average Heat Flux, BTU/hr ft^2	1.647×10^5
Hydraulic Diameter, ft	.05577
Wetted Perimeter, ft	.1474
Inlet Conditions	
Core Mass Flow, lbm/hr	7.55×10^7
Mass Flux, lbm/hr ft^2	1.285×10^6
Temperature, °F	525.0
Pressure, PSI	1005.0
Enthalpy, BTU/lbm	518.1

Table 3.5

Shoreham Core Results With
Flat Heat Flux Distribution

(British Engineering Units)

	WABCORE	COBRA IIIC/MIT	PSAR
Outlet Fluid Temp.	544.3	545.2	
Outlet Clad Temp.	564.8	577.9	
Inlet Clad Temp.	563.1	558.0	
Outlet Centerline Temp.	2563.0	2411.0	
Peak Centerline Temp.	2608.8	2436.0	
Inlet Centerline Temp.	2582.8	2412.0	
Pressure Drop	8.7[2] 4.8[3,4]	8.2[2] 7.5[5]	
Outlet Enthalpy	6627.5	628.3	
MDNBR	7.74	4.07[1] 4.0[6]	1.9 (Hot CHN.) ∿ 6 (Nominal)
Outlet Quality	.131	.131	.141 (AVG)
Outlet Void Frac.	.758[2] .536[3] .520[4]	.755[2] .646[5]	.431 (AVG) .768 (MAX)

1 - W-3 CHF correlation

2 - Homogeneous model with Slip 1 = 1 and Slip 2 = 1

3 - Homogeneous model with Slip 1 = 1 and Slip 2 = 2.7

4 - Armad-Trechev model

5 - Modified Armad model

6 - B&W CHF correlation

Table 3.6

Shoreham Core Results With
Cosine Heat Flux Distribution

(British Engienering Units)

	WABCORE	COBRA IIIC/MIT	PSAR
Outlet Fluid Temp.	544.2	545.2	
Outlet Clad Temp.	554.8	562.7	
Inlet Clad Temp.	542.3	542.5	
Outlet Centerline Temp.	1472.9	1545.4	
Peak Centerline Temp.	3067.9	2872.9	
Inlet Centerline Temp.	1460.4	1524.7	
Pressure Drop	9.0[2] 4.9[3,4]	8.2[2] 7.5[5]	
Outlet Enthalpy	628.2	628.3	
MDNBR	6.35	4.0[1] 4.2[6]	1.9 (Hot CHN.) ∿ 6 (Nominal)
Outlet Quality	.133	.131	.141 (AVG)
Outlet Void Frac.	.760[2] .538[3] .521[4]	.755[2] .646[5]	.431 (AVG) .768 (MAX)

1 - W-3 CHF correlation

2 - Homogeneous model with Slip 1 = 1 and Slip 2 = 1

3 - Homogeneous model with Slip 1 = 1 and Slip 2 = 2.7

4 - Armad-Trechev model

5 - Modified Armad model

6 - B&W CHF correlation

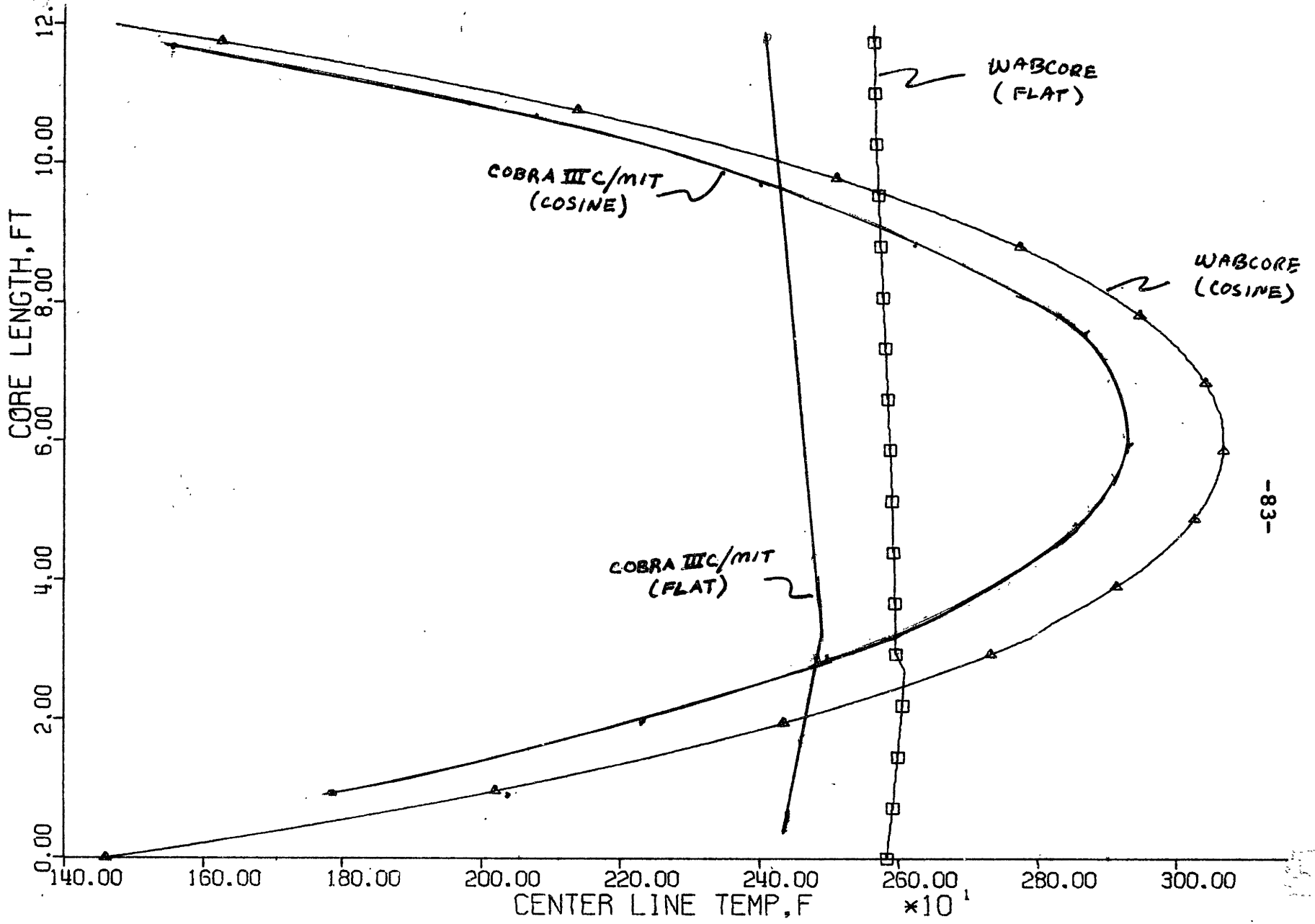

FIGURE 3.2, SHOREHAM CENTER LINE TEMP. DISTRIBUTION

The sudden change in centerline temperature by the WABCORE calculation is caused the application of the Chen heat transfer coefficient in the two-phase region. This results in good agreement with predicted results, however, because WABCORE is a single pass code, the proper two-phase heat transfer coefficient is not applied until the end of subcooled boiling. Application at this point results in a small error in the subcooled boiling region clad temperature from using the single-phase heat transfer coefficient. The Chen heat transfer coefficient should be applied at the beginning of the subcooled boiling region to eliminate this error.

COBRA IIIC/MIT does calculate the DNB ratio in the bulk boiling region with the shape correction factor included. However, the correlation used for this calculation, could not be found in the literature and is obviously not the original as recommended by Tong or B&W. As a result of this, no real conclusions could be drawn about the differences of the MDNB ratios. It should be pointed out that the MDNBR is calculated to occur at the axial center of the channel by WABCORE whereas, it occured close to the outlet of the channel as determined by COBRA IIIC/MIT.

In nonuniform heat flux experiments there are usually several CHF indications along the channel length between

the heat flux peak and exit. The value used for computation is the one located farthest upstream or nearest the peak of the flux shape[6]. This would lead one to believe that both calculations of DNBR could have merit, however, which result is the most accurate is not known for sure.

The effect upon quality by modeling vapor production as a linear phenomenon from the point of fully developed boiling to the point of thermodynamic equilibrium is illustrated in Figure 3.3. This approximation appears to give a better prediction of quality in the subcooled boiling region as compared to COBRA IIIC/MIT. This is due to the linear approximation of vapor production in the subcooled boiling region. The axial variation of the void fraction for several two-phase models is illustrated in Figure 3.4.

FIGURE 3.3

VAPOR AXIAL DISTRIBUTION

SHOREHAM CORE

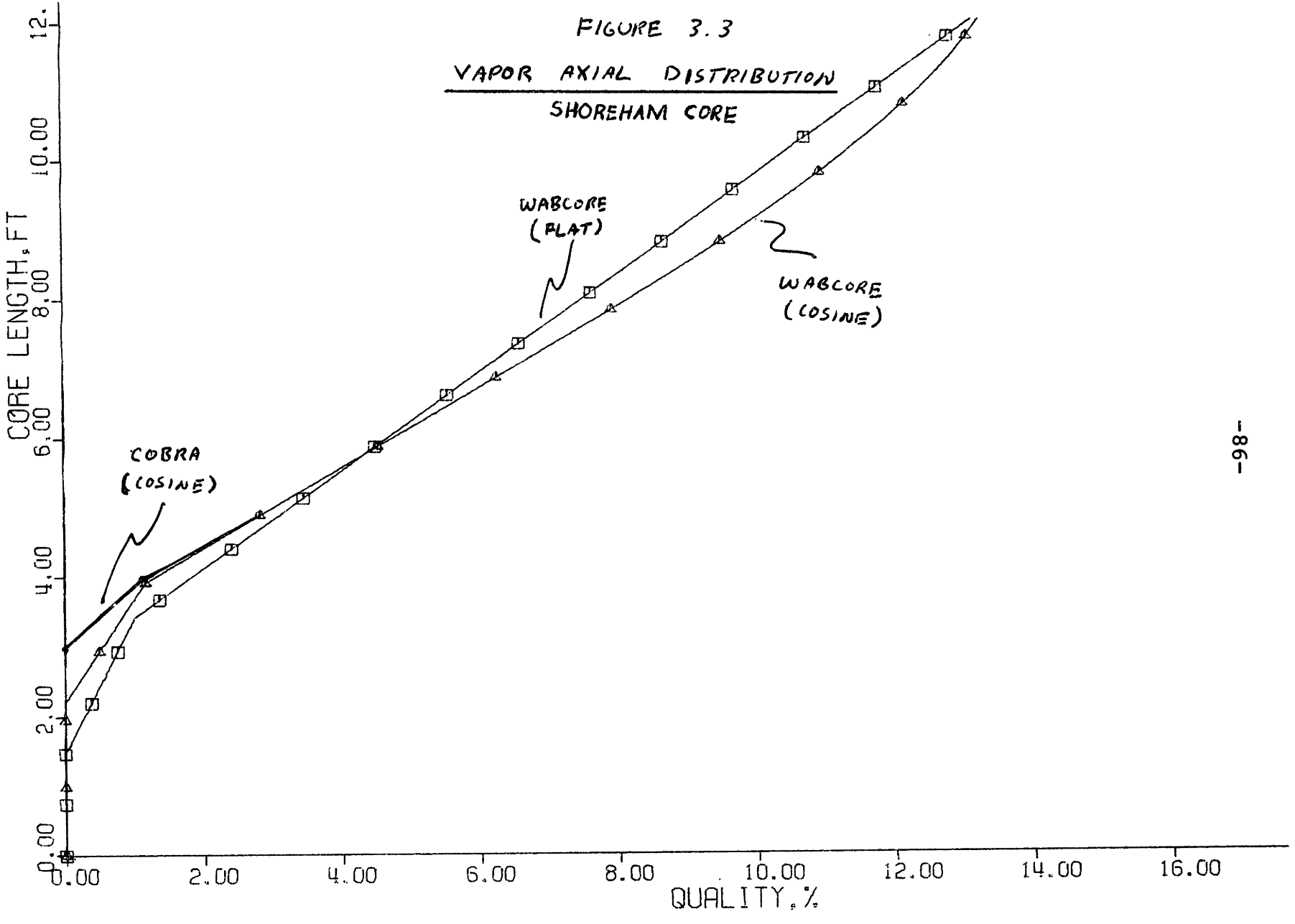

Figure 3.4

Different Void Distributions With Flat Heat Flux Distribution Shoreham Reactor

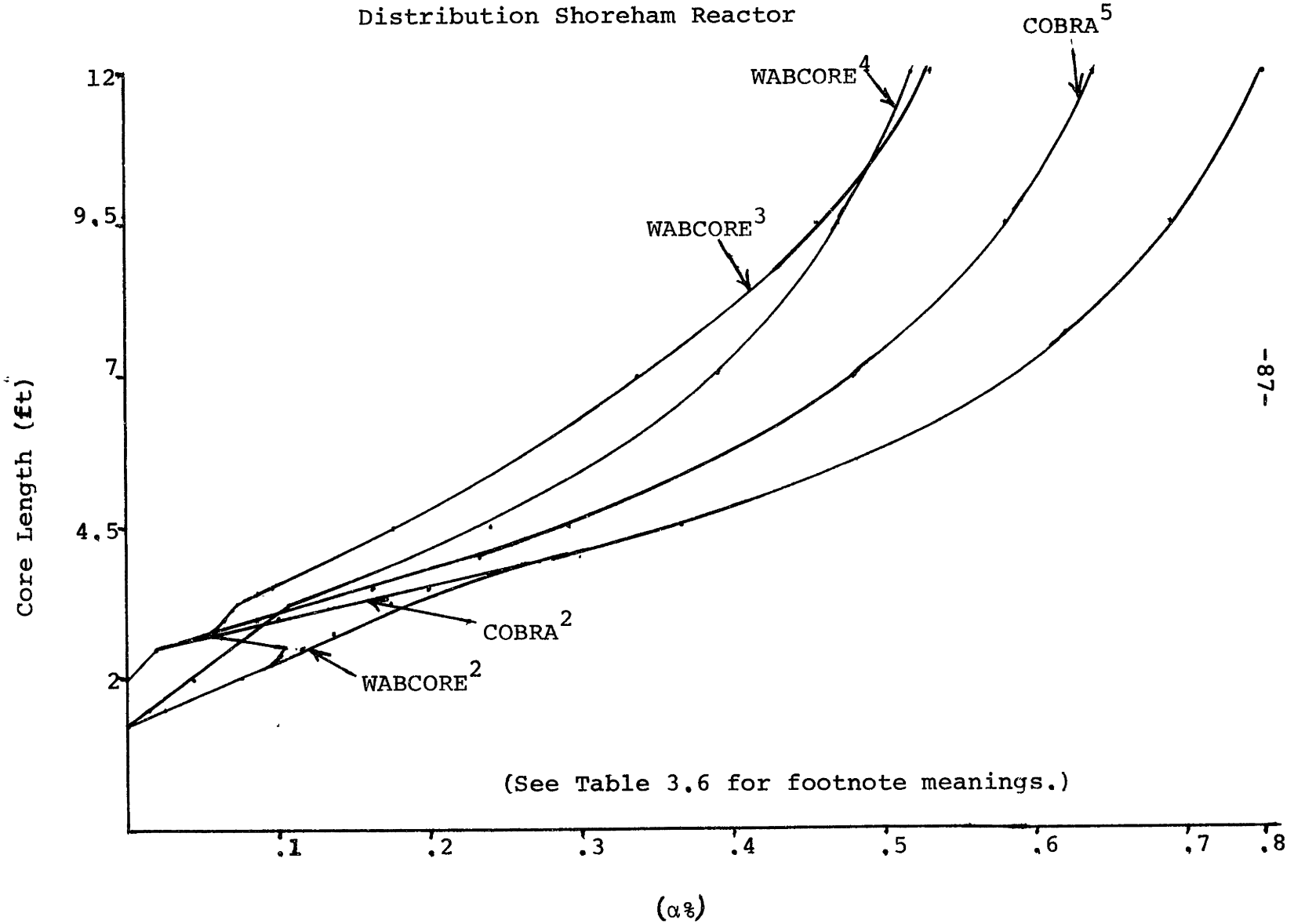

(See Table 3.6 for footnote meanings.)

CHAPTER IV

RESULTS AND DISCUSSION OF THE SENSITIVITY STUDY

The objectives of this sensitivity study is to first answer the four questions put forth in Chapter I and second, to define a range of themal-hydraulic reactor parameters applicable to tight pitch lattice designs. The Main Yankee reactor is used as the base case in this study. Reactor parameters for this particular core are illustrated in Table 3.1 of Chapter III.

4.1 Reactor Core Constraints

Due to the desire to maintain as many of the present reactor characteristics as possible while using at the same time, a core with a tighter pitch, the following initial constraints were established in order to use the same reactor system components (i.e., pressure vessel, pumps, etc.),

- Maintain initial core cross-sectional area (A_c)
- Maintain initial enthalpy rise (δh)
- Maintain initial coolant outlet temperature (T_{Fo})
- Maintain initial core power (q)
- Maintain initial coolant mass flow (w).

To bound the results of the sensitivity study, the two following general constraints will be used,

- Engineering thermal-hydraulic limitations as used

in today's LWR designs) and

- Safety limitations as used in present day LWR design .

Economic constraints will not be used directly in the study. Neglecting this impact, however, is not expected to invalidate the results of the sensitivity study because of the many constraints established in view of an already existant reactor system. It should be understood that if this were not the case and the reactor system (i.e., pressure vessel, pumps, etc.) was nonexistant, then a sensitivity study of reactor characteristics would require economic constraints for a complete study.

The economic implications imposed by the results of the sensitivity study, as far as they are known at this point in time, will be presented in the final section of this chapter.

4.2 Sensitivity Study Approach

The approach used in this study as believed to lead to an orderly and systematic representation of possible core design changes and results due to these changes. This sensitivity study approach includes the effects of changing the following parameters in the following order:

1. A Reference (i.e., initial reactor characteristics held constant) case study of the effect of several axial heat flux profiles to determine the sensitivity of coolant and centerline temperature, system pressure loss, DNBR, and

enthalpy rise.

2. Variation of linear heat rate to study the effect of core length on DNBR and channel pressure loss.

3. Variation of rod pitch for each linear heat rate to observe the effects on DNBR and channel pressure loss.

4. Variation of rod diameter for each pitch to study the same effects.

4.3 Results

To examine the effects of the heat flux shape profiles, five different flux shapes were used with all other Main Yankee reactor parameters held constant. These shapes included a lower bump, cosine, flat, and two saddle type profiles (Figure 4.1).

The results indicated that there is no dependence of flux shape on core pressure loss and very little effect on coolant temperature and enthalpy rise. The changes in the centerline temperature (Figure 4.2) and DNBR (Figure 4.3) were, however, directly dependent on heat flux shape. Figure 4.3 indicates that the lowest DNBR is approximately 5.5 corresponding to the lower bump flux profile with $q' = 5.7$ KW/ft . This factor is established as a lower DNBR limit, and the additional constraint resulting from this is,

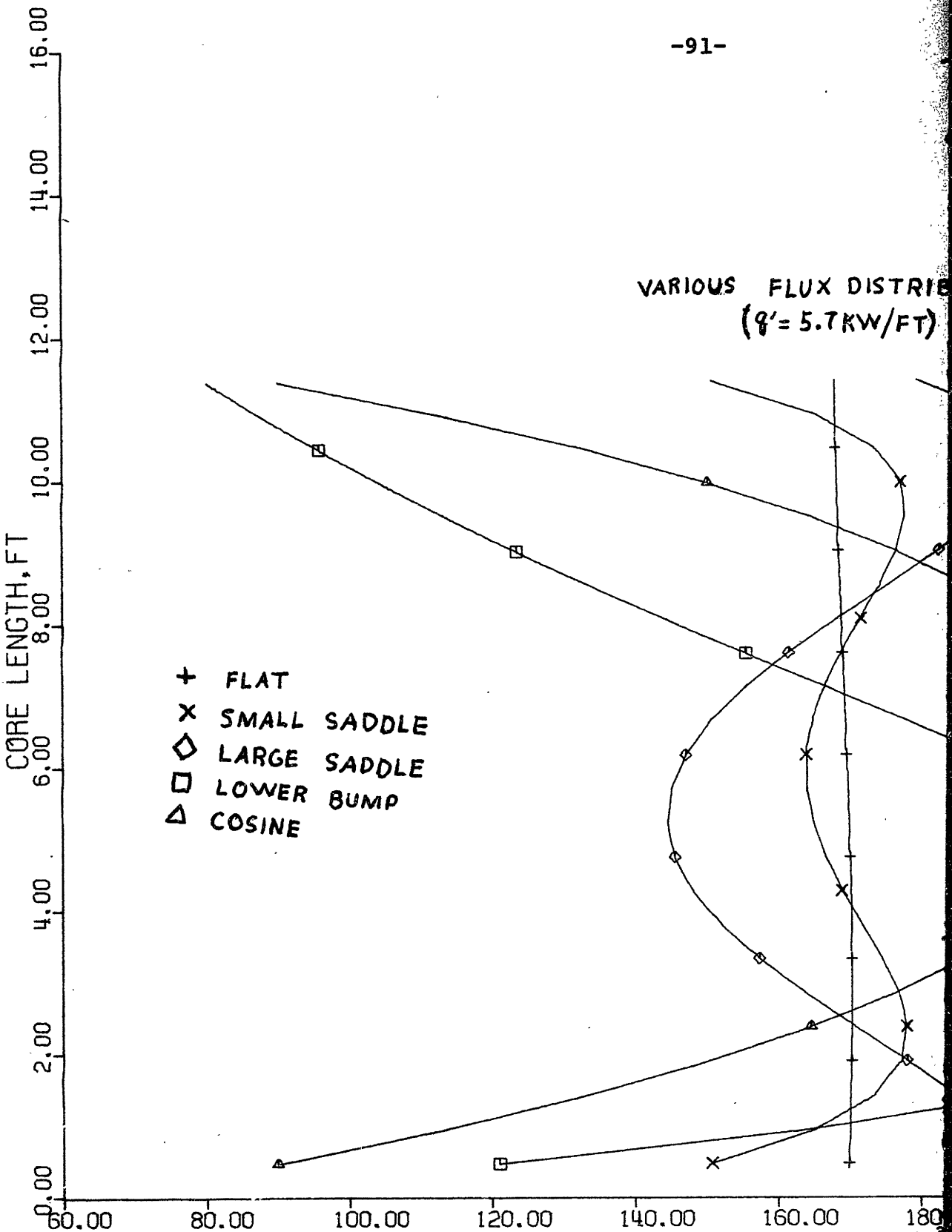
VARIOUS FLUX DISTRIE
(q'= 5.7KW/FT)
CORE LENGTH, FT
0.00
2.00
4.00
6.00
8.00
10.00
12.00
14.00
16.00
+ FLAT
× SMALL SADDLE
◇ LARGE SADDLE
□ LOWER BUMP
△ COSINE
60.00
80.00
100.00
120.00
140.00
160.00
180
FLUX, BTU/SQFT
*10

FIGURE 4.1

VARIOUS FLUX DISTRIBUTIONS
($q' = 5.7$ KW/FT)

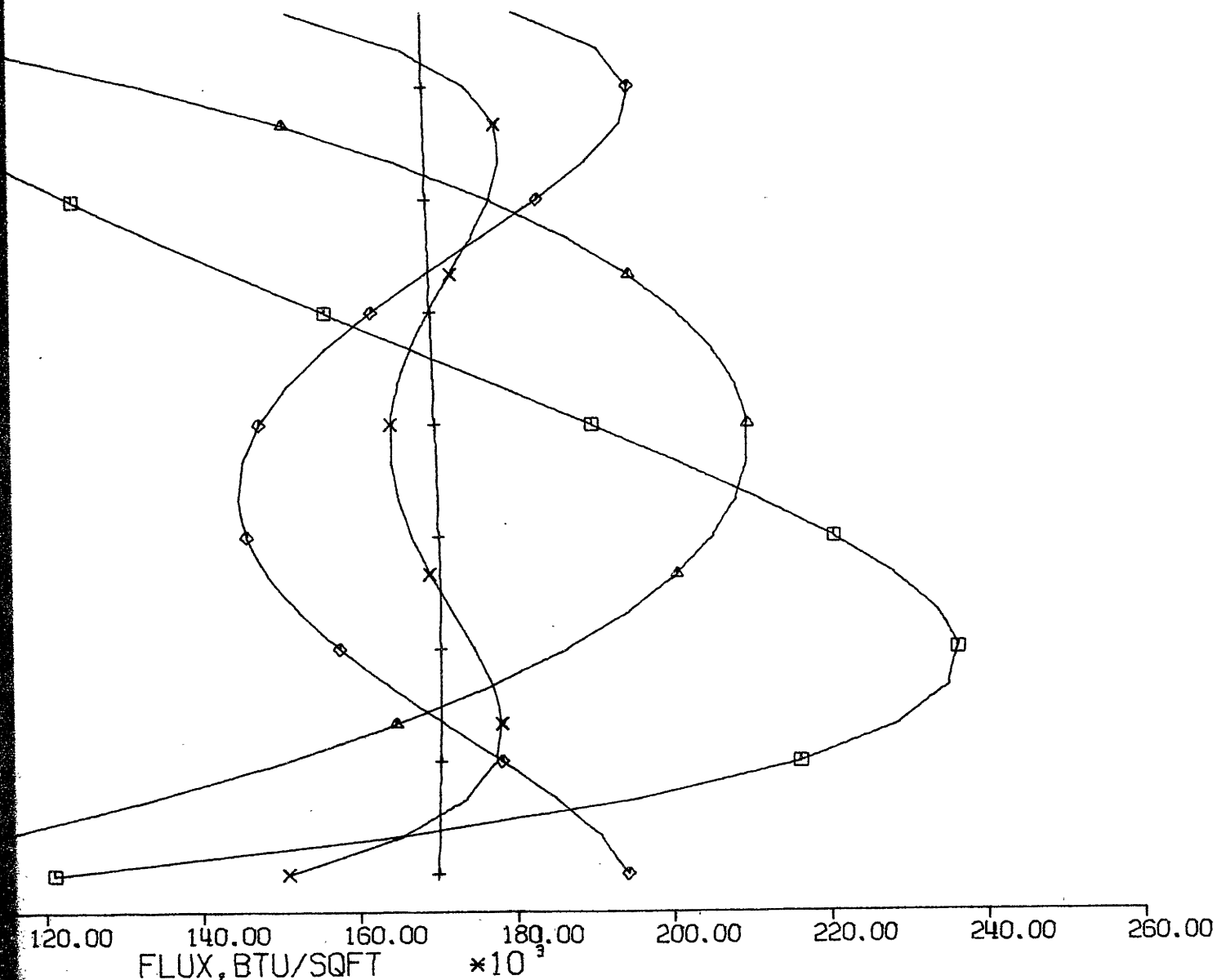

FIGURE 4.1

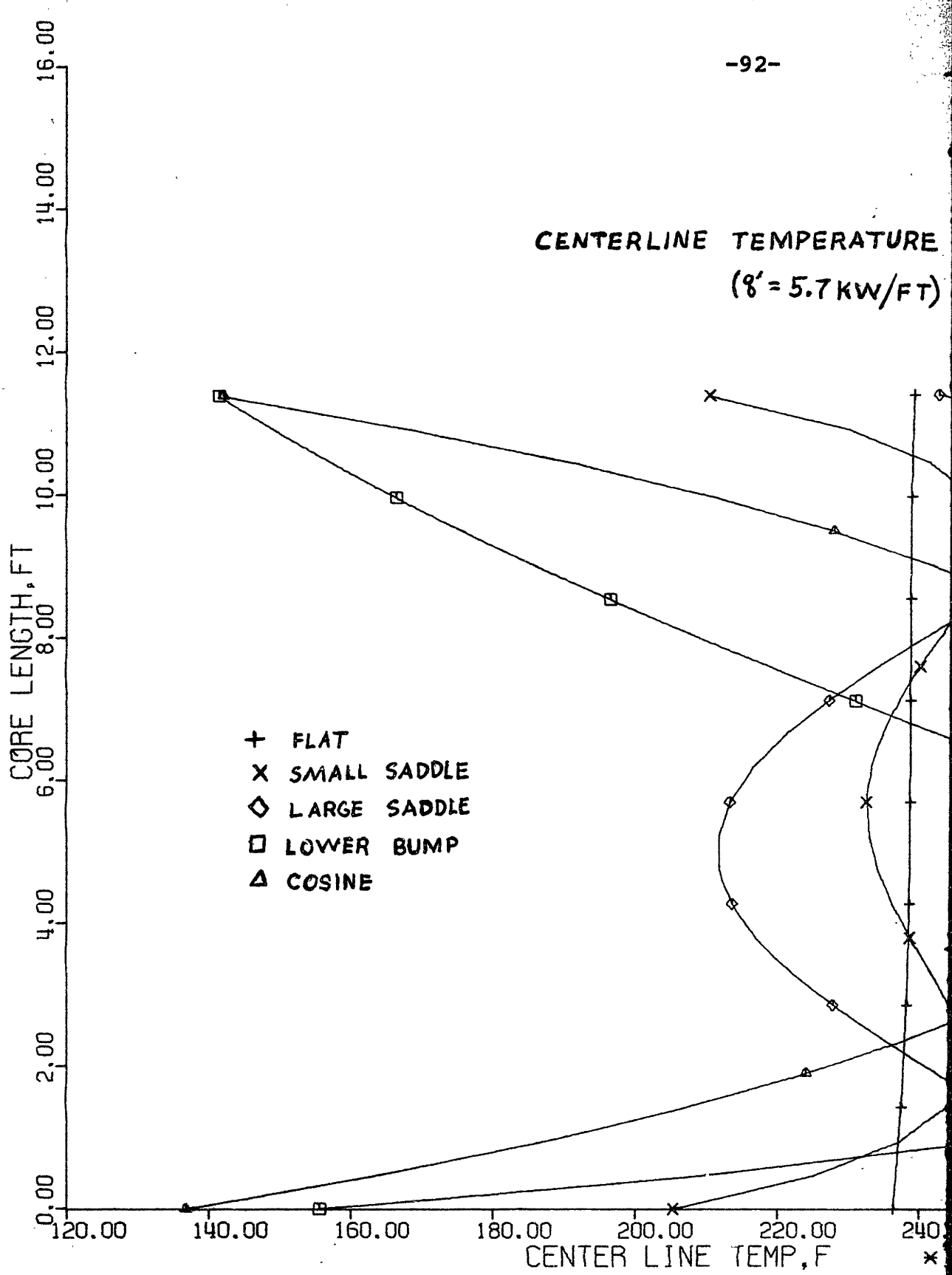
CENTERLINE TEMPERATURE
(q' = 5.7 KW/FT)
CORE LENGTH, FT
0.00
2.00
4.00
6.00
8.00
10.00
12.00
14.00
16.00
120.00
140.00
160.00
180.00
200.00
220.00
240
CENTER LINE TEMP, F
+ FLAT
X SMALL SADDLE
◇ LARGE SADDLE
□ LOWER BUMP
Δ COSINE

FIGURE 4.2

NTERLINE TEMPERATURE DISTRIBUTION
(q' = 5.7 KW/FT)

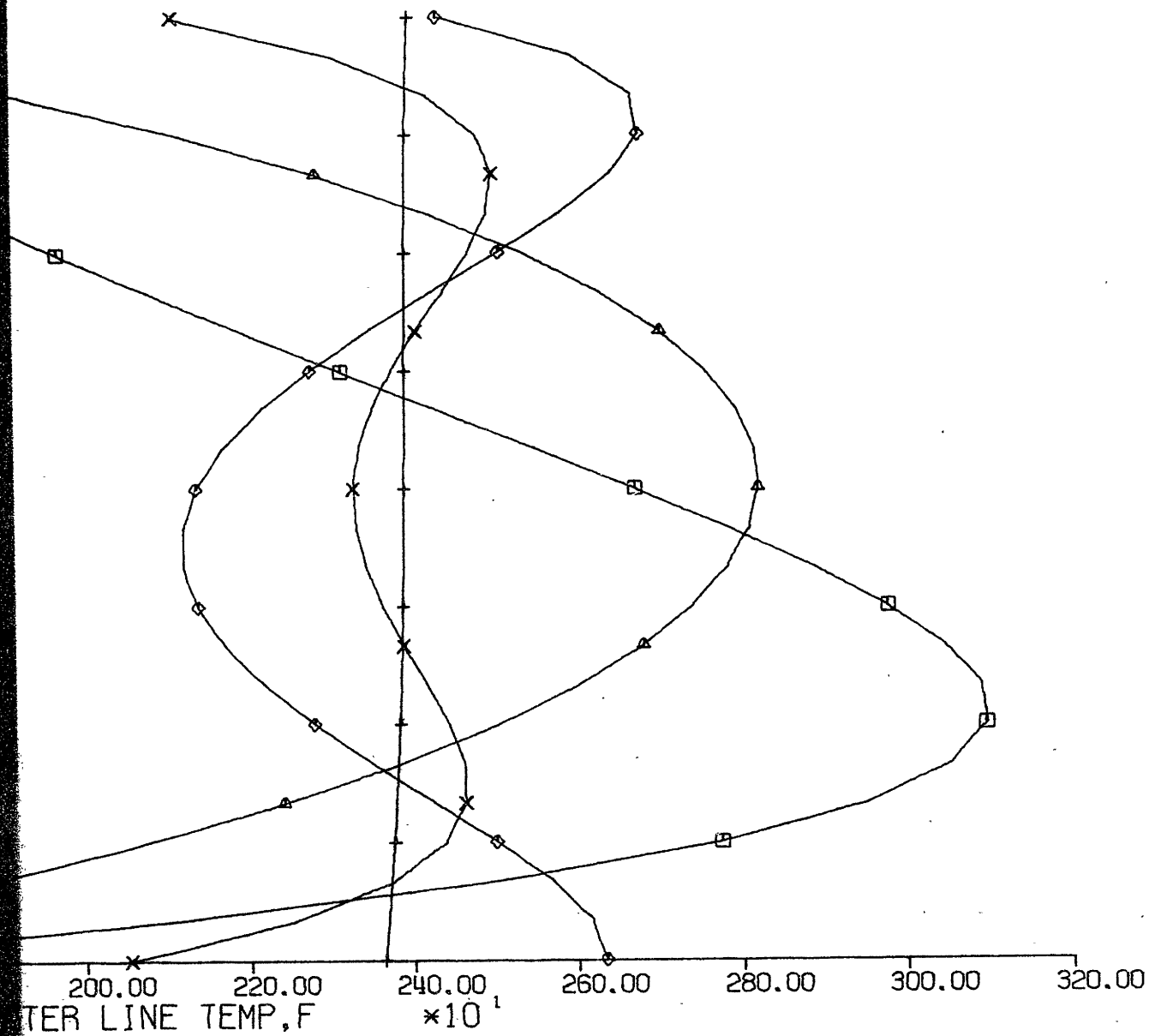

FIGURE 4.2

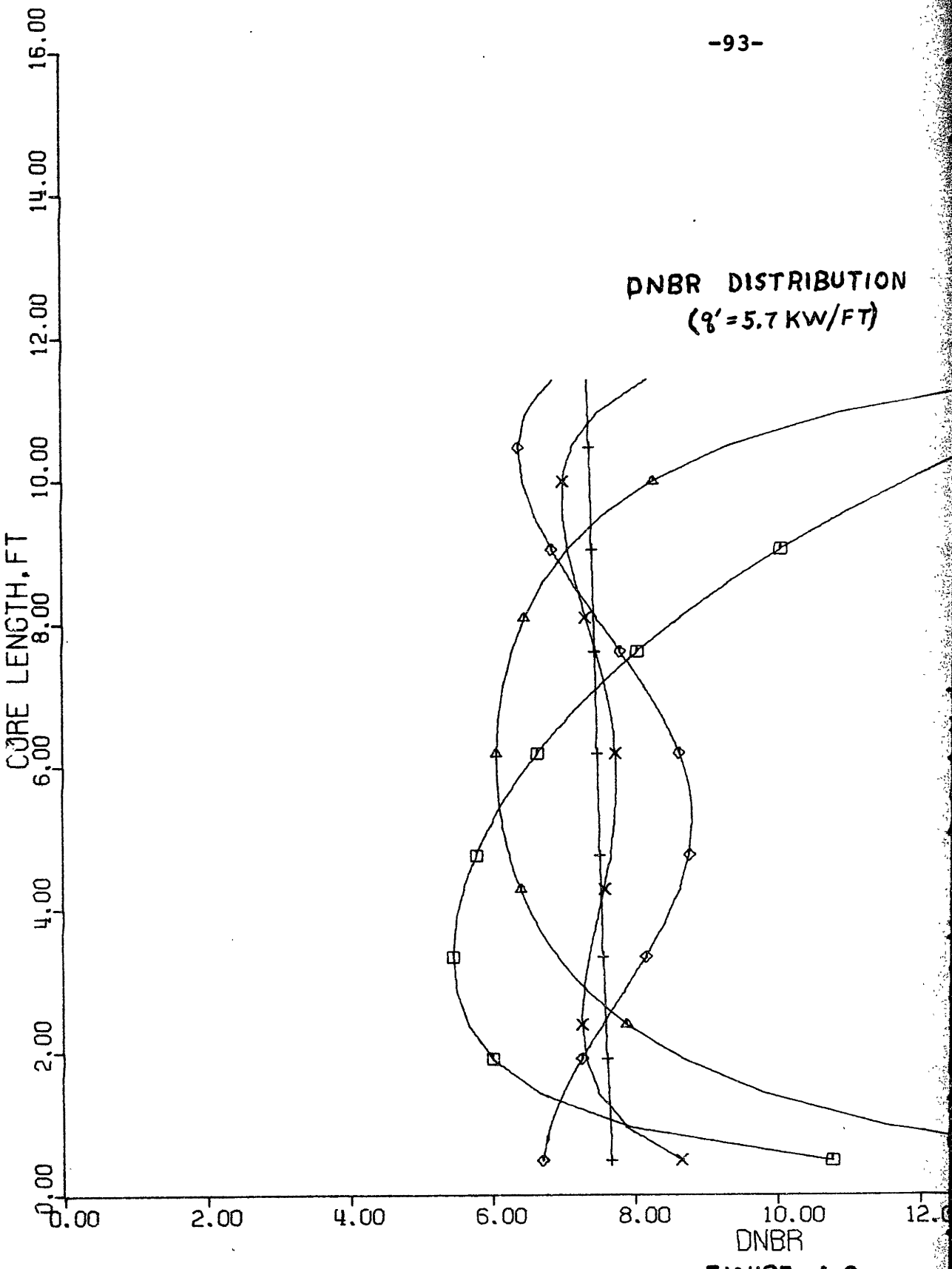
DNBR DISTRIBUTION
(q' = 5.7 KW/FT)
CORE LENGTH, FT
0.00
2.00
4.00
6.00
8.00
10.00
12.00
14.00
16.00
0.00
2.00
4.00
6.00
8.00
10.00
12.
DNBR

FIGURE 4.3

DNBR DISTRIBUTION
($q' = 5.7$ KW/FT)

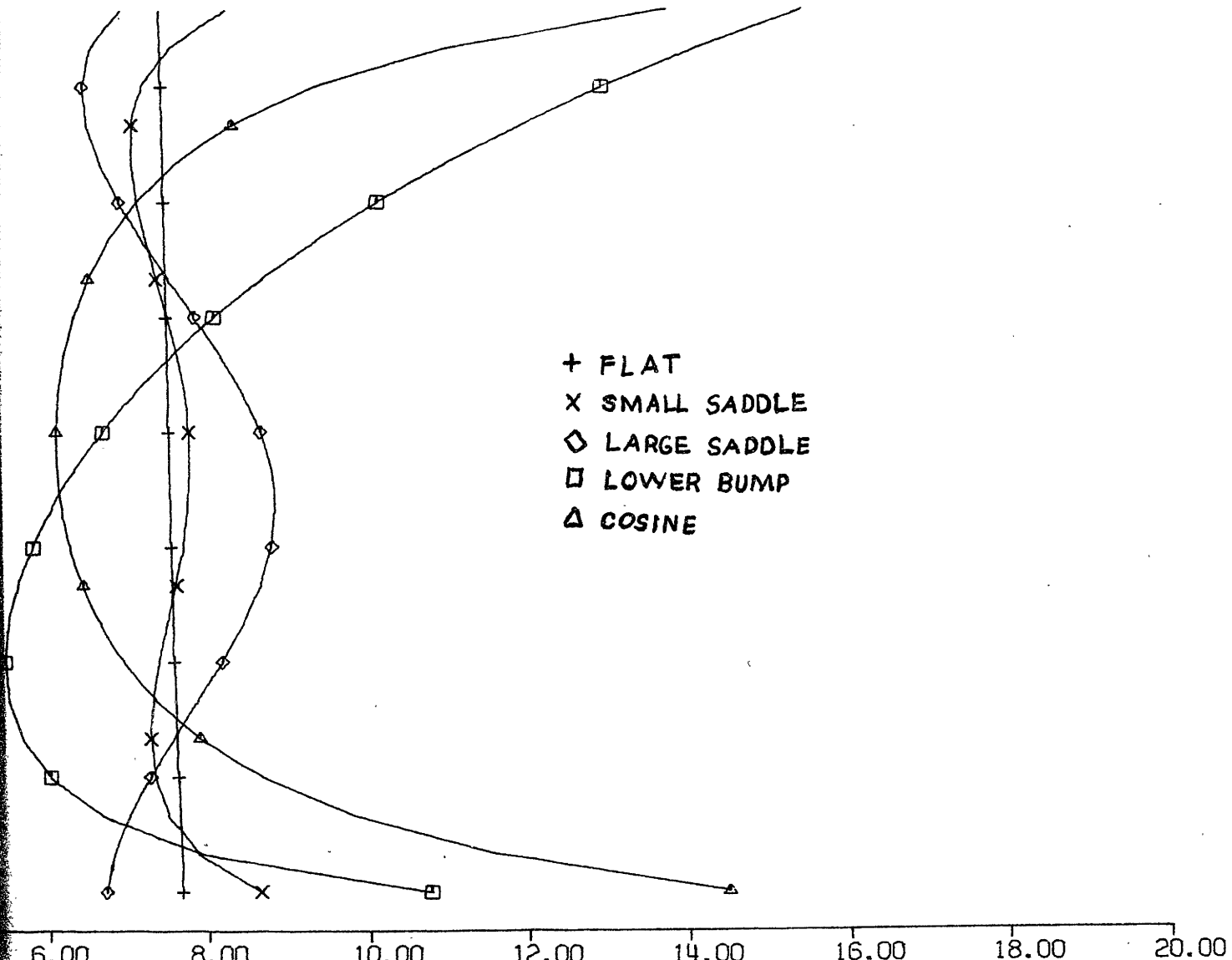

FIGURE 4.3

- Minimum acceptable DNBR will be approximately 6.

Because efforts are being made to flatten the neutron flux shape as much as possible, thereby causing a more even fuel rod burn up, the heat flux profile used in the remainder of the study is basically a flat profile with a 1.5% deviation from peak to average. This slight deviation is caused by the exponentials used to make the shape.

Variation of the linear heat rate using a flat flux profile produced the curves drawn in Figure 4.4. The curve for $q' = 15$ KW/ft is extrapolated to intercept with the initial power level of the Main Yankee reactor. This linear heat generation rate was not followed beyond the point of intersection because of resulting low MDNBR (5.5) and a high centerline temperature of about 5000°F. The pressure losses associated with these linear heat rates at the initial total power level of 2630 MW(th), decrease linearly from 13 PSI for $q' = 5.7$ KW/ft to 8PSI for $q' = 10$ KW/ft. Therefore, increasing the linear heat generation rate leads to a decrease in pressure drop and MDNBR but increases the centerline temperature.

To obtain the maximum linear heat generation rate possible it is desirable to increase the MDNBR value for $q' = 10$ KW/ft from the 4.5 shown on Figure 4.4 towards a MDNBR of 6. Tightening the pitch while keeping the core cross-sectional area and rod diameter constant produces

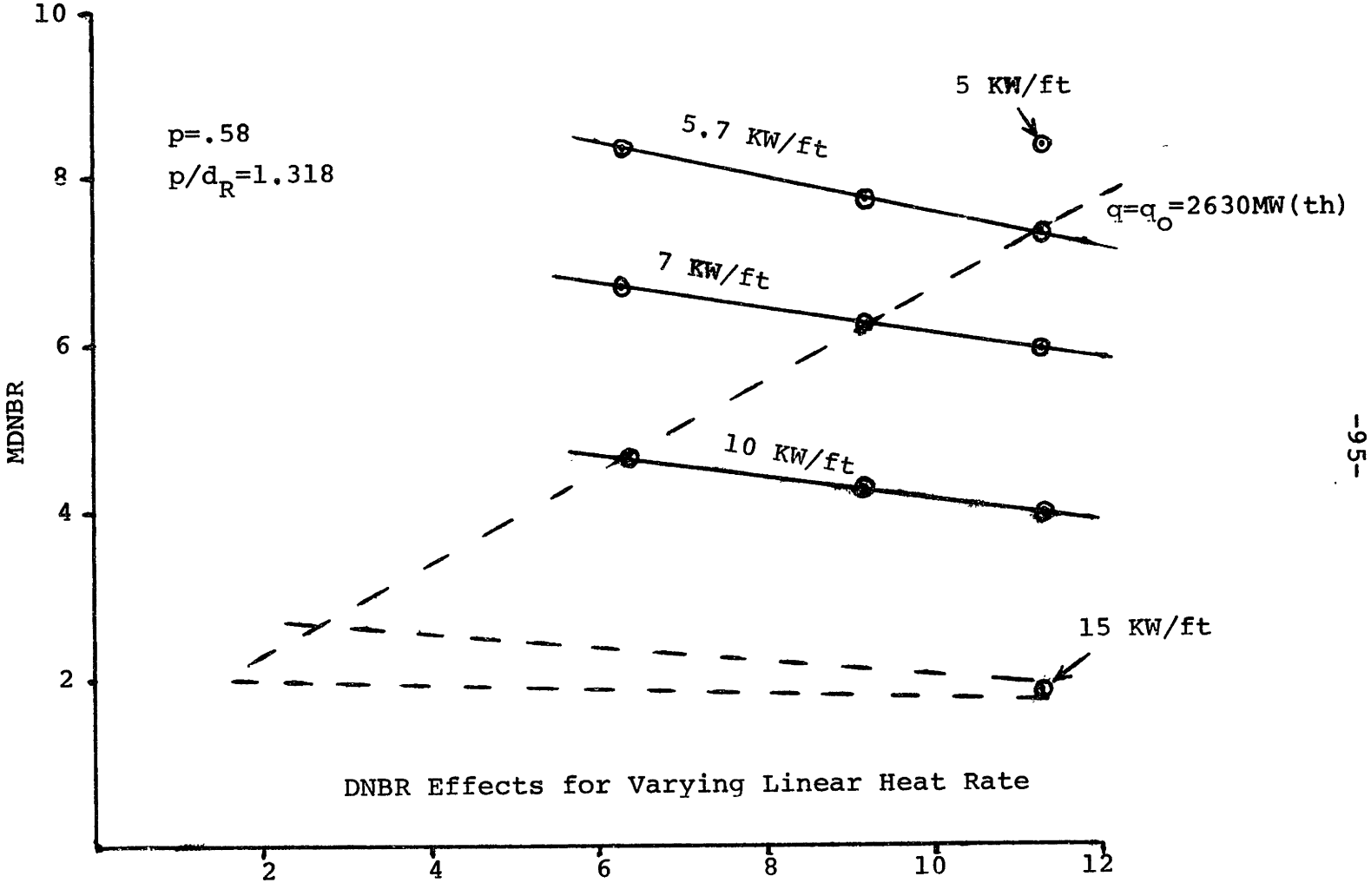

DNBR Effects for Varying Linear Heat Rate

Figure 4.4

just this result (Figure 4.5). The 10 KW/ft cases approach the MDNBR limit of six while the 7 and 5.7 KW/ft cases are now above this limit. Pressure losses across the channel lengths are not prohibitively large and seen technically feasible as Figure 4.6 shows. At this point, no specific constraints have been placed on the allowable pressure loss. To bound the pressure loss within technical limitations, the following constraint is established,

- Maintain the pressure loss as close as possible to the base case, but below 150% of the base case $P \leq 1.5\ P_{REF}$.

Results at this point already indicate that the linear heat generation rate can be seemingly increased to 7.0 KW/ft with no major impact upon the initial pressure loss and a small decrease in the initial MDNBR.

Further variation of the spacing between rods is produced by varying the rod diameter about its initial value of .44 inches. The results of this variation are illustrated in Figure 4.8 through 4.13 for q' varying from 5.7, 7.0 and 10.0 KW/ft . At this point, the increased coolant mass flux will become an important parameter in limiting the sensitivity study results. Figure 4.7 shows the variation of the mass flux versus the rod diameter and the pitch. To meet the engineering and technical limits of reactor design the following constraint on coolant mass flux is established.

- Maintain the coolant mass flux as close to the base case but less than 150% of the base case

$$G_i \leq (1.5)G_{i(REF)} \quad .$$

From the plotted data and imposed constraints there is now ample information to outline regions of operation where smaller rod spacing can be applied for various linear heat generation rates.

A general procedure for performing this optimization would be to

1. Use Figure 4.7 to determine the upper limit of rod diameter and pitch combinations with the coolant mass flux constraint.

2. Apply the pressure loss constraint to Figures 4.9, 4.11, and 4.13 and determine the second upper limit of rod diameter and pitch combinations meeting the established criterion.

3. Apply the MDNBR constraint to Figures 4.8, 4.10 and 4.12 to determine the lower limit of rod diameter and pitch combinations meeting this criterion.

4. Transfer the mass flux and pressure loss, rod diameter and pitch limits to the MDNBR plots of Figures 4.8, 4.10 and 4.12 to outline a region where all constraints are met.

These optimized regions can be optimized further (decreased

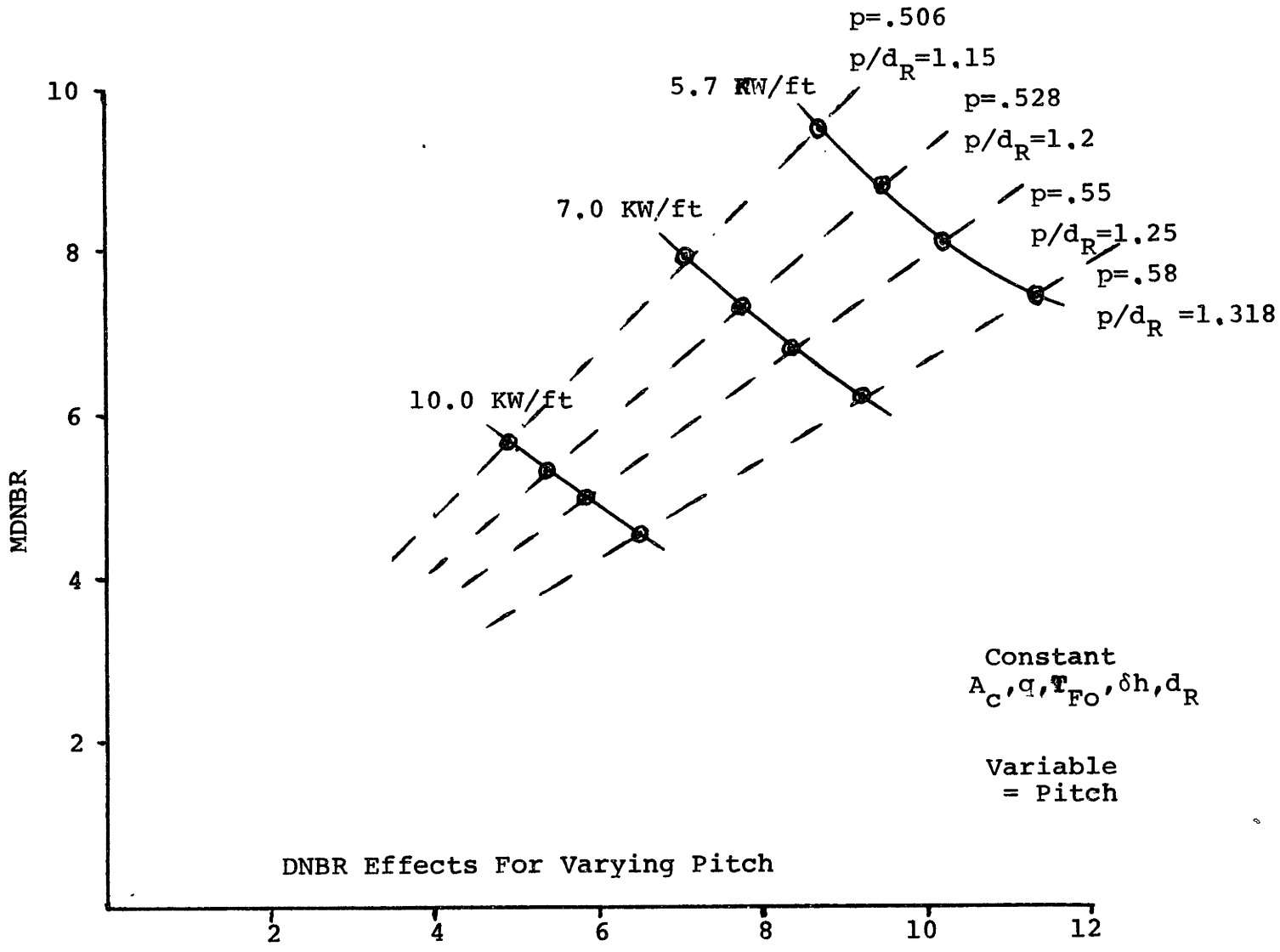

DNBR Effects For Varying Pitch

Figure 4.5

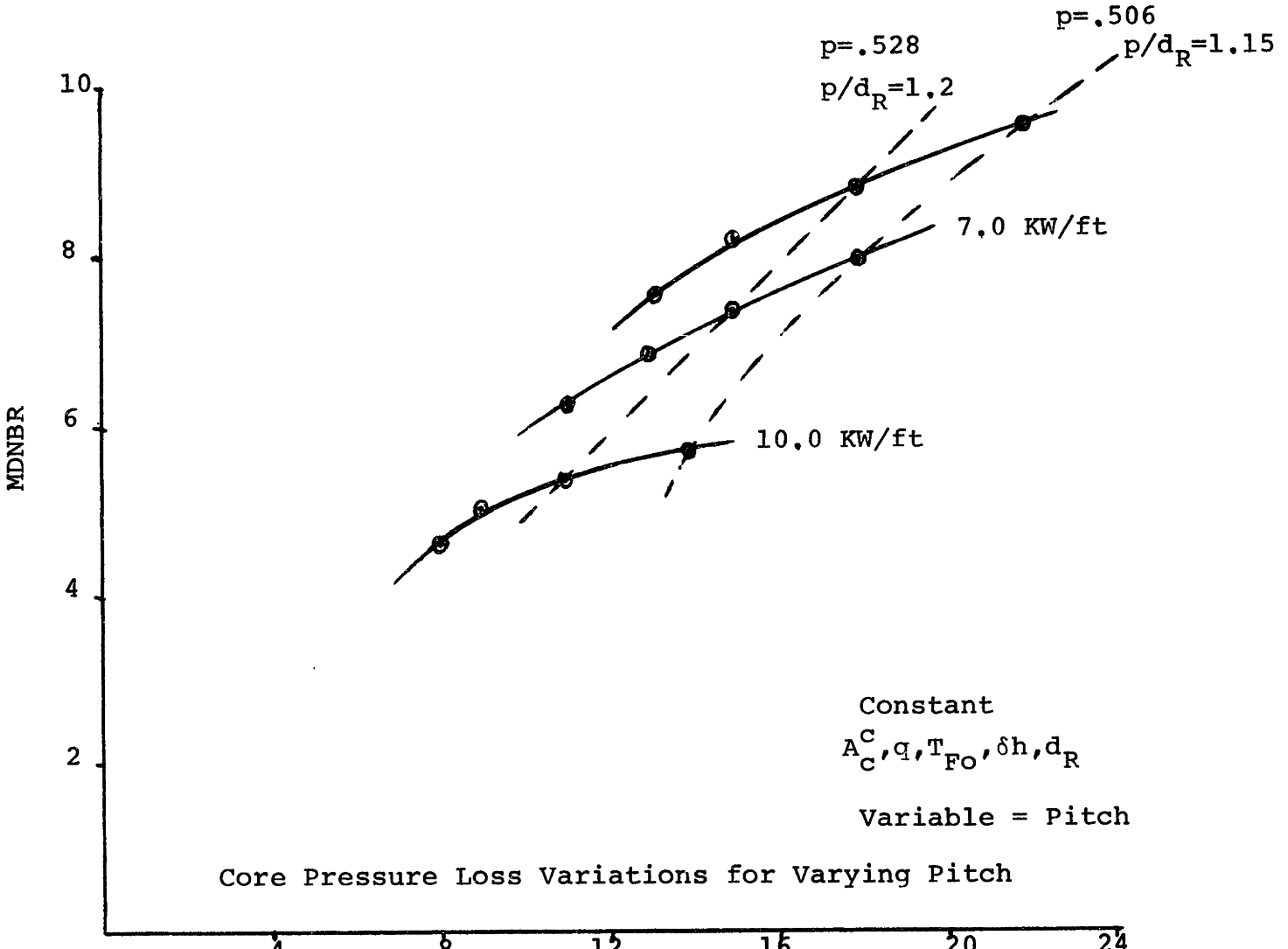

Core Pressure Loss Variations for Varying Pitch

Figure 4.6

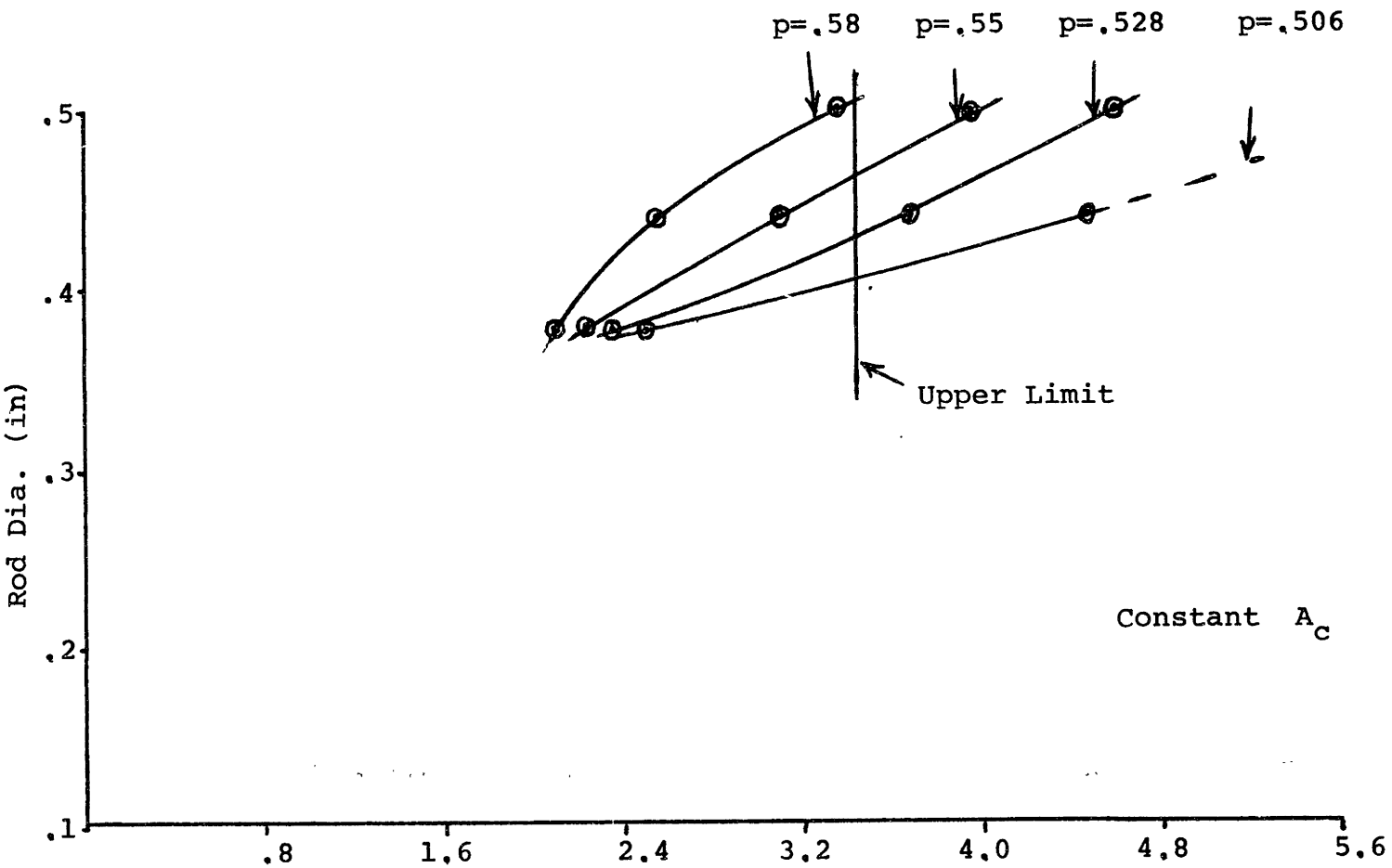

Figure 4.7

Mass Flux Variations for Varying Pitch and Rod Diameter

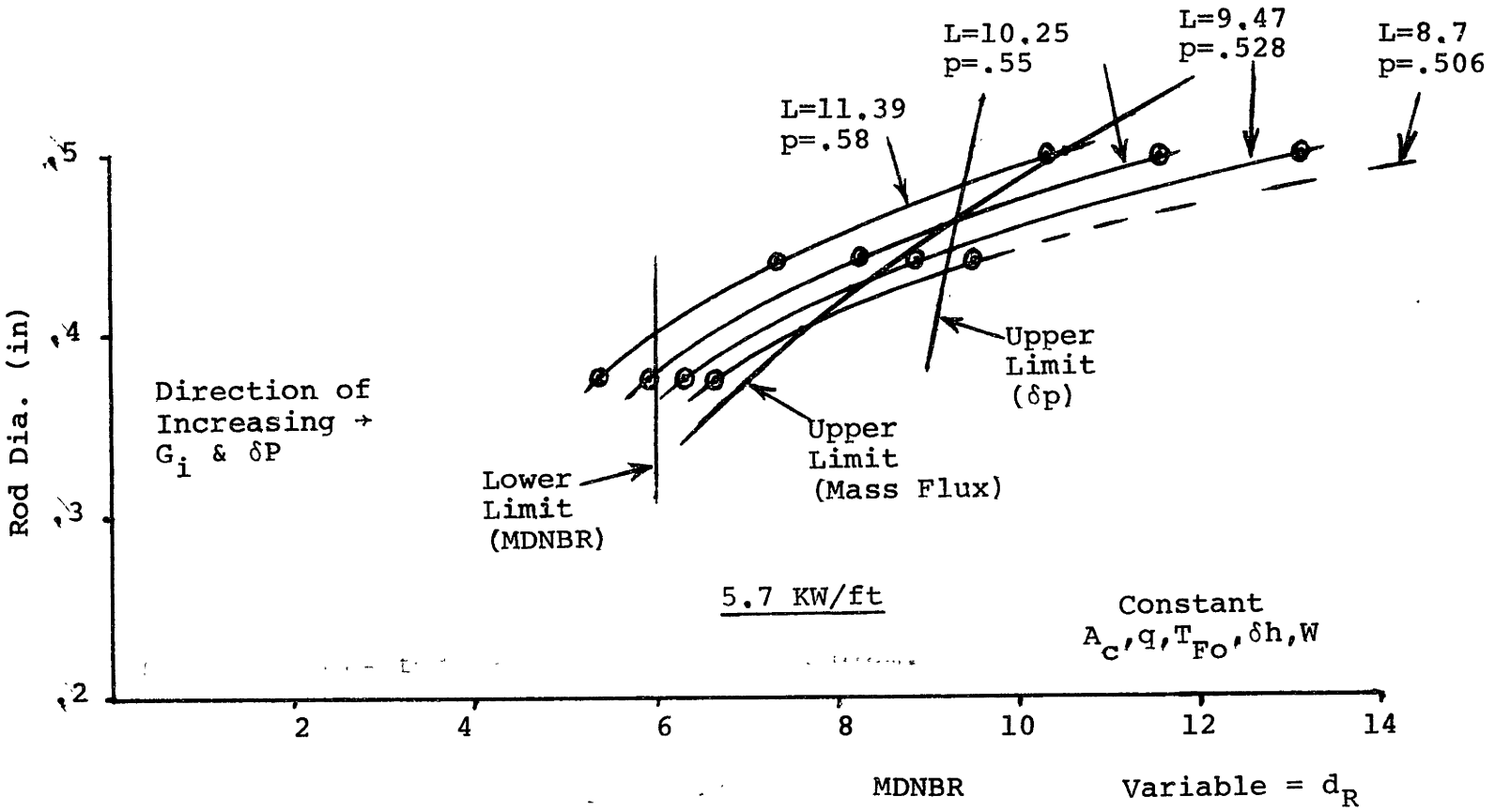

Figure 4.8

MDNBR Effects for Varying Pitch and Rod Diameter

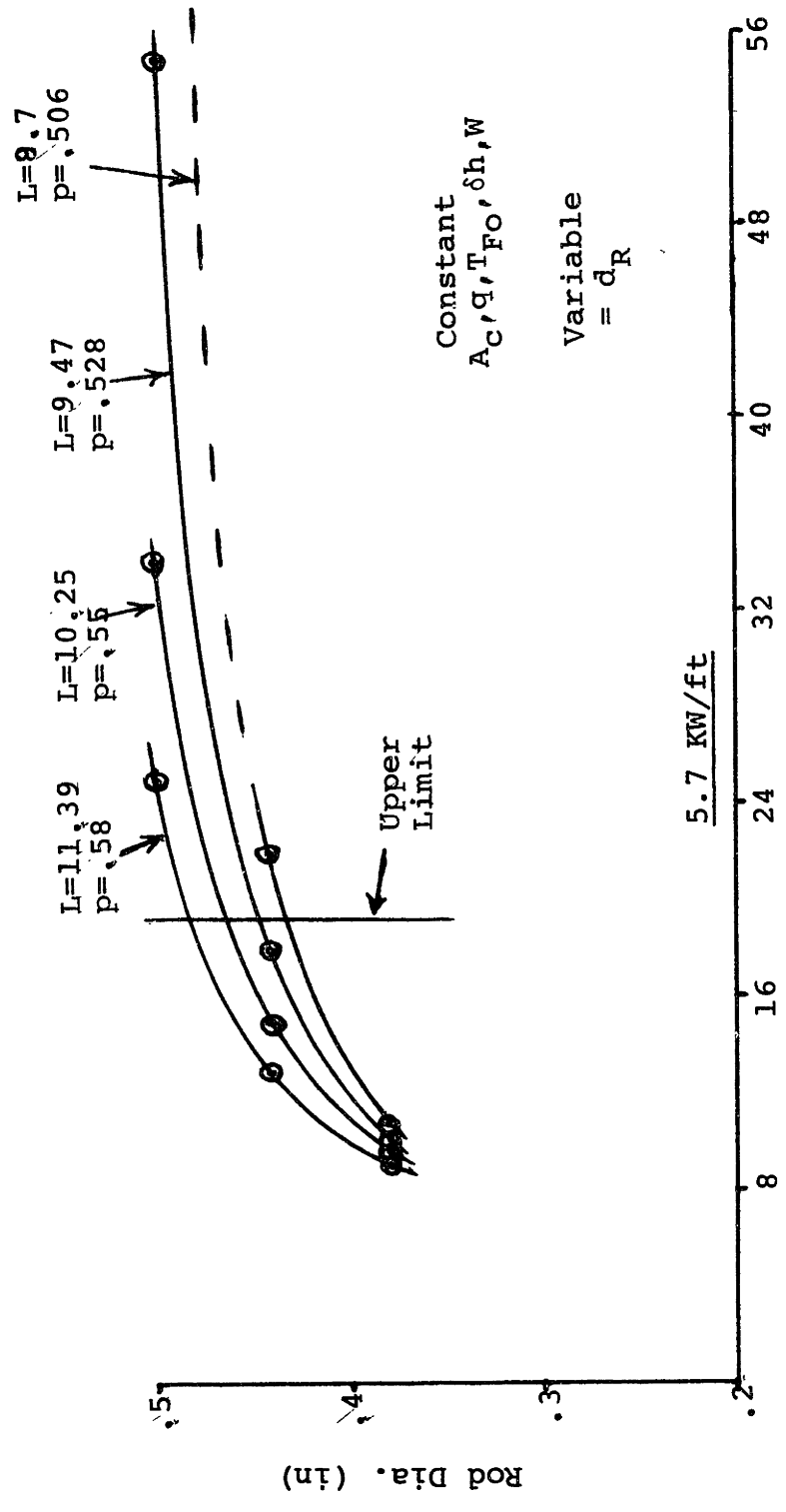

Figure 4.9

Core Pressure Loss Variations for Varying Pitch and Rod Diameter

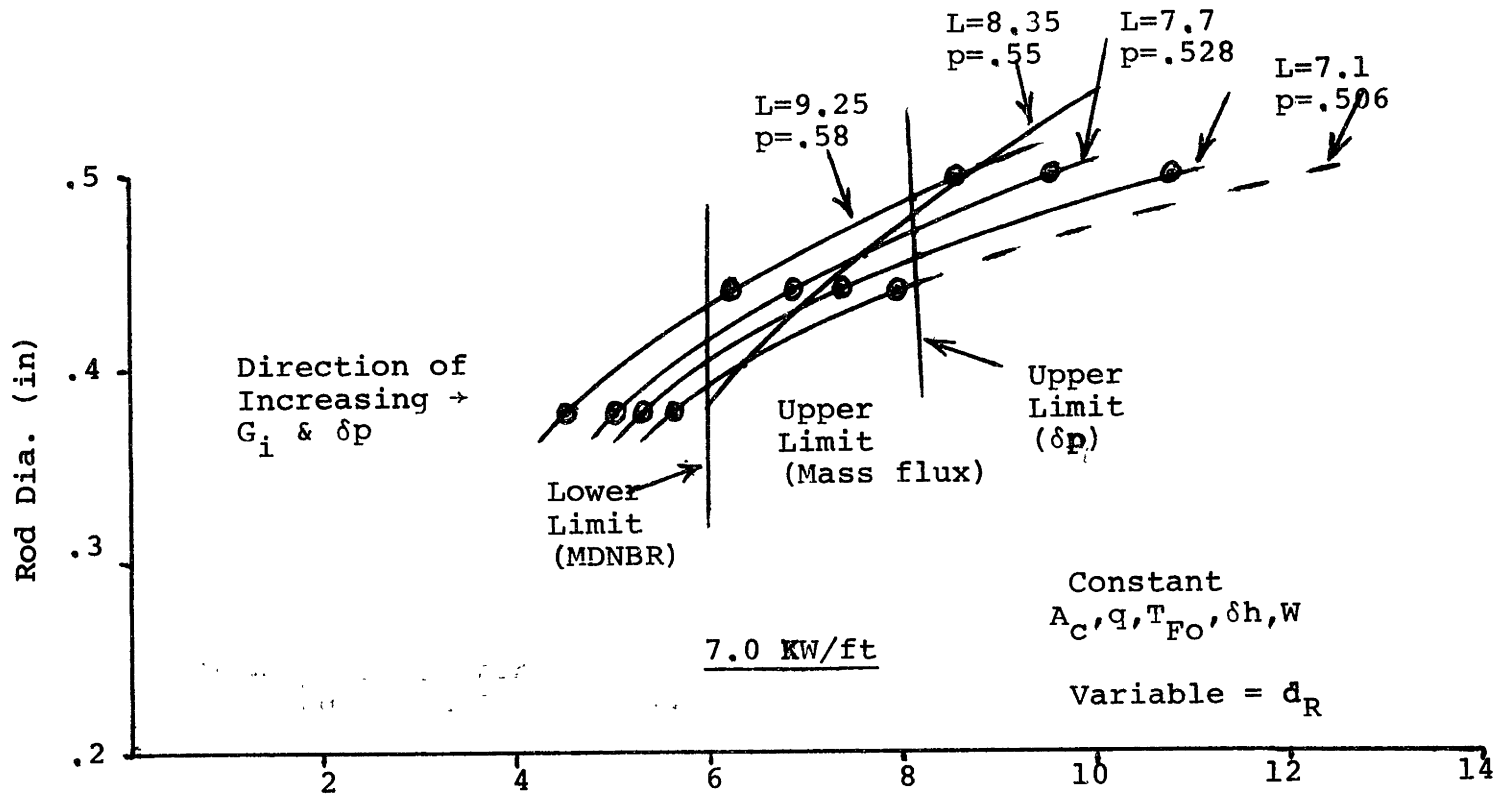

Figure 4.10

MDNBR Effects for Varying Pitch and Rod Diameter

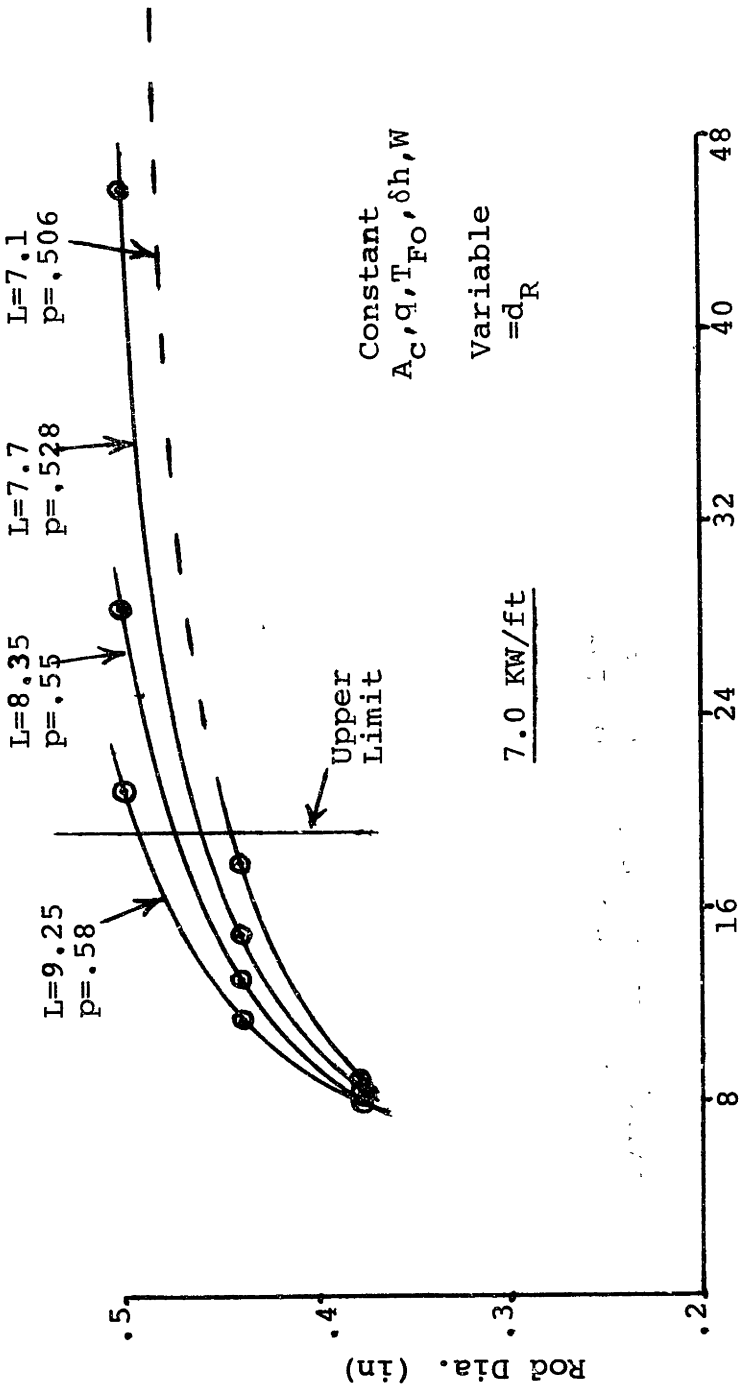

Figure 4.11

Core Pressure Loss Variation for Varying Pitch and Rod Diameter

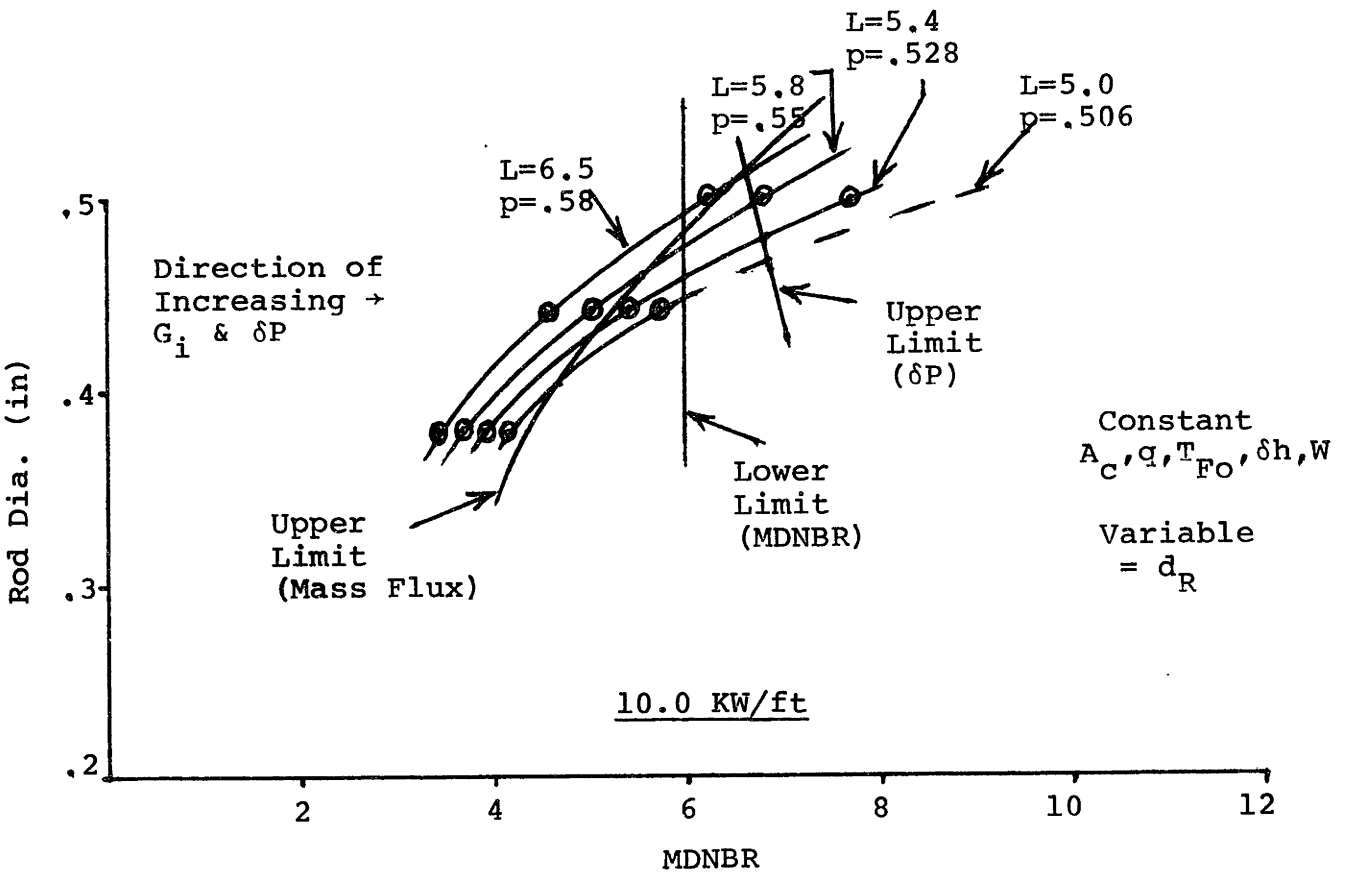

Figure 4.12

MDNBR Effects for Varying Pitch and Rod Diameter

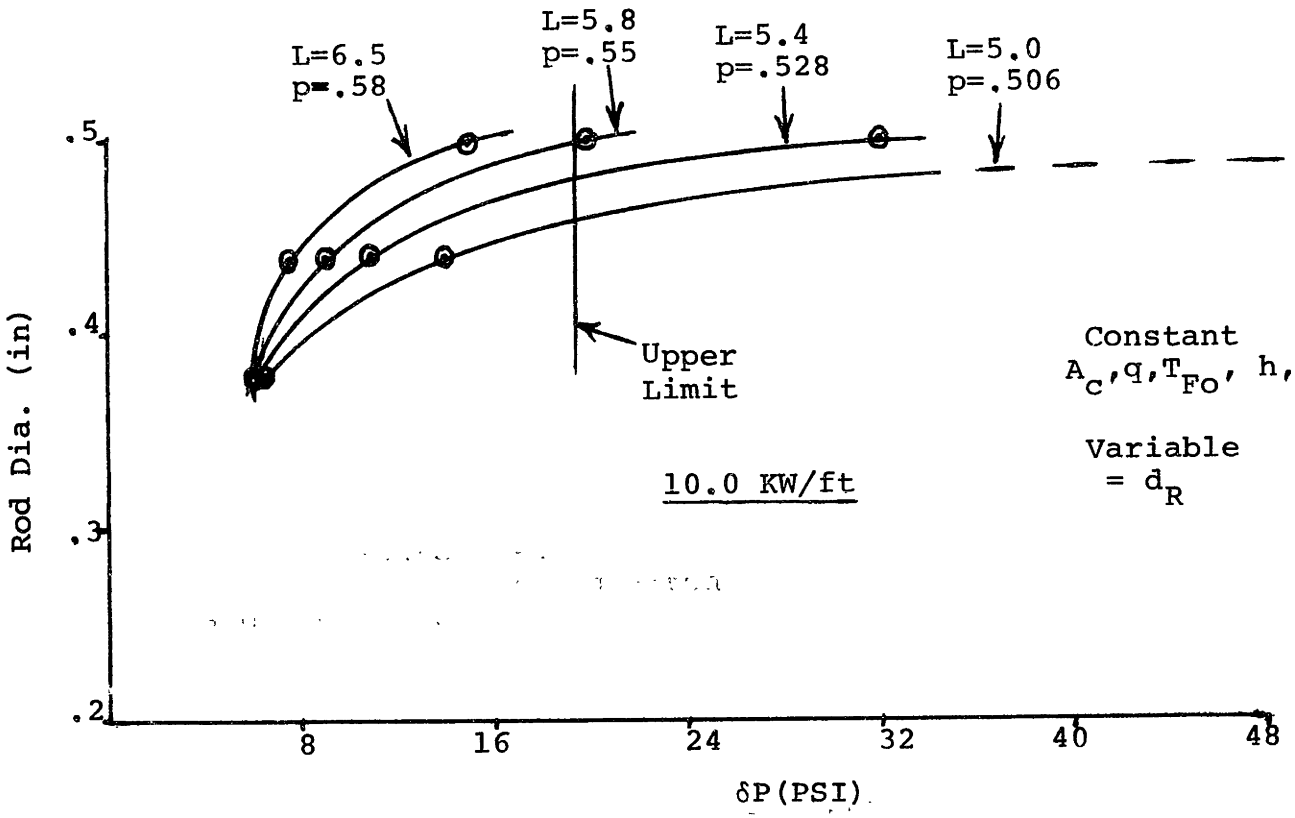

Figure 4.13

Core Pressure Loss Variation for Varying Pitch and Rod Diameter

in size) by tightening the constraints on the governing parameters, thereby decreasing the ranges of rod diameter and pitch combinations that are applicable. Notice, with the constraints used, the area of validity is so small in the 10 KW/ft case (Figure 4.12) that there is only a small range of variations which fall into this area. The minimum geometrical parameters which correspond to this region for $q' = 10$ KW/ft are

- rod length $\geq$ 6.2 feet
- pitch $\geq$ .57 inches
- rod diameter $\geq$ .48 inches versus initial conditions for $q' = 5.7$ KW/ft
- rod length = 11.39 feet
- rod diameter = .44 inches .

Variations can be made on these geometrical parameters while still obtaining results which fall into this optimized region, however, the upper limit for these parametric variations has not been determined in this study. Note that if,

1. The pitch and core length are increased, more points can be obtained in the optimized area while decreasing pressure loss and mass flux.

2. The linear heat generation rate is decreased, all curves of Figures 4.8, 4.10 and 4.12 (except the MDNBR constraint line) will move to the right in the direction of conservative values. (Compare Figures 4.10 and 4.12.)

The curves of Figure 4.7 through 4.13 therefore, show the complete thermal-hydraulic effects of varying rod geometry and linear heat generation rate for the Main Yankee reactor design with the designated parameters held constant.

The results of this preliminary study indicate that if a flat flux profile is used, the linear power level of the Main Yankee reactor may be increased to 10 KW/ft with a slight increase in pressure loss to 14.8 PSI and a decrease in MDNBR to 6.25. Rod temperatures for this special case in the optimized region are shown in Table 4.1 as obtained by WABCORE. A comparison with COBRA IIIC/MIT results is illustrated in Table 4.2. These results include the basically flat heat flux profile with a 1.5% difference from peak to average and a cosine flux profile with a 25.0% difference from peak to average. The results show that the DNBR minimum has been violated and the rod centerline temperature is becoming unusually high for LWR operation. The results predicted by WABCORE are generally more conservative then the COBRA IIIC/MIT results. The core pressure loss and maximum clad temperature are in good agreement and well within engineering limits for both cases.

Table 4.1

Main Yankee Channel Temperatures
At 10 KW/ft Calculated by WABCORE

TEMPERATURES IN DEG. F				
FLUID	CLAD	FUEL SURFACE	CENTER LINE	
541.0000	571.9182	1644.9536	3593.1077	1
543.2693	574.2026	1648.5400	3599.0581	2
545.5325	576.4490	1651.7554	3604.0325	3
547.7888	578.6802	1654.6470	3608.1233	4
550.0376	580.8958	1657.2388	3611.3979	5
552.2781	583.0962	1659.5574	3613.9314	6
554.5095	585.2810	1661.6252	3615.7871	7
556.7317	587.4502	1663.4663	3617.0325	8
558.9436	589.6047	1665.1067	3617.7397	9
561.1450	591.7444	1666.5708	3617.9768	10
563.3357	593.8694	1667.8809	3617.8074	11
565.5151	595.9805	1669.0635	3617.3040	12
567.6831	598.0774	1670.1421	3616.5342	13
569.8394	600.1611	1671.1409	3615.5630	14
571.9836	602.2317	1672.0852	3614.4622	15
574.1157	604.2900	1672.9998	3613.3008	16
576.2356	606.3364	1673.9087	3612.1443	17
578.3433	608.3718	1674.8369	3611.0623	18
580.4385	610.3965	1675.8108	3610.1284	19
582.5215	612.4111	1676.8535	3609.4070	20
584.5925	614.4167	1677.9910	3608.9680	21
586.6514	616.4138	1679.2490	3608.8845	22
588.6982	618.4031	1680.6519	3609.2224	23
590.7336	620.3857	1682.2246	3610.0515	24
592.7576	622.3625	1683.9932	3611.4419	25

Table 4.2

Comparison of Main Yankee Core (10 KW/ft) Calculated by WABCORE and COBRA IIIC/MIT

	WABCORE	COBRA IIIC/MIT	WABCORE	COBRA IIIC/MIT
Outlet Coolant Temp.	592.7	592.5	592.7	592.5
Maximum Centerline Temp.	3617.9	3149.2	4338.5	3456.8
Core Pressure Lors	14.8	14.5	14.8	14.5
MDNBR	6.25	8.11 (1) 6.0 (2)	5.15	7.57 (1) 5.42
Maximum Clad Temp.	622.4	642.3 (3)	615.1	637.7 (3)

1 - W-3 CHF correlation

2 - $B\&W_2$ CHF correlation

3 - Temperature not calculated until second axial node

4.4 Economic Implications

Since fuel inventory cost has an inverse dependence on linear heat generation rate, it is apparent that fuel cost will go down if the limits can be increased. Physically, an increased linear heat generation rate at constant burnup and annual refueling increases the refueling fraction. This must be compensated by a corresponding enrichment increase. Previous work in this area has shown that the cost incentive for increased specific power is surprisingly small, for a PWR with a 10% increase in specific power[7]. This lack of sensitivity is due to the fact that the reduced cost are offset by the additional enrichment to maintain burnup levels. It is therefore expected that even though an increase in the Main Yankee linear heat generation rate from 5.7 to 10.0 KW/ft results in approximately a 25% reduction in fuel mass, there will be a small economic benefit. However, on the other hand, there will be substantial savings in core heavy metal mass.

CHAPTER V

CONCLUSION AND RECOMMENDATIONS

Results of the preliminary sensitivity study of the Main Yankee reactor core have indicated that the linear heat generation rate could be approximately doubled to 10 KW/ft with a basically flat heat flux profile (i.e., 1.5% deviation from peak to average) which leads to the following consequences with a pitch of .58 inches

- An increase in rod diameter from .44 to .5 inches
- An increase in coolant mass flux from 2.5 to 3.34 x 10^6 lbm/hr ft^2
- A decrease in rod length from 11.39 to 6.5 feet
- An increase in core pressure loss from 12.8 to 14.8 PSI
- A decrease in MDNBR from 7.3 to 6.25 .

With the parametric constraints used in this sensitivity study, no pitches were found that were more than .01 inches smaller than the initial of .58 inches with a linear heat generation rate of 10 KW/ft. The reason for this is due to the constraint of maintaining the initial core cross-sectional area and flow rate. Because of this more rods must be used in the core when the pitch is tightened, thereby causing a greater increase in the mass flux than that caused by a rod diameter increase only. As a result, a

linear heat generation rate smaller than 10 KW/°F would be necessary for the use of a tighter pitch than .57 inches.

During the course of this study, core area, total power, coolant outlet temperature, enthalpy use and total mass flow were held constant. If any one of these parameters are varied, then for each variation, a set of 36 cases must be run to present the same amount of information presented in this study (3 rod diameter x 4 rod pitches x 3 linear heat rates). WABCORE has been specifically designed to handle this situation efficiently and the number of cases will not cause a loss of organization or time.

Because of the inherent conservatism of a single-channel thermal-hydraulic code and the extra conservatism built into WABCORE, the results can usually be interpreted as being conservative for most parts. This conclusion can be substantiated by the comparison with COBRA IIIC/MIT results presented in Chapter III.

Finally, it is believed that the results in this sensitivity study present a complete thermal-hydraulic overview of the changes expressed by the Main Yankee core within the framework of the given set of parametric constraints. Extrapolations based on these results can be made within reasonable limits.

5.1 Recommendations

To extend the scope of this sensitivity study on a thermal-hydraulic and economic basis, the following recommendations can be made

1. Although the conservative results of the sensitivity study indicate that there is a margin for increased peaking of the axial heat flux shape, a hot-channel analysis should be performed. Prescribed hot spot factors can be applied to the heat flux and fuel rod using a deterministic or statistical approach. It is suggested, however, that the hot-channel conditions from the Main Yankee PSAR be used and results checked against the PSAR hot-chennel MDNBR.

2. When the reactor parameters held constant in this study are varied for further study, the amount of information needed to predict an optimum will increase significantly. To handle this information efficiently, it is recommended that an optimization program should be developed to use and optimize the results of the thermal-hydraulic calculations. To do this, nonlinear relationships would have to be derived with variable rod diameter, pitch, linear heat generation rate, MDNBR, pressure loss, mass flux, core length and any other reactor parameters which are varied. A non-linear optimization technique can then be used to apply the desired constraints and outline a feasible region of operation.

3. If the above optimization method is introduced, the results would be valid only from a thermal-hydraulic point of view. A necessary step would be to add economic constraints. These additions should include,

- Cost of initial ore for core start-up
- Cost of fuel rod fabrication
- Cost implied by the number of refuelings over a time period .

As a result, the optimized core would be validated on a thermal-hydraulic and economic basis. These results will nevertheless be preliminary and should be followed by more extensive studies before final decisions are made.

4. The last optimization consideration would be that of the entire reactor system (i.e., primary and secondary loops, steam generators, etc.). Several ways of performing this type of optimization are presented in the literature, mostly in chemical journels on chemical systems. The most valuable method in this context seems to be a technique presented by Weisman and Holzman[8] which optimizes a system by minimizing the economic loss caused by the unoptimized system.

5. A complete study of the transient capabilities of the core (i.e., LOCA, ATWS, etc.) must be performed to determine any final deficiencies which might necessitate changes.

LIST OF REFERENCES

1. DeStordeui, A.N., "Drag Coefficients for Fuel-Element Spacers", Nucleonics, June, 1961.

2. ElWakel, M.M., "Nuclear Heat Transport", International Textbook Company, 1971.

3. Tong, L.S., "Critical Heat Fluxes in Rod Bundles", Westinghouse Electric Company Paper, 1970.

4. Indsinga, W., "An Assessment of Two-Phase Pressure Drop Correlations for Steam-Water Systems", thesis, MIT, May, 1975.

5. Andrade, G.G., DaSilva, O.L.P., "Parametric Thermal-Hydraulic Analysis of a Core Substitition in a PWR", Special Problem in Nuclear Engineering, MIT, Sept., 1976.

6. Wilson, R.H., et al., "Critical Heat Flux in a Nonuniformily Heated Rod Bundle", ASME Winter Meeting, 1969.

7. Gallagher, W.J., McLeod, N.B., "Higher Power Densities in Water Reactors-Economic and Technical Bases", Reactor and Fuel-Processing Technology, Vol. 12, No. 1, Winter, 1968-1969.

8. Weisman, J., Holzman, A.G., "Optimal Process System Design Under Conditions of Risk", Ind. Eng. Chem. Process Des. Develop., Vol. 11, No. 3, 1972.

9. Collier, J.G., "Convective Boiling and Condensation" McGraw-Hill, 1972.

10. Keenan, J.H., Keyes, F.G., Hill, P.G., Moore, J.G., "Steam Tables", John Wiley & Sons, Inc., 1969.

11. Green, S.J., Letourneau, B.W., Saladna, E.F., Sherba, P.S., "Critical Heat Flux Test on a Coolant Channel Simulating a Closely Spaced Lattice of Rods", ASME Winter Annual Meeting, 1969.

12. Towell, R.H., "Effect of Rod Spacing on Heat Transfer Burnout in Rod Bundles", USAEC Report DP-1013, 1965.

13. Matzmer, B., Casterline, J.E., Moech, E.O., Wikhammer, G.A., "Experimental Critical Heat Flux Measurements Applied to a Boiling Reactor Channel", ASME Paper No. 66-WA/HT-46, 1966.

14. Moeck, E.O., Stern, F., Wikhammer, G.A., Dempster, R.J., "Dryout in a 19-Rod Bundle Cooled by Steam/Water Fog at 515 PSIA", ASME Paper No. 65-HT-50, 1965.

15. Gellerstedt, J.S., Lee, R.A., Oberjohn, W.J., Wilson, R.H., Stanek, L.J., "Correlation of Critical Heat Flux in Bundle Cooled by Pressurized Water", ASME Winter Meeting, 1969.

16. Bergles, A.E., "Two-Phase Flow Structure Observations for Pressure Water in a Rod Bundle", MIT Paper.

17. Janssen, E., Schraub, F.A., Nixon, R.B., Matzner, B., Casterline, J.F., "Sixteen-Rod Critical Heat Flux Investigation, Steam-Water at 600 to 1250 PSIA", ASME Winter Annual Meeting, 1968.

18. Williams, J.S., Jr., "Thermal Analysis of the Effect of Axial Flux Distribution On Steady-State Performance of Nuclear Reactors", Bettis Atomic Power Division Report.

19. Castellana, F.S., Bonilla, C.F., "Two-Phase Pressure Drop and Heat Transfer in Rod Bundles", Columbia University Paper.

20. LeTourneau, B.W., Gevin, M.E., Green, S.J., "Critical Heat Flux and Pressure Drop Test with Parallel Upflow of High Pressure Water in Bundles of Twenty 3/4-in. Rods", Nuclear Science and Engineering, Pg. 214, 1974.

21. DeStordeur, A.N., "Drag Coefficients for Fuel Element Spaces", Nucleonics, June, 1961.

APPENDIX A

Users Manual for WABCORE

A.1 Full Reactor Core Input Data

Card	Variable	Format	Descritpion	Units
1	ITYPE	I4	(=0) for this input option	
1	TITAL	A76	Any user title	
2	TEMPI	F10.4	Inlet temperature	°F
2	PRESSI	F10.4	Inlet pressure	PSI
2	HI	F10.4	Inlet enthalpy	BTU/lbm
2	FKC	F10.4	Clad thermal conductivity	BTU/hr,ft°F
2	FHG	F10.4	Gap heat transfer coefficient	BTU/hr,ft^2, °F
2	FKF	F10.4	Fuel pellet thermal conductivity	BTU/hr,ft, PF
3	Q	E10.4	Reactor power	BTU/hr
3	W	E10.4	Coolant mass flow rate	lbm/hr
3	AVGQ	E10.4		
3	AVGQ	E10.4	Rod avg. heat flux	BTU/ft^2,hr
3	POVD	F10.4	Pitch over diameter ratio	
3	FL	F10.4	Rod length	ft
3	LSTEP	F10.4	Core cross sectional area	ft^2
4	DELTA	F10.4	Ratio of total lgth. of spacers to lgth. of rod	
4	T	F10.4	Grid thickness*	ft
5	FS	F10.4	Starting point of heat flux shape (Figure 2.5)	

Card	Variable	Format	Description	Units
5	FBPLSS	F10.4	End point of heat flux shape (Figure 2.5)	
5	FKN	F10.4	Shape normalization constant (K_n)	(Eq. 2.15)
5	FN	F10.4	Exponential multiplication constant (N)	(Eq. 2.15)
5	FA	FF10.4	Exponential shape constant (A)	(Eq. 2.15)
5	FK	F10.4	Exponential multiplication constant (K)	(Eq. 2.15)
5	FC	F10.4	Exponential shape constant (C)	(Eq. 2.15)
6	SPSLO	10F8.4	Spacer location* -Grid only,10 per card	ft
7	SPSCOF	10F8.4	Spacer coefficient- -Grid only, 9 per card	
8	ISPAC	I5	(=1)-Sq. array w/grid spacers (=2)-Sq. array w/wire wrap (=3)-Hexagonal array w/wire wrap	
8	ITPM	I5	(=1)-Homogeneous TPM (Eq.-3.20A) (=2)-Homogeneous TPM (Eq.-3.20B) (=3)-Armad-Treschev TPM (Eq.-3.21)	
8	IPLOT	I5	(=0)-No plots (=1)-Plot*	
8	IRAD	I5	(=1) (=2)	
8	AON1	F6.3	Ratio of pellet to rod dia. (IRAD=2)* Volume of moderator to fuel ratio (IRAD=1)*	

Card	Variable	Format	Description	Units
8	AON2	F6.3	Ratio of inside clad to rod dia. (IRAD=2)* Fraction of clad to clad+gap thickness (IRAD=1)*	
8	SLIP1	F6.3	Subcooled boiling slip factor (Eq. 2.32C)	
8	SLIP2	F6.3	Bulk boiling slip factor (Eq. 2.32C)	

A2 Single Channel Input Option

Card	Variable	Format	Description	Units
1	ITYP	I4	(=1)-For this input options	
1	TITAL	A76	Any user title	
2	TEMP1	F10.4	Inlet temperature (°F)	
2	PRESSI	F10.4	Inlet pressure (PSI)	
2	HI	F10.4	Inlet enthalpy	BTU/lbm
2	FKC	F10.4	Clad thermal conductivity	BTU/lbm, ft,°F
2	FHG	F10.4	Gap heat transfer coefficient	BTU/lbm,ft^2, °F
2	FKF	F10.4	Fuel pellet thermal conductivity	BTU/lbm,ft, °F
3	AVGQ	E10.4	Avg. heat flux	BTU/ft^2,hr
3	GI	E10.4	Coolant mass flux	lbm/hr,ft^2
3	DEI	F10.6	Subchannel hydraulic dia.	ft
3	FL	F10.6	Rod length	ft
3	ACIF	F10.6	Subchannel flow area	ft^2
3	LSTEP	I5	No. of axial nodes	

Card	Variable	Format	Description	Units
4	FS	F8.4	Starting point of heat flux shape (Figure 2.5)	
4	FBPLSS	F8.4	End point of heat flux shape (Figure 2.5)	
4	FKN	F8.4	Shape normalization constant (K_n)	(Eq. 2.15)
4	FN	F8.4	Exponential multiplication constant (N)	(Eq. 2.15)
4	FA	F8.4	Exponential shape constant (A)	(Eq. 2.15)
4	FK	F8.4	Exponential multiplication constant (K) (Eq. 2.15)	
4	FC	F8.4	Exponential shape constant (C) (Eq. 2.15)	
5	SPSLO	10F8.4	Spacer location* -Grid only,10 per card	ft
6	SPSCOF	10F8.4	Spacer coefficient -Grid only, 9 per card	
7	ITPM	I5	(=1)-Homogeneous TPM (Eq.-3.20A) (=2)-Homogeneous TPM (Eq.-3.20B) (=3)-Armad-Treschev TPM (Eq.-3.21)	
7	IPLOT	I5	(=0)-No plot (=1)-Plot*	
7	RODDI	F10.5	Rod diameter	
7	RFS	F10.5	Fuel pellet radius	
7	RCI	F10.5	Inside clad radius	
7	SLIP1	F10.5	Subcooled boiling slip factor (Eq.2.32C)	

Card	Variable	Format	Description	Units
7	SLIP2	F10.5	Bulk boiling slip factor (Eq.2.32C)	
7	PITCH	F10.5	Rod pitch	

*See Section A.3 for further input explanation.

A3 Input Explanations

1. Spacer Location (SPSLO) - This is the axial position of the grid along the channel. To indicate that there are no other grid locations, the last entry must be larger than the channel length (i.e., 99ft). No spacer coefficient corresponds with this entry. If the wrie wrap option is selected, these cards must still be included with an entry of 99 in the first location of the spacer location card.

2. Plots (IPLOT) - Any number of cases may be computed in a single run, however, only five may be plotted. These plots are made on the corresponding set of axis versus core length. The plotted variables are

- Coolant temperature
- Centerline temperature
- Enthalpy
- System pressure
- DNBR

- Void fraction
- Quality
- Heat Flux .

The five plotted cases need not be in sequence and are chosen by setting IPLOT=1. If a particular run consists of boiling cases (i.e., x>0), then the last case of the run must be a boiling case also, otherwise, the quality and void graphs will not be plotted.

The plot results are placed on a 7-track tape at LNS and are displayed by the user via a calcomp unit at 37-678 of MIT.

3. (AON1) - If IRAD=1 then AON1 is the volume of moderator to fuel ratio

$$AON1 = \frac{V_m}{V_f} = \frac{A_{cif}}{\pi R_{fs}^2} \quad .$$

If IROD=2, then AON1 is the ratio of pellet to rod diameter

$$AON1 = \frac{2 \cdot R_{fs}}{d_R} \quad .$$

4. (AON2) - If IROD=1, then AON2 is the ratio of clad thickness to the clad plus gap thickness

$$AON2 = \frac{T_c}{d_R - 2 \cdot R_{fs}}$$

where

$$T_c = \text{clad thickness} \quad .$$

If IROD=2, then AON2 is the ratio of inside clad diameter to rod diameter

$$AON2 = \frac{d_R - 2 \cdot T_c}{d_R} \quad .$$

5. Grid Thickness (T) - This is the thickness of the projected face with a normal parallel to the channel length.

APPENDIX B

WABCORE LISTING

```
      DIMENSION BUFF(1000)
      DIMENSION FLE1(52),FLE2(52),FLE3(52),FLE4(52),FLE5(52)
      DIMENSION TPM1(50),TPM2(50),VOID(50),X(50),QSQFT(50)
      DIMENSION PRESF(50),TEMPF(50),TEMPC(50),TEMPFS(50),H(50),Z(50)
      DIMENSION TEMPCL(50),CRITQ1(50),ZFDB(50),ZSC(50),ZSTAR(50)
      DIMENSION PFRIC(50),PACC(50),PSPAC(50),SPSCOF(10),SPSLO(10)
      DIMENSION DNB(50),FF(50)
      DIMENSION A1(52),A2(52),A3(52),A4(52),A5(52),B1(52),B2(52),B3(52)
      DIMENSION B4(52),B5(52),C1(52),C2(52),C3(52),C4(52),C5(52),D1(52)
      DIMENSION D2(52),D3(52),D4(52),D5(52),E1(52),E2(52),E3(52)
      DIMENSION E4(52),E5(52),F1(52),F2(52),F3(52),F4(52),F5(52)
      DIMENSION TITAL(20)
      DIMENSION G1(52),G2(52),G3(52),G4(52),G5(52),H1(52),H2(52),H3(52)
      DIMENSION H4(52),H5(52),QTY(50),VOD(50)
      COMMON FA,FN,FK,FKN,FLPRIM,FC
      COMMON /SPACR/  PITCH,RODDI,T,DELTA,W,EFFNO,ISPAC
      COMMON /DNBR1/ CRITQ1,H,Z,X,QSQFT,FF,DNB,GI,DEI,MXQFLX,RFS
      COMMON /TPM/ TPM1,VOID,DUM1,DUM2,DUM3,DUM4,ITPM,SLIP1,SLIP2
      COMMON /CHN/ TEMPF,HCOEF,GC,HDIF
      REAL K1
      REAL MXQFLX
10    FORMAT(3(E10.4),3(F10.4),I5)
11    FORMAT(8(F10.4))
12    FORMAT(10F8.4)
13    FORMAT(4I5,4F6.3)
14    FORMAT(I4,19A4)
16    FORMAT(2I5,6F10.5)
17    FORMAT(2E10.4,3F10.6,I5)
501   FORMAT('0','TOTAL HEAT=',E10.4,' BTU/HR',22X,'MASS FLOW RATE=',E10
     1.4,' LBM/HR',/,' AVG FLUX=',E10.4,' BTU/SQ.FT',21X,'PITCH/DIA.=',F
     210.4)
502   FORMAT('0','CORE LENGTH=',F10.4,' FT',25X,'CORE AREA=',F10.4,' SQ.
     1FT',/,' STEP NO.=',I5,36X,'SPACE/ROD LENGTH=',F6.4,/,' SPACER THIC
     2KNESS=',F6.4,' FT')
503   FORMAT('0','CLAD THER COND=',F10.4,' BTU/HR.FT.F',13X,'GAS CONV CO
     1EF=',F10.4,' BTU/HR.SQ.FT.F',/,' FUEL COND=',F10.4,' BTU/HR.FT.F')
```

```
504  FORMAT('0','S=',F6.4,' FT',39X,'B"+S=',F6.4,' FT',/,' KN=',F6.4,41
    1X,'N=',F8.4,/,' A=',F8.4,' /FT',38X,'K=',F8.4,/,' C=',F8.4,' /FT')
505  FORMAT('0','DELTA H=',F10.4,' BTU/LBM',24X,'ROD DIA.=',F6.4,' FT',
    1/,' PITCH=',F6.4,' FT',35X,'ROD NO.=',F10.3)
506  FORMAT('0','CHANNEL  FLOW AREA=',E9.4,' SQ.FT',16X,'MASS FLOW RATE
    1=',E10.4,' LBM/HR.SQ.FT',/,' WET PER=',E10.4,' FT',29X,'HYD. DIA.=
    2',E10.4,' FT')
507  FORMAT('0','FUEL RAD=',F6.4,' FT',32X,'INSIDE CLAD RAD=',F6.4,' FT
    1',/,' NORMALIZED ROD LENGTH=',F10.4,' FT')
508  FORMAT('0','MAX HEAT FLUX DEN=',E10.4,' BTU/HR.CU.FT')
516  FORMAT('0','ROD INCRAMENT=',F6.4,' FT')
510  FORMAT('1',10X,'TEMPERATURES IN DEG. F')
511  FORMAT(' ','FLUID',9X,'CLAD',10X,'FUEL SURFACE',2X,'CENTER LINE')
509  FORMAT(' ',4(F9.4,5X),I3)
512  FORMAT(' ',2(F10.4,5X),E10.4,5X,3(F10.4,5X),I3)
513  FORMAT('1','PRESSURE',7X,'ENTHALPY',5X,'CRITICAL HEAT FLUX',3X,'FR
    1IC LOSS',6X,'ACC LOSS',7X,'DRAG LOSS')
514  FORMAT('1','FDB LENGTH',5X,'SC LENGTH',6X,'SAT LENGTH')
515  FORMAT(' ',3(F10.5,5X),I3)
519  FORMAT('0','2 PHAS MULT1',3X,'2 PHAS MULT2',3X,'VOID FRACT',5X,'QU
    1ALITY')
517  FORMAT(' ',4(E10.4,5X),I3)
518  FORMAT(' ','SUBCOOLED BOILING REGION')
520  FORMAT('0','DRAG COEF',6X,'SPACER LOCATION')
521  FORMAT(' ',2(F10.4,5X))
522  FORMAT('1','   DNB',9X,'CORR FACTOR',4X,'BTU /SQ.FT.')
523  FORMAT(' ',2(F10.4,5X),E10.4,5X,I3)
526  FORMAT(' ','BOILING REGION')
527  FORMAT('1','2 PHAS MULT',3X,'VOID FRACT',5X,'QUALITY')
528  FORMAT(' ',3(E10.5,5X),I3)
530  FORMAT('1',25X,20A4)
531  FORMAT(' ','   PSI',9X,'BTU/LBM',10X,'BTU/SQ.FT.',10X,'PSI',11X,'P
    1SI',13X,'PSI')
532  FORMAT('0','FUEL RADIUS FRAC.=',F6.4,26X,'INNER CLAD RADIUS FRAC.=
    1',F6.4)
533  FORMAT('0','VOL. OF MODERATOR TO FUEL RATIO=',F6.4,12X,'CLAD THICK
```

```
     1NESS FRAC.=',F6.4)
534   FORMAT(' ','SUBCOOLED SLIP=',F6.4,29X,'FULLY DEVELOPED SLIP=',F6.4
     1)
535   FORMAT('0','CHANNEL  FLOW AREA=',E9.4,' SQ.FT',16X,'MASS FLOW RATE
     1=',E10.4,' LBM/HR.SQ.FT',/,' AVG FLUX=',E10.4,' BTU/SQ.FT',21X,'HY
     2D. DIA.=',E10.4,' FT',/,' PITCH=',F6.4,' FT')
536   FORMAT('0','DELTA H=',F10.4,' BTU/LBM',24X,'ROD DIA.=',F6.4,' FT',
     1/,' ROD LENGTH=',F10.4,' FT',26X,'STEP NO.=',I5)
537   FORMAT(' ','ARMAD-TRECHEV TWO-PHASE MODEL')
      NRUN=0
      N1=0
      N2=0
      N3=0
      N4=0
      N5=0
3     READ(5,14,END=450)ITYP,(TITAL(I),I=1,19)
      IF(ITYP.EQ.1)GO TO 35
      READ(5,11)TEMPI,PRESSI,HI,FKC,FHG,FKF
      READ(5,10)Q,W,AVGQ,POVD,FL,AC,LSTEP
      READ(5,11)DELTA,T
      READ(5,11)FS,FBPLSS,FKN,FN,FA,FK,FC
      READ(5,12)(SPSLO(I),I=1,10)
      READ(5,12)(SPSCOF(I),I=1,10)
      READ(5,13)ISPAC,ITPM,IPLOT,IRAD,AON1,AON2,SLIP1,SLIP2
      WRITE(6,530)(TITAL(I),I=1,19)
      WRITE(6,501)Q,W,AVGQ,POVD
      WRITE(6,502)FL,AC,LSTEP,DELTA,T
      WRITE(6,503)FKC,FHG,FKF
      WRITE(6,504)FS,FBPLSS,FKN,FN,FA,FK,FC
      IF(IRAD.EQ.1)WRITE(6,533)AON1,AON2
      IF(IRAD.EQ.2)WRITE(6,532)AON1,AON2
      IF(ITPM.EQ.1 .OR. ITPM.EQ.2)WRITE(6,534)SLIP1,SLIP2
      IF(ITPM.EQ.3)WRITE(6,537)
      WRITE(6,520)
      DO 15 I=1,10
15    WRITE(6,521)SPSCOF(I),SPSLO(I)
```

```
      DELTAH=Q/W
      CON=1.
      IF(ISPAC.EQ.3)CON=(2./3.**.5)
      RODDI=(AVGQ*3.1416*FL*AC)/(Q*(POVD)**2)*CON
      RODRD=RODDI/2.
      PITCH=POVD*RODDI
      EFFNO=AC/PITCH**2*CON
      CALL SPACER(ACIF,GI,PI,DEI)
      IF(IRAD.EQ.2)GO TO 25
      RFS=(ACIF/(3.1416*AON1))**.5
      RCI=RODRD-(RODRD-RFS)*AON2
      GO TO 30
25    RFS=AON1*RODDI/2.
      RCI=AON2*RODDI/2.
30    FLPRIM=1.*FL/(FBPLSS-FS)
      MXQFLX=Q/(3.1416*(RFS**2)*EFFNO*SHAP(FS,FBPLSS))
      FLSTEP=LSTEP
      DLSTEP=FL/(FLSTEP-1.)
      WRITE(6,505)DELTAH,RODDI,PITCH,EFFNO
      WRITE(6,506)ACIF,GI,PI,DEI
      WRITE(6,507)RFS,RCI,FLPRIM
      WRITE(6,508)MXQFLX
      WRITE(6,516)DLSTEP
      GO TO 45
35    READ(5,11)TEMPI,PRESSI,HI,FKC,FHG,FKF
      READ(5,17)AVGQ,GI,DEI,FL,ACIF,LSTEP
      READ(5,11)FS,FBPLSS,FKN,FN,FA,FK,FC
      READ(5,12)(SPSLO(I),I=1,10)
      READ(5,12)(SPSCOF(I),I=1,10)
      READ(5,16)ITPM,IPLOT,RODDI,RFS,RCI,SLIP1,SLIP2,PITCH
      DELTAH=AVGQ*3.1416*RODDI*FL/(GI*ACIF)
      RODRD=RODDI/2.
      FLPRIM=1.*FL/(FBPLSS-FS)
      MXQFLX=AVGQ*3.1416*RODDI*FL/(3.1416*RFS**2*SHAP(FS,FBPLSS))
      FLSTEP=LSTEP
      DLSTEP=FL/(FLSTEP-1.)
```

```
      W=ACIF*GI
      POVD=PITCH/RODDI
      EFFNO=1.
      WRITE(6,530) (TITAL(I),I=1,19)
      WRITE(6,535)ACIF,GI,AVGQ,DEI,PITCH
      WRITE(6,536)DELTAH,RODDI,FL,LSTEP
      WRITE(6,507)RFS,RCI,FLPRIM
      WRITE(6,503)FKC,FHG,FKF
      IF(ITPM.EQ.1 .OR. ITPM.EQ.2)WRITE(6,534)SLIP1,SLIP2
      IF(ITPM.EQ.3)WRITE(6,537)
      WRITE(6,504)FS,FBPLSS,FKN,FN,FA,FK,FC
      WRITE(6,508)MXQFLX
      WRITE(6,516)DLSTEP
      WRITE(6,520)
      DO 40 I=1,10
40    WRITE(6,521)SPSCOF(I),SPSLO(I)
45    CRITQ1(1)=0.
      PFRIC(1)=0.
      PACC(1)=0.
      ZFDB(1)=0.
      ZSC(1)=0.
      ZSTAR(1)=0.
      KIP1=0
      KIP2=0
      KIP3=0
      KCT=0
      X(1)=0.
      VOID(1)=0.
      TPM1(1)=1.
      SUM=0.
      II=1
      DO 5 I=1,50
      QTY(I)=0.
      VOD(I)=0.
      ZFDB(I)=0.
      ZSC(I)=0.
```

```
      ZSTAR(I)=0.
5     PSPAC(I)=0.
      M=1
      GC=4.17E08
      TEMPF(1)=TEMPI
      PRESF(1)=PRESSI
      H(1)=HI
      Z(1)=FS
      P=PRESSI
      PRESSA=PRESSI
      Y=HI
      B=.042*POVD-.024
      IF(ISPAC.EQ.3)B=.026*POVD-.006
      DO 100 I=1,LSTEP
      IF(I.EQ.1)GO TO 60
      Z(I)=DLSTEP*(FBPLSS-FS)/FL+Z(I-1)
      P=PRESF(I-1)
      H(I)=H(I-1)+MXQFLX*3.1416*RFS**2*SHAP(Z(I-1),Z(I))*EFFNO/W
      Y=.5*(H(I)+H(I-1))
      TEMPF(I)=TEMPF(I-1)+MXQFLX*3.1416*RFS**2*EFFNO*SHAP(Z(I-1),Z(I))/(
     1CP(Y)*W)
      U=TEMPF(I)
60    HCOEF=(B*HF(Y)/DEI**.2)*(GI/VISL(Y))**.8*(CP(Y)*VISL(Y)/HF(Y))**.3
     11333
      FLSHAP=FKN*(FN*FA*(1.-Z(I))*EXP((Z(I)-1.)*FA)+FK*FC*Z(I)*EXP(-Z(I)
     11*FC))
      TEMPC(I)=TEMPF(I)+RFS**2*MXQFLX*FLSHAP/(HCOEF*RODDI)
      TEMPFS(I)=TEMPC(I)+(ALOG(RODRD/RCI)/(2.*FKC)+1./(2.*RFS*FHG)+1./(2
     11.*RCI*FHG))*RFS**2*MXQFLX*FLSHAP
      TEMPCL(I)=TEMPFS(I)+RFS**2*MXQFLX*FLSHAP/(4.*FKF)
      IF(I.EQ.1)GO TO 100
      PFRIC(I)=(.221/(2.*DINS(U)*GC))*(VISL(Y)**.2*DLSTEP*GI**1.8)/(DEI*
     11*1.2*144.)
      IF(Z(I).LT.(SPSLO(M)*(FBPLSS-FS)/FL+FS))GO TO 50
      PSPAC(I)=SPSCOF(M)*GI**2/(2.*GC*DINS(U)*144.)
      M=M+1
```

```
50    PRESF(I)=PRESF(I-1)-PFRIC(I)-PSPAC(I)
      PACC(I)=(1./DINS(TEMPF(I))-1./DINS(TEMPF(I-1)))*GI**2/(GC*144.)
      PRESF(I)=PRESF(I)-PACC(I)-32.2*1.296E7*DINS(U)*DLSTEP/(GC*144.)
      DELTI=SATTEM(P)-TEMPF(I)
      PRESSA=.5*(PRESF(I)+PRESF(I-1))
      DELTAQ=MXQFLX*RFS**2*SHAP(Z(I-1),Z(I))/(RODDI*DLSTEP)
      QSOFT(I)=DELTAQ
      CALL DNBR(I,PRESSA,II)
      FNEW=.067*(14.+.0068*PRESSA)
      IF(KIP1.NE.0)GO TO 85
      ZFDB(I)=GI*CP(Y)*DEI*(DELTI/DELTAQ-(FNEW*DINS(U))/GI)/4.
      IF(ZFDB(I).LE.DLSTEP)KIP1=I
85    IF(KIP3.NE.0)GO TO 90
      ZSC(I)=GI*CP(Y)*DEI*DELTI/(4.*DELTAQ)
      IF(ZSC(I).LE.DLSTEP)KIP3=I
90    ZSTAR(I)=GI*CP(Y)*DEI*(DELTI/DELTAQ+FNEW/(GI*1.6*(1./DINS(U))))/4.
      IF(ZSTAR(I).GT.DLSTEP)GO TO 100
      K=I
      KIP2=I
      GO TO 110
100   CONTINUE
      KCT=1
      KIP2=LSTEP
      K=LSTEP
110   IF(KIP1.EQ.0)GO TO 385
      IF(KIP1.EQ.KIP2)GO TO 270
      P=PRESF(K)
      XZSR=CP(H(K))*FNEW*DELTAQ/(GI*1./DENL(P)*1.6*(HVAP(PRESF(K))-HLIQ(
     1PRESF(K))))
      IF(KCT.EQ.1)GO TO 230
      XZSRRR=XZSR/(KIP2-KIP1)
      GO TO 235
230   XZSRRR=XZSR*DLSTEP/ZSTAR(K)
235   KIP33=KIP3-1
      DO 240 I=KIP1,KIP33
      II=II+1
```

```
      J=II
      P=PRESF(I+1)
      X(J)=XZSRRR*(J-1)
      Y=HLIQ(P)
      CALL VOIDX(Y,P,II,1)
234   PFRIC(I+1)=PFRIC(I+1)*TPM1(J)
      PRESF(I+1)=PRESF(I)-PFRIC(I+1)-PSPAC(I+1)
      H(I+1)=H(I+1)+X(J)*(HVAP(P)-HLIQ(P))
238   SVOLGI=1./DENG(PRESF(I))
      SVOLLI=1./DENL(PRESF(I))
      SVOLGO=1./DENG(PRESF(I+1))
      SVOLLO=1./DENL(PRESF(I+1))
      PACC(I+1)=(DUM1*SVOLLO-DUM2*SVOLLI+DUM3*SVOLGO-DUM4*SVOLGI)*GI**2/
     1(GC*144.)
      PRESF(I+1)=PRESF(I+1)-PACC(I+1)
      N=I+1
      P=(PRESF(I+1)+PRESF(I))*.5
      CALL DNBR(N,P,II)
240   CONTINUE
270   K=KIP3+1
      DO 380 I=K,LSTEP
      II=II+1
      J=II
      Z(I)=DLSTEP*(FBPLSS-FS)/FL+Z(I-1)
      P=PRESF(I-1)
      HDIF=HVAP(P)-HLIQ(P)
      QSQFT(I)=MXQFLX*RFS**2*SHAP(Z(I-1),Z(I))/(RODDI*DLSTEP)
      IF(I.GT.KIP2)GO TO 290
      X(J)=XZSRRR*(J-1)
      GO TO 295
290   IF(SUM.NE.0.)GO TO 294
      KIP22=KIP2+1
      DO 292 I=KIP3,KIP22
292   SUM=SUM+QSQFT(I)
      AVSQFT=SUM/(KIP2-KIP3+2)
      X(J)=4.*AVSQFT*(KIP2-KIP3+1)*DLSTEP/(DEI*GI*HDIF)
```

```
294   X(J)=X(J-1)+4.*QSQFT(I)*DLSTEP/(DEI*GI*HDIF)
295   H(I)=HLIQ(P)+X(J)*HDIF
      Y=HLIQ(P)
      TEMPF(I)=SATTEM(P)
      CALL CHEN(Y,P,I,J)
      FLSHAP=FKN*(FN*FA*(1.-Z(I))*EXP((Z(I)-1.)*FA)+FK*FC*Z(I)*EXP(-Z(I)
     1*FC))
      TEMPC(I)=TEMPF(I)+RFS**2*MXQFLX*FLSHAP/(HCOEF*RODDI)
      TEMPFS(I)=TEMPC(I)+(ALOG(RODRD/RCI)/(2.*FKC)+1./(2.*RFS*FHG)+1./(2
     1.*RCI*FHG))*RFS**2*MXQFLX*FLSHAP
      TEMPCL(I)=TEMPFS(I)+RFS**2*MXQFLX*FLSHAP/(4.*FKF)
      CALL VOIDX(Y,P,II,2)
      DENMAV=(1.-VOID(J))*DENL(P)+VOID(J)*DENG(P)
       PFRIC(I)=(.221/(2.*DENMAV*GC))*(VISL(Y)**.2*DLSTEP*GI**1.8)/(DEI*
     1*1.2*144.)
330   PFRIC(I)=PFRIC(I)*TPM1(J)
      IF(Z(I).LT.(SPSLO(M)*(FBPLSS-FS)/FL+FS))GO TO 340
      PSPAC(I)=SPSCOF(M)*GI**2/(2.*GC*DENMAV*144.)
      M=M+1
340   PRESF(I)=PRESF(I-1)-PFRIC(I)-PSPAC(I)
      SVOLGI=1./DENG(PRESF(I-1))
      SVOLLI=1./DENL(PRESF(I-1))
      SVOLGO=1./DENG(PRESF(I))
      SVOLLO=1./DENL(PRESF(I))
      PACC(I+0)=(DUM1*SVOLLO-DUM2*SVOLLI+DUM3*SVOLGO-DUM4*SVOLGI)*GI**2/
     1(GC*144.)
      PRESF(I)=PRESF(I)-PACC(I)
      P=(PRESF(I-1)+PRESF(I))*.5
      CALL DNBR(I,P,II)
380   CONTINUE
385   DO 386 I=2,LSTEP
      QUALTY=0.
      IF((I.GT.KIP1).AND.(KIP1.NE.0))QUALTY=X(I-KIP1+1)
      K1=.44/(GI/1.E6)**1.72*12*(1.-QUALTY)**7.9
      F=FA+K1*1./FLPRIM
      G=K1*1./FLPRIM-FC
```

```
      E=K1*Z(I)*1./FLPRIM
      D=FA*1.+K1*Z(I)*1./FLPRIM
      P1=K1*MXQFLX*RFS**2*FKN*FLPRIM/(QSQFT(I)*(1.-EXP(-K1*FLPRIM/1.*(Z(
     1I)-Z(I-1))))*RODDI*1.)
      P2=FN*FA*1.*(EXP(Z(I)*F-D)-EXP(F*Z(I-1)-D))/F
      P3=FN*FA*((F*Z(I)-1.)*EXP(F*Z(I)-D)-(F*Z(I-1)-1.)*EXP(F*Z(I-1)-D))
     1/(F**2)
      P4=FK*FC*((G*Z(I)-1.)*EXP(G*Z(I)-E)-(G*Z(I-1)-1.)*EXP(G*Z(I-1)-E))
     1/(G**2)
      FF(I)=P1*(P2-P3+P4)
386   DNB(I)=CRITQ1(I)/(QSQFT(I)*FF(I))
      WRITE(6,514)
      DO 220 I=1,KIP2
220   WRITE(6,515)ZFDB(I),ZSC(I),ZSTAR(I),I
      WRITE(6,510)
      WRITE(6,511)
      DO 400 I=1,LSTEP
      IF(I.EQ.KIP1)WRITE(6,518)
      IF((I.EQ.(KIP3+1)).AND.(KIP3.NE.0))WRITE(6,526)
400   WRITE(6,509)TEMPF(I),TEMPC(I),TEMPFS(I),TEMPCL(I),I
      WRITE(6,513)
      WRITE(6,531)
      DO 405 I=1,LSTEP
      IF(I.EQ.KIP1)WRITE(6,518)
      IF((I.EQ.(KIP3+1)).AND.(KIP3.NE.0))WRITE(6,526)
405   WRITE(6,512)PRESF(I),H(I),CRITQ1(I),PFRIC(I),PACC(I),PSPAC(I),I
      IF(KIP1.EQ.0)GO TO 411
      WRITE(6,527)
      DO 410 I=1,J
      K=I+KIP1-1
410   WRITE(6,528)TPM1(I),VOID(I),X(I),K
411   WRITE(6,522)
      DO 415 I=2,LSTEP
415   WRITE(6,523)DNB(I),FF(I),QSQFT(I),I
      IF(IPLOT.NE.1)GO TO 3
      IF(II.EQ.1)GO TO 421
```

```
      DO 420 I=2,J
      QTY(I+KIP1-1)=X(I)*100.
420   VOD(I+KIP1-1)=VOID(I)*100.
421   WRITE(6,1)
1     FORMAT('0','$$$')
      NRUN=NRUN+1
      GO TO(425,430,435,440,445),NRUN
425   N1=LSTEP
      DO 427 I=1,N1
      A1(I)=TEMPF(I)
      B1(I)=TEMPCL(I)
      C1(I)=PRESF(I)
      FLE1(I)=DLSTEP*(I-1)
      G1(I)=QTY(I)
      H1(I)=VOD(I)
426   IF(I.EQ.1)GO TO 427
      F1(I-1)=QSQFT(I)
      E1(I-1)=DNB(I)
427   D1(I)=H(I)
      GO TO 3
430   N2=LSTEP
      DO 433 I=1,N2
      A2(I)=TEMPF(I)
      B2(I)=TEMPCL(I)
      C2(I)=PRESF(I)
      FLE2(I)=DLSTEP*(I-1)
      G2(I)=QTY(I)
      H2(I)=VOD(I)
432   IF(I.EQ.1)GO TO 433
      F2(I-1)=QSQFT(I)
      E2(I-1)=DNB(I)
433   D2(I)=H(I)
      GO TO 3
435   N3=LSTEP
      DO 437 I=1,N3
      A3(I)=TEMPF(I)
```

```
      B3(I)=TEMPCL(I)
      C3(I)=PRESF(I)
      FLE3(I)=DLSTEP*(I-1)
      G3(I)=QTY(I)
      H3(I)=VOD(I)
436   IF(I.EQ.1)GO TO 437
      F3(I-1)=QSQFT(I)
      E3(I-1)=DNB(I)
437   D3(I)=H(I)
      GO TO 3
440   N4=LSTEP
      DO 443 I=1,N4
      A4(I)=TEMPF(I)
      B4(I)=TEMPCL(I)
      C4(I)=PRESF(I)
      FLE4(I)=DLSTEP*(I-1)
      G4(I)=QTY(I)
      H4(I)=VOD(I)
442   IF(I.EQ.1)GO TO 443
      F4(I-1)=QSQFT(I)
      E4(I-1)=DNB(I)
443   D4(I)=H(I)
      GO TO 3
445   N5=LSTEP
      DO 447 I=1,N5
      A5(I)=TEMPF(I)
      B5(I)=TEMPCL(I)
      C5(I)=PRESF(I)
      FLE5(I)=DLSTEP*(I-1)
      G5(I)=QTY(I)
      H5(I)=VOD(I)
446   IF(I.EQ.1)GO TO 447
      F5(I-1)=QSQFT(I)
      E5(I-1)=DNB(I)
447   D5(I)=H(I)
450   IF(NRUN.EQ.0)STOP
```

```
      WRITE(6,1)
      CALL PLOTS(BUFF(1),1000)
      CALL PICTUR (10.,8.,'COOLANT TEMP,F',-14,'CORE LENGTH,FT',14,A1,FL
     1E1,N1,3,0,A2,FLE2,N2,4,2,A3,FLE3,N3,3,3,A4,FLE4,N4,4,4,A5,FLE5,N5,
     13,5,NRUN)
      CALL PLOT (3.,0.,-3)
      CALL PICTUR (10.,8.,'CENTER LINE TEMP,F',-18,'CORE LENGTH,FT',14,B
     11,FLE1,N1,3,0,B2,FLE2,N2,4,2,B3,FLE3,N3,3,3,B4,FLE4,N4,4,4,B5,FLE5
     1,N5,3,5,NRUN)
      CALL PLOT (3.,0.,-3)
      CALL PICTUR (10.,8.,'PRESSURE,PSI',-12,'CORE LENGTH,FT',14,C1,FLE1
     1,N1,3,0,C2,FLE2,N2,4,2,C3,FLE3,N3,3,3,C4,FLE4,N4,4,4,C5,FLE5,N5,3,
     15,NRUN)
      CALL PLOT (3.,0.,-3)
      CALL PICTUR (10.,8.,'ENTHALPY,BTU/LBM',-16,'CORE LENGTH,FT',14,D1,
     1FLE1,N1,3,0,D2,FLE2,N2,4,2,D3,FLE3,N3,3,3,D4,FLE4,N4,4,4,D5,FLE5,N
     15,3,5,NRUN)
      CALL PLOT (3.,0.,-3)
      IF(KIP1.EQ.0)GO TO 453
      CALL PICTUR (10.,8.,'QUALITY,%',-9,'CORE LENGTH,FT',14,G1,FLE1,N1,
     13,0,G2,FLE2,N2,4,2,G3,FLE3,N3,3,3,G4,FLE4,N4,4,4,G5,FLE5,N5,3,5,NR
     2UN)
      CALL PLOT (3.,0.,-3)
      CALL PICTUR (10.,8.,'VOID,%',-6,'CORE LENGTH,FT',14,H1,FLE1,N1,3,0
     1,H2,FLE2,N2,4,2,H3,FLE3,N3,3,3,H4,FLE4,N4,4,4,H5,FLE5,N5,3,5,NRUN)
      CALL PLOT (3.,0.,-3)
453   DO 455 I=2,50
      FLE1(I-1)=FLE1(I)
      FLE2(I-1)=FLE2(I)
      FLE3(I-1)=FLE3(I)
      FLE4(I-1)=FLE4(I)
455   FLE5(I-1)=FLE5(I)
      N1=N1-1
      N2=N2-1
      N3=N3-1
      N4=N4-1
```

```
 N5=N5-1
 CALL PICTUR (10.,8.,'DNBR',-4,'CORE LENGTH,FT',14,E1,FLE1,N1,3,0,E
12,FLE2,N2,4,2,E3,FLE3,N3,3,3,E4,FLE4,N4,4,4,E5,FLE5,N5,3,5,NRUN)
 CALL PLOT (3.,0.,-3)
 CALL PICTUR (10.,8.,'FLUX,BTU/SQFT',-13,'CORE LENGTH,FT',14,F1,FLE
11,N1,3,0,F2,FLE2,N2,4,2,F3,FLE3,N3,3,3,F4,FLE4,N4,4,4,F5,FLE5,N5,3
2,5,NRUN)
 CALL PLOT (10.,0.,-3)
 CALL PLOT (0.,0.,999)
 STOP
 END
```

```
      FUNCTION SHAP(A,B)
      COMMON FA,FN,FK,FKN,FLPRIM,FC
      SHAP=(FKN*FLPRIM/1.)*(FN*1.*(EXP((B-1.)*FA)-EXP((A-1.)*FA))-(FK/FC
     1)*(EXP(-B*FC)*(FC*B+1.)-EXP(-A*FC)*(FC*A+1.))-(FN/FA)*(EXP((B-1.)*
     2FA)*(FA*B-1.)-EXP((A-1.)*FA)*(FA*A-1.)))
      RETURN
      END
C
CC
C
      FUNCTION SATTEM(P)
      U=ALOG(P)
      U=U-7.
      SATTEM=((((-.16074*U-.69679)*U+.61781)*U+14.65778)*U+124.05875)*U+
     1555.99496
      RETURN
      END
C
CC
C
      FUNCTION DENL(P)
      U=ALOG(P)-7.
      VLIQ=((((-.2638E-03*U+.14267E-02)*U+.21252E-02)*U+.11923E-02)*U+.
     119742E-02)*U+.40469E-02)*U+.21963E-01
      DENL=1./VLIQ
      RETURN
      END
C
CC
C
      FUNCTION CP(H)
      X=.001*H
      X3=X*X*X
      CP=1./(.864+1.66*X-7.*X*X+10.6*X3-7.*X*X3)
      RETURN
      END
```

```
      FUNCTION VISL(H)
      VISL=.008+118./H
      RETURN
      END
C
C
C
      FUNCTION HLIQ(P)
      U=ALOG(P)-7.
      HLIQ=(((((-.5873*U+.11491E1)*U+7.41534)*U+10.8011)*U+13.8916)*U+3
     17.49243)*U+160.7816)*U+557.1533
      RETURN
      END
C
C
C
      FUNCTION DENG(P)
      U=ALOG(P)-7.
      PVG=(((((04.7459*U-6.5913)*U-22.4306)*U-27.967)*U-53.0073)*U-61.51
     147)*U+439.9746
      DENG=P/PVG
      RETURN
      END
C
C
C
      FUNCTION HVAP(P)
      U=ALOG(P)-7.
      HVAP=(((((3.7170*U-9.1118)*U-24.4478)*U-27.2172)*U-44.2069)*U-46.3
     1516)*U+1187.6082
      RETURN
      END
```

```
      FUNCTION VISG(P)
      VISG=.04059+8.36E-6*(P-405.78)
      RETURN
      END
C
C
C
      FUNCTION HF(H)
      X=.001*H-.25
      HF=.47-.45*X-.072/EXP(6.25*X)
      RETURN
      END
C
C
C
      FUNCTION DINS(T)
      IF(T.GT.550.)GO TO 2
      DINS=76.1196-.05324*T
      GO TO 5
 2    DINS=92.0748-.08222*T
 5    CONTINUE
      RETURN
      END
C
C
C
      SUBROUTINE PICTUR(XLEN,YLEN,XLABEL,NCX,YLABEL,NCY,X1,Y1,N1,J1,L1,X
     12,Y2,N2,J2,L2,X3,Y3,N3,J3,L3,X4,Y4,N4,J4,L4,X5,Y5,N5,J5,L5,N)
      DIMENSION X5(2),X4(2),X3(2),X2(2),X1(2)
      DIMENSION Y5(2),Y4(2),Y3(2),Y2(2),Y1(2)
      DIMENSION XM(12),YM(12)
      DIMENSION N5(2),N4(2),N3(2),N2(2),N1(2)
      DIMENSION J5(2),J4(2),J3(2),J2(2),J1(2)
      DIMENSION L5(2),L4(2),L3(2),L2(2),L1(2)
      DIMENSION XLABEL(2),YLABEL(2)
 11   GO TO(1,2,3,4,5),N
```

```
5     CALL MINMAX(X5,N5,XM(9),XM(10))
      CALL MINMAX(Y5,N5,YM(9),YM(10))
4     CALL MINMAX(X4,N4,XM(7),XM(8))
      CALL MINMAX(Y4,N4,YM(7),YM(8))
3     CALL MINMAX(X3,N3,XM(5),XM(6))
      CALL MINMAX(Y3,N3,YM(5),YM(6))
2     CALL MINMAX(X2,N2,XM(3),XM(4))
      CALL MINMAX(Y2,N2,YM(3),YM(4))
1     CALL MINMAX(X1,N1,XM(1),XM(2))
      CALL MINMAX(Y1,N1,YM(1),YM(2))
      NN=2*N
      CALL SCALE(XM,XLEN,NN,1)
      CALL SCALE(YM,YLEN,NN,1)
      CALL AXIS(0.0,0.0,XLABEL,NCX,XLEN,0.0,XM(NN+1),XM(NN+2))
      CALL AXIS(0.0,0.0,YLABEL,NCY,YLEN,90.0,YM(NN+1),YM(NN+2))
      GO TO(6,7,8,9,10),N
10    K=N5(1)+1
      X5(K)=XM(NN+1)
      X5(K+1)=XM(NN+2)
      Y5(K)=YM(NN+1)
      Y5(K+1)=YM(NN+2)
      CALL LINE(X5,Y5,N5,1,J5,L5)
      CALL PLOT(0.0,0.0,3)
9     K=N4(1)+1
      X4(K)=XM(NN+1)
      X4(K+1)=XM(NN+2)
      Y4(K)=YM(NN+1)
      Y4(K+1)=YM(NN+2)
      CALL LINE(X4,Y4,N4,1,J4,L4)
      CALL PLOT(0.0,0.0,3)
8     K=N3(1)+1
      X3(K)=XM(NN+1)
      X3(K+1)=XM(NN+2)
      Y3(K)=YM(NN+1)
      Y3(K+1)=YM(NN+2)
      CALL LINE(X3,Y3,N3,1,J3,L3)
```

```
      CALL PLOT(0.0,0.0,3)
7     K=N2(1)+1
      X2(K)=XM(NN+1)
      X2(K+1)=XM(NN+2)
      Y2(K)=YM(NN+1)
      Y2(K+1)=YM(NN+2)
      CALL LINE(X2,Y2,N2,1,J2,L2)
      CALL PLOT(0.0,0.0,3)
6     K=N1(1)+1
      X1(K)=XM(NN+1)
      X1(K+1)=XM(NN+2)
      Y1(K)=YM(NN+1)
      Y1(K+1)=YM(NN+2)
      CALL LINE(X1,Y1,N1,1,J1,L1)
      CALL PLOT(XLEN+3.,0.,-3)
      WRITE(6,100)
100   FORMAT('0','$$$$$')
      RETURN
      END
      SUBROUTINE SPACER(ACIF,GI,PI,DEI)
      COMMON /SPACR/  PITCH,RODDI,T,DELTA,W,EFFNO,ISPAC
524   FORMAT('1',25X,'SQUARE ARRAY WITH GRID SPACERS')
525   FORMAT('1',25X,'SQUARE ARRAY WITH WIRE WRAP')
529   FORMAT('1',25X,'HEXAGONAL ARRAY WITH WIRE WRAP')
      GO TO(16,18,20),ISPAC
16    ACIF=(PITCH)**2-3.1416*(RODDI)**2/4.-(2.*PITCH*T-T**2)*DELTA
      GI=W/(EFFNO*ACIF)
      PI=3.1416*RODDI+4.*DELTA*(PITCH-T)
      DEI=4.*ACIF/PI
      WRITE(6,524)
      GO TO 25
18    SPACDI=PITCH-RODDI
      ACIF=PITCH**2-(3.1416/4.)*(RODDI**2+SPACDI**2)
      GI=W/(EFFNO*ACIF)
      PI=3.1416*(RODDI+SPACDI)
      DEI=4.*ACIF/PI
```

```
      WRITE(6,525)
      GO TO 25
20    SPACDI=PITCH-RODDI
      ACIF=(3.**.5/4.)*PITCH**2-(3.1416/8.)*(RODDI**2+SPACDI**2)
      GI=W/(EFFNO*ACIF)
      PI=(3.1416/2.)*(RODDI+SPACDI)
      DEI=4.*ACIF/PI
      WRITE(6,529)
25    CONTINUE
      RETURN
      END
      SUBROUTINE DNBR(I,P,J)
      DIMENSION CRITQ1(50),H(50),Z(50),X(50),QSQFT(50),FF(50),DNB(50)
      COMMON /DNBR1/ CRITQ1,H,Z,X,QSQFT,FF,DNB,GI,DEI,MXQFLX,RFS
      CRITQ1(I)=1.E6*((2.022-.0004302*P)+(.1722-.0000984*P)*EXP((18.177-
     1.004129*P)*X(J)))*((.1484-1.596*X(J)+.1729*X(J)**2)*GI/1.E6+1.037)
     2*(1.157-.869*X(J))*(.2664+.8357*EXP(-3.151*DEI))*(.8258+.000794*(H
     3LIQ(P)-H(I-1)))
      RETURN
      END
      SUBROUTINE VOIDX(Y,P,II,M)
      DIMENSION CRITQ1(50),H(50),Z(50),X(50),QSQFT(50),FF(50),DNB(50)
      DIMENSION TPM1(50),VOID(50)
      COMMON /DNBR1/ CRITQ1,H,Z,X,QSQFT,FF,DNB,GI,DEI,MXQFLX,RFS
      COMMON /TPM/ TPM1,VOID,DUM1,DUM2,DUM3,DUM4,ITPM,SLIP1,SLIP2
      J=II
      SVOLG=1./DENG(P)
      SVOLL=1./DENL(P)
      GO TO(231,232,233),ITPM
231   TPM1(II)=(1.+X(J)*((SVOLG-SVOLL)/SVOLL))*(1.+X(J)*(VISL(Y)/VISG(P)
     1-1.))**(-.25)
      GO TO 234
232   TPM1(II)=(1.+X(J)*((SVOLG-SVOLL)/SVOLL))*(1.+X(J)*(VISG(P)/VISL(Y)
     1-1.))**(.25)
      GO TO 234
233   BB=(X(J)/SVOLL)/((1.-X(J))/SVOLG+X(J)/SVOLL)
```

```
      VOID(J)=(.833+.05*ALOG(BB/14.22))*BB
      TPM1(J)=(1.-X(J))**1.75/(1.-VOID(J))**1.2
234   IF(ITPM.EQ.3)GO TO 236
      SLIP=SLIP2
      IF(M.EQ.1)SLIP=SLIP1
      V=X(J)*1./DENG(P)+(1.-X(J))*1./DENL(P)*SLIP
      VOID(II)=(X(J)*1./DENG(P))/V
236   DUM1=(1-X(J))**2/(1-VOID(J))
      DUM2=(1-X(J-1))**2/(1-VOID(J-1))
      DUM3=X(J)**2/VOID(J)
      IF(J.EQ.2)GO TO 237
      DUM4=X(J-1)**2/VOID(J-1)
      GO TO 238
237   DUM4=0.
238   CONTINUE
      RETURN
      END
```

```
      FUNCTION SUFTN(P)
      X=DENL(P)-DENG(P)
      X=.000001*X**4.
      SUFTN=X*(4.6+1.84/EXP(.685*X)+.232*EXP(1.56*(X-15.)))
      SUFTN=SUFTN*6.8525E-5
      RETURN
      END
C
C
C
      FUNCTION SATP(T)
      Z=(T-32.)*5./9.
      TT=ABS(.65-.01*Z)
      SATP=220.88*EXP((1000./(Z+273.15))*1.0E-5*(374.136-Z)*((-741.9242)
     1+(29.721*TT)+(-11.55286*(TT**2.))+(.86856*(TT**3.))+(.10941*(TT**4
     1.))+(-.44*(TT**5.))+(.2521*(TT**6.))+(-5.21870E-2*(TT**7.))))
      SATP=SATP*14.5038
      RETURN
      END
C
C
C
      SUBROUTINE CHEN(Y,P,I,J)
      DIMENSION CRITQ1(50),H(50),Z(50),X(50),QSQFT(50),FF(50),DNB(50)
      COMMON /DNBR1/ CRITQ1,H,Z,X,QSQFT,FF,DNB,GI,DEI,MXQFLX,RFS
      COMMON /CHN/ TEMPF(50),HCOEF,GC,HDIF
      HCSP=(.023*HF(Y)/DEI**.2)*(GI*(1.-X(J))/VISL(Y))**.8*(CP(Y)*VISL(Y
     1)/HF(Y))**.4
      DELTS=.072*QSQFT(I)**.5*EXP(-P/1260.)
      IF(Y.GE.HLIQ(P))GO TO 6
      QTEST=HCSP*(DELTS+SATTEM(P)-TEMPF(I))
      IF(QTEST.LT.QSQFT(I))GO TO 6
      HCOEF=(.023*HF(Y)/DEI**.2)*(GI/VISL(Y))**.8*(CP(Y)*VISL(Y)/HF(Y))*
     1*.4
      GO TO 2
    6 XTT=((1.-X(J))/X(J))**.9*(DENG(P)/DENL(P))**.5*(VISL(Y)/VISG(Y))**
```

```
     1.1
      IF((1./XTT).GE..5)GO TO 8
      F=.5/(XTT*XTT)+.95/XTT+1.
      GO TO 9
8     F=1.6*(2./XTT)**.738
9     IF(Y.LT.HLIQ(P))F=1.
      HCSP=HCSP*F
      RETP=(GI*(1.-X(J))*DEI/VISL(Y))*F**1.25
      IF(RETP.LE.0)GO TO 10
      IF(RETP.GE.3.E5)GO TO 11
      S=.17-.232*ALOG(RETP/3.E5)
      GO TO 12
11    S=.17-.0617*ALOG(RETP/3.E5)
      GO TO 12
10    S=1.
12    B=(HF(Y)**.79*CP(Y)**.45*DENL(P)**.49)/(VISL(Y)**.29*HDIF**.24*DEN
     1G(P)**.24*SUFTN(P)**.5)
      ACHEN=.00122*B*S*GC**.25
      TWALL=SATTEM(P)+DELTS
      TM=SATTEM(P)
      IC=0
      IFLAG=0
13    SATPW=SATP(TWALL)
      IC=IC+1
      IF(IC.GT.100)GO TO 26
      HCTP=ACHEN*(TWALL-SATTEM(P))**.24*((SATPW-P)*144.)**.75
      IF(Y.GE.HLIQ(P))GO TO 14
      QNEW=HCSP*(TWALL-TEMPF(I))+HCTP*(TWALL-SATTEM(P))
      GO TO 15
14    QNEW=(HCSP+HCTP)*(TWALL-SATTEM(P))
15    TESTQ=(ABS(QNEW-QSQFT(I)))/QSQFT(I)
      IF(TESTQ.LE..01)GO TO 16
      IF(IC.GT.1)GO TO 17
18    QOLD=QNEW
      TOLD=TWALL
      IF(QNEW-QSQFT(I))19,16,20
```

```
19    TWALL=TWALL+10.
      GO TO 13
20    TWALL=TWALL-10.
      GO TO 13
17    TEST2=(QOLD-QSQFT(I))/(QNEW-QSQFT(I))
      IF(IFLAG.EQ.1)GO TO 21
      IF(TEST2.GT.0.)GO TO 18
      IFLAG=1
      IF(QNEW-QSQFT(I))22,22,23
22    QHI=QOLD
      QLO=QNEW
      THI=TOLD
      TLO=TWALL
      GO TO 24
23    QLO=QOLD
      QHI=QNEW
      THI=TWALL
      TLO=TOLD
24    SLOPE=(QHI-QLO)/(THI-TLO)
      TWALL=(QSQFT(I)+(SLOPE*THI)-QHI)/SLOPE
      GO TO 13
21    IF(QNEW.GT.QSQFT(I))GO TO 25
      QLO=QNEW
      TLO=TWALL
      GO TO 24
25    QHI=QNEW
      THI=TWALL
      GO TO 24
16    IF(Y.GE.HLIQ(P))GO TO 26
      QTRUE=HCSP*(TWALL-TEMPF(I))+HCTP*(TWALL-SATTEM(P))
      HCOEF=QTRUE/(TWALL-TEMPF(I))
      GO TO 2
26    HCOEF=HCSP+HCTP
2     CONTINUE
      RETURN
      END
```